

Aus dem Institut für Molekulare Medizin
der Universitätsmedizin der Johannes Gutenberg-Universität Mainz

NECAB2/MitoNEET represents an alternative activity-triggered mitochondrial quality
control system

NECAB2/MitoNEET repräsentiert ein alternatives aktivitätsinduziertes Kontrollsystem
der mitochondrialen Qualität

Inauguraldissertation
zur Erlangung des Doktorgrades der
Medizin
der Universitätsmedizin
der Johannes Gutenberg-Universität Mainz

Vorgelegt von

Elena Morpurgo

aus Arona

Mainz, 2021

Wissenschaftlicher Vorstand:

1. Gutachter:

2. Gutachter:

Tag der Promotion:

7. Dezember 2021

Table of contents

Abbreviations	VI
Table Directory	IX
Image Directory	X
1. Introduction	1
2. Literary discussion	3
2.1. Neuronal Calcium Binding protein 2 (NECAB2)	3
2.1.1. The Neuronal Calcium binding protein family	3
2.1.2. Localization of NECAB proteins	3
2.1.3. Function of NECAB proteins	3
2.1.4. NECAB2 structure	5
2.2. The striatum	6
2.2.1. Anatomy of the striatum and connectivity	6
2.2.2. The basal ganglia and the motor circuit	6
2.2.3. Clinical significance	7
2.2.3.1. Hyperkinetic disorders and neuropsychiatric diseases	7
2.3. Mitochondria	8
2.3.1. Structure and function of mitochondria	8
2.3.2. Clinical relevance of mitochondrial impairment	9
2.4. Autophagy	9
2.4.1. Macroautophagy.....	10
2.4.1.1. Mitophagy.....	10
2.4.2. Endocytosis	11
2.5. Parkinson’s Disease	11
2.6. The PINK1/Parkin pathway	12
2.6.1. Alternative quality control pathways	13
2.6.1.1. Parkin-independent pathways	14
2.6.1.2. PINK1 can operate without Parkin	14
2.6.1.3. Mitophagy depends on other organelles	14
2.7. The CDGSH iron-sulfur domain-containing protein 1	17
3. Materials	21
3.1. Cell lines	21
3.1.1. HT22.....	21
3.1.2. Primary striatal neurons	21
3.1.3. Induced pluripotent stem cells (iPSCs)	21
3.2. Chemicals, buffers, markers	22
3.3. PCR primers	23
3.4. Plasmids	23

3.5. Antibodies	24
3.6. Consumables	25
3.7. Devices	26
3.8. Software	27
4. Methods	28
4.1. Cell culture – neuronal striatal primary cultures	28
4.2. Cell culture – HT22.....	29
4.2.1. Defrosting HT22	29
4.2.2. Splitting HT22.....	29
4.2.3. Transfection of HT22 cells.....	29
4.3. Cell culture – iPSCs	30
4.4. Molecular biology	31
4.4.1. Genotyping.....	31
4.5. Protein biochemistry	33
4.5.1. Protein isolation from cells	33
4.5.2. BCA protein assay.....	33
4.5.3. SDS-PAGE.....	33
4.5.4. CCCP treatment.....	35
4.6. Immunocytochemistry.....	36
4.6.1. Murine primary striatal neurons.....	36
4.6.2. Human iPSC-derived dopaminergic neurons	37
4.7. Image analysis	38
4.7.1. Imaris analysis of z-stacks	38
4.7.2. ImageJ Deconvolution and Pearson’s Coefficient.....	38
4.8. Statistical analysis.....	38
5. Results.....	39
5.1. NECAB2 is present at mitochondria and potentially at endosomes.....	39
5.2. Mitophagy is significantly lower in N2-expressing cells.....	42
5.3. Parkin and MitoRed colocalization increases with FCCP	43
5.4. NECAB2 and MitoNEET may colocalize	44
5.5. HT22 N2 cells express higher amounts of mNT when compared to EV	45
5.6. MitoNEET and Rab5 colocalize.....	46
5.7. Endosomal and mitochondrial overlap increases upon Antimycin A treatment and decreases upon FCCP treatment in HT22 cells	47
5.8. TOM20 and Rab5 colocalization increases upon AMA treatment in HT22 cells ..	49
5.9. TOM20 and Rab5 colocalization increases upon FCCP treatment in KO primary striatal neurons	50
5.10. NECAB2 is upregulated in human iPSC-derived dopaminergic neurons with PD mutations	52

5.11. NECAB2 colocalizes more with Rab5 in isogenic control	55
6. Discussion	57
6.1. NECAB2 is present at mitochondria and in endosomes.....	58
6.2. NECAB2 is involved in mitochondrial quality control.....	58
6.3. NECAB2 could act on mtQC through endosomes.....	59
6.4. NECAB2 could interact with MitoNEET	61
6.5. MitoNEET and Rab5 colocalization increases upon FCCP treatment	62
6.6. NECAB2 and MitoNEET represent a novel mtQC mechanism	63
6.7. NECAB2's potential implications in disease.....	65
6.8. NECAB2 is upregulated in human dopaminergic neurons with PD mutations but colocalizes more with Rab5 in isogenic control	65
7. Summary	67
8. Zusammenfassung.....	69
Literature	I
Acknowledgement.....	XIII
Curriculum Vitae.....	XIV

Abbreviations

°C	Degrees Celsius
A2AR	Adenosine A2A receptor
ABM	Antibiotic monooxygenase domain
AD	Alzheimer's disease
AL	Autolysosome
Alfy	Autophagy-linked FYVE protein
ALS	Amyotrophic lateral sclerosis
ALS2/Alsin	Amyotrophic lateral sclerosis protein 2
AMPH	Amphisome
APH	Autophagosomes
APP	amyloid precursor protein
ATG	Autophagy-related protein
ATL3	Atlastin 3
ATP	Adenosine triphosphate
A β	β -amyloid
A β	β -amyloid
BCA	bicinchoninic acid assay
BFP2	Blue fluorescent protein 2
Bid	BH3 interacting-domain death agonist
bp	Base pair
BSA	Bovine serum albumin
cAMP	Cyclic adenosine monophosphate
CCCP	Carbonyl cyanide m-chlorophenyl hydrazone
CCPG1	Cell cycle progression 1
CF	Cystic fibrosis
CFTR	Cystic fibrosis transmembrane conductance regulator
cGMP	Cyclic guanosine monophosphate
CISD1	CDGSH iron sulfur domain 1; gene coding for MitoNEET, also abbreviated as mNT
CMA	Chaperone-mediated autophagy
DAPI	4',6-diamidino-2-phenylindole
DFCP1	Double FYVE-containing protein 1
DMEM	Dulbecco's Modified Eagle's medium
DMSO	Dimethyl sulfoxide
DNA	Deoxyribonucleic acid
DRP1	Dynamin-related protein 1
EBs	Embryoid bodies
EDTA	Ethylenediaminetetraacetic acid
EE	Early endosomes
EOPD	Early onset Parkinson's Disease
ER	Endoplasmic reticulum
ESCRT	Endosomal Sorting Complex Required for Transport
FBS	Fetal bovine serum
FCCP	Carbonyl cyanide-4-(trifluoromethoxy)phenylhydrazone
Fe-S (clusters)	Iron sulphur (clusters)
GABA	Gamma-aminobutyric acid
GABARAP	GABA type A receptor-associated protein
GBA1	Acid β -glucocerebrosidase
GEF	guanine nucleotide exchange factor

GFP	Green fluorescent protein
GPe	Globus pallidus pars externa
GPi	Globus pallidus pars interna
GPR3	G-protein coupled receptor 3
GTP	Guanosine triphosphate
h/hr/hrs	Hour/hours
HBSS	Hanks' Balanced Salt Solution
HSAN1	Hereditary sensory and autonomic neuropathy type 1
HT22	Immortalized mouse hippocampal neuronal cell line
ICC	Immunocytochemistry
IMM	Inner mitochondrial membrane
iPSC	Induced pluripotent stem cell
kDa	kiloDalton
KO	Knockout
LC3	Microtubule-associated protein 1A/1B-light chain 3
LHON	Leber hereditary optic neuropathy
LIR	LC3-interacting region
LRRK2	Leucine-rich repeat serine/threonine-protein kinase 2
MAP2	Microtubule associated protein 2
MAPK	Mitogen-activated protein kinase
MCS	Membrane contact sites
MEF	Mouse embryonic fibroblasts
Mfn1	Mitofusin 1
Mfn2	Mitofusin 2
MG132	Carbobenzoxy-Leu-Leu-leucinal
mGlu5	Metabotropic glutamate receptor
min	Minute(s)
ml	Milliliter
MM	Mitochondrial membrane
mM	Millimolar
mNT	MitoNEET, also abbreviated as CISD1
MPT	Mitochondrial Permeability Transition
MSN	Medium spiny neuron
mtDNA	Mitochondrial DNA
mtQC	Mitochondrial quality control
MUL1	Mitochondrial ubiquitin ligase 1
MVB	Multivesicular bodies
NAF-1	Nutrient-deprivation autophagy factor-1
NBM	Neurobasal medium
NDP52	Nuclear domain 10 protein 52
NECAB1-3	Neuronal calcium binding protein or N-terminal calcium binding protein 1-3
NEET	Asn-Glu-Glu-Thr amino acid sequence
Nek2	NIMA-related kinase 2
NHR	NECAB homology region
NIP1	Nek2-Interacting Protein 1/NECAB3
Nix	Nip3-like protein X
NPCs	Neuronal progenitor cells
OMM	Outer mitochondrial membrane
Opa1	Optic Atrophy1 protein
OPTN	Optineurin

p62/SQSTM1	Sequestosome 1
Pax6	Paired Box 6
PBS(T)	Phosphate buffered saline (with Tween20/Polysorbate 20)
PCR	Polymerase chain reaction
PD	Parkinson's disease
PDE10A	cAMP and cAMP-inhibited cGMP 3',5'-cyclic phosphodiesterase 10A
PFA	Paraformaldehyde
PINK1	PTEN-induced kinase 1
PPAR	Peroxisome proliferator activated receptors
PTEN	Phosphatase and tensin homolog
QSBB	Queen Square Brain Bank
RAB GTPases	Rab guanosine triphosphates
RETREG1	Reticulophagy regulator 1
RIPA	radioimmunoprecipitation assay buffer
ROS	Reactive oxygen species
SCI	Spinal cord injury
SDS-PAGE	Sodium Dodecyl Sulfate Polyacrylamide Gel Electrophoresis
SNc	Substantia nigra pars compacta
SNCA	α -Synuclein
SNr	Substantia nigra pars reticulata
Syt1	Synaptotagmin 1
TAE	Tris-acetate-EDTA
TALEN	Transcription activator-like effector nucleases
TBI	Traumatic brain injury
TBS(T)	Tris-buffered saline (with Tween20/Polysorbate 20)
TEMED	Tetramethylethylenediamine
TGN	Trans-Golgi network
TH	Tyrosine hydroxylase
TOM20	Translocase of outer membrane
TP53	Tumor protein 53
TRPV1	Transient receptor potential vanilloid 1
WT	Wildtype
XB51	X11-like binding protein of clone number 51
$\Delta\psi_m$	Mitochondrial membrane potential
μ l	Microliter
μ m	Micrometer
μ M	Micromolar

Table Directory

Table 1: Chemicals, buffers, markers	22
Table 2: PCR primers	23
Table 3: Plasmids	23
Table 4: Antibodies	24
Table 5: Consumables	25
Table 6: Devices	26
Table 7: Software	27
Table 8: Plating and cultivation medium	28
Table 9: Differentiation media for iPSCs	30
Table 10: Protein buffer composition	34
Table 11: Running and stacking gel composition	34

Image Directory

Figure 1: Model of mNT and NAF-1 interaction in cells, from (Karmi et al., 2017):	19
Figure 2: Example of genotyping PCR.	32
Figure 3: MitoRed and NECAB2 may colocalize in WT in striatal neurons.....	39
Figure 4: NECAB2 is predominantly present at crude mitochondria in WT mouse brain.	40
Figure 5: NECAB2 may colocalize with endosomal markers.	41
Figure 6: Mitophagy is significantly increased in HT22 BFP2 EV cells.....	42
Figure 7: Parkin and MitoRed colocalization increases in HT22 BFP2 N2 cell lines transiently transfected with Parkin-GFP treated with FCCP	43
Figure 8: NECAB2 may colocalize with MitoNEET in mouse WT primary striatal neurons	44
Figure 9: Western blot showing increased mNT expression in N2 HT22 cells..	45
Figure 10: Rab5 colocalizes with MitoNEET (mNT) in striatal neurons.....	46
Figure 11: Rab5 and MitoRed colocalization increases upon AMA treatment, decreases upon FCCP treatment in HT22 BFP2 cell lines transiently transfected with Rab5.....	47
Figure 12: Rab5 and TOM20 colocalization increases upon AMA treatment in HT22 BFP2 cell lines transiently transfected with Rab5.....	49
Figure 13: Rab5 increasingly colocalizes with TOM20 in KO mouse primary striatal neurons upon FCCP treatment.....	51
Figure 14: NECAB2 and tyrosine hydroxylase are present in iPSC-derived dopaminergic neurons.....	52
Figure 15: NECAB2 and MitoNEET are upregulated in human iPSC-derived dopaminergic neurons with PD mutations compared to isogenic control.	54
Figure 16: MitoNEET/NECAB2 and Rab5/NECAB2 colocalize in human iPSC-derived dopaminergic neurons.	55
Figure 17: Canonical mitophagy.	63
Figure 18: Proposed model of NECAB2 and MitoNEET-dependent mitophagy	63

1. Introduction

Mitochondria have traditionally been described as the “powerhouses of the cell” given their role in energy production in the form of adenosine triphosphate (Siekevitz, 1957). In recent years, however, mitochondria have been implicated in many more cellular processes, including calcium buffering/signaling, the formation of reactive oxygen species, the biosynthesis of co-factors, and the generation of iron sulphur (Fe-S) clusters (Lill et al., 1999, Alberts et al., 2017).

High-energy demand tissues such as muscles, the heart, and the brain require particularly effective mitochondrial energy production. The brain is especially dependent on well-functioning mitochondria, given that neurons are post-mitotic and therefore the effect of faulty mitochondria cannot be diluted by proliferation (Gegg et al., 2010). Mitochondrial dysfunction has been linked to neurodegenerative diseases like Alzheimer’s and Parkinson Disease (PD), but also to neuropathies and to amyotrophic lateral sclerosis (Schapira, 2006). In recent years, more and more pathways ensuring mitochondrial quality control have been uncovered (reviewed in Killackey et al., 2020). Some of these pathways and their proteins have specifically been linked to disease. For example, homozygous or compound heterozygous Parkin (a protein involved in canonical mitochondrial quality control) mutations result in early-onset PD (Lucking et al., 2000).

Neuronal Calcium Binding Protein 2 (NECAB2) is part of the Neuronal Calcium Binding protein family and is expressed mainly in the striatum (Canela et al., 2007), a brain structure involved in motor planning and coordination (Bamford and Bamford, 2019). Striatal degeneration plays a role in PD (DeLong and Wichmann, 2007), and NECAB2 was upregulated in neurons derived from GBA-PD¹ induced pluripotent stem cells (iPSCs) (Schondorf et al., 2014). Previous work from our group showed NECAB2 could play a role in mitochondrial quality control (Dey et al., 2021).

The CDGSH iron-sulfur domain-containing protein 1 (CISD1), also known as MitONEET (mNT), which is located at the outer mitochondrial membrane, was originally identified as a target of the antidiabetic drug pioglitazone (Colca et al., 2004). It has since been linked to autophagy and mitochondrial functioning (Karmi et al., 2017). mNT KO mice display a PD phenotype (Geldenhuys et al., 2017), suggesting mNT is

¹ The *GBA1* gene encodes a lysosomal enzyme, β -glucocerebrosidase (GBA). Mutations in the *GBA1* gene have been linked to PD (Sidransky et al., 2009).

involved in mitochondrial quality control. Furthermore, label-free proteomics from our group show MitoNEET dysregulation in NECAB2 knockout mice striata (unpublished data).

The aim of this thesis was to study if and how NECAB2 is involved in mitochondrial quality control.

2. Literary discussion

2.1. Neuronal Calcium Binding protein 2 (NECAB2)

2.1.1. The Neuronal Calcium binding protein family

NECAB2 (N-Terminal EF-Hand Calcium Binding Protein 2 or Neuronal Calcium-Binding Protein 2) is part of the Neuronal Calcium Binding protein family, along with NECAB1 and NECAB3 (Sugita et al., 2002). All NECAB proteins contain three homologous domains: an N-terminal EF hand domain that binds calcium; a unique highly conserved sequence with a coiled-coil termed NECAB homology region (NHR); and a C-terminal DUF167 domain (Sugita et al., 2002), also known as an antibiotic monooxygenase domain (ABM). In *Streptomyces* bacteria, monooxygenases containing the ABM motif are involved in antibiotic biosynthesis (Yeats et al., 2003).

2.1.2. Localization of NECAB proteins

While NECAB 1 and 2 are found primarily in the brain, NECAB3 is expressed in the brain, heart and skeletal muscle in vertebrates (Sugita et al., 2002). NECAB2 is expressed mainly in the striatum (Canela et al., 2007) and in pyramidal cells in the CA2 region and some interneurons of the hippocampus (Canela et al., 2009, Zimmermann et al., 2013, Gerber et al., 2019). Recently, NECAB2 was also identified as a reliable marker from postnatal development to adulthood for the indusium griseum and the fascicula cinerea in mice (Sanders et al., 2021). Furthermore, NECAB2 expression also characterizes A δ low-threshold mechanosensitive neurons in mice, which play a role in the detection of light touch and hair deflection (Peng et al., 2018).

2.1.3. Function of NECAB proteins

Synaptotagmins are localized at the cell membrane and contain an N-terminal transmembrane region and two C-terminal C2 domains (C2A and C2B) which bind calcium (Pang et al., 2006). Synaptotagmins likely function as calcium sensors and are thus involved in the secretion of hormones and neurotransmitters (Pang et al., 2006). NECAB1 was initially isolated by affinity chromatography on the immobilized C2A domain of Synaptotagmin 1 (Syt1) (Sugita et al., 2002). Subsequent cloning and characterization of the previously unknown protein showed it belonged to the NECAB family (Sugita et al., 2002).

NECAB3, also known as Nek2-Interacting Protein 1 (NIP1), was isolated as interacting partner of the neuron-specific X11-like protein (X11L) (Lee et al., 2000). NECAB3

may play a role in the Golgi apparatus as a substrate of Nek2, a mitotic regulator (Yoo et al., 2004). X11L associates with β -amyloid precursor protein (APP) and in this manner suppresses β -amyloid ($A\beta$) generation (Tomita et al., 1999). $A\beta$ is pathognomonic in Alzheimer's disease (AD). Interestingly, Sumioka et al. (2003) found that two isoforms of NECAB3 both have the ability to bind X11L and cause a change in its conformation, impairing its ability to suppress $A\beta$ secretion.

NECAB2 was shown to be a downstream target of Pax6 in the early developing retina (Bernier et al., 2001). Pax6 is part of a group of homeobox genes required for eye development in humans, mice and insects (Bernier et al., 2001). NECAB2 also binds to the A2A receptor (A2AR), a heptaspanning membrane receptor important for striatal function (Canela et al., 2007). A2AR's C-terminal tail interacts with cytosolic proteins and is linked to the actin cytoskeleton through α -actinin, thereby anchoring it to the plasma membrane. NECAB2 reduces A2AR cell surface expression when the two are co-expressed (Canela et al., 2007). By contrast, the Mitogen-activated protein kinase (MAPK) cascade is increased; therefore, it seems that NECAB2 association with A2AR at the plasma membrane level can modulate the coupling efficiency of A2AR with the signal transduction machinery (Canela et al., 2007). An increased calcium concentration promotes dissociation of NECAB2 from A2AR but association to other proteins, which suggests NECAB2 plays a role in neuronal physiology (Canela et al., 2007). A2AR was known to interact with metabotropic glutamate receptor 5 (mGlu₅) and Canela et al. also showed that NECAB2 interacts with both forms of the mGlu₅ receptor (mGlu_{5a} and mGlu_{5b}) in a calcium-dependent manner. This receptor interaction is dose-dependent: like with A2AR, at high calcium levels, NECAB2 dissociates from mGlu₅ (Canela et al., 2009). mGlu₅ promotes plasma membrane expression of NECAB2, whereas NECAB2 expressed by itself is more present in the cytoplasm (Canela et al., 2009).

A recent study found that NECAB2 highly colocalizes with G-protein coupled receptor 3 (GPR3, which has been linked to Alzheimer's disease) in the CA2 region of the hippocampus, but also in the thalamus, striatum and dorsal brainstem (Ikawa et al., 2020). Given that NECAB2 was shown to interact with A2AR, the authors speculate NECAB2 and GPR3's potential interaction could be anti-apoptotic and play a role in presynaptic functions (Ikawa et al., 2020). Indeed, the CA2 hippocampus region is more trauma-resistant than the CA1 and CA3 regions, likely due to its higher calcium buffering capability (Simons et al., 2009). Furthermore, in zebra fish, the Necab2

gene was identified as a direct p53 target (Mandriani et al., 2016); P53 is a tumor suppressor protein (Chen et al., 1990), encoded by the *tumor protein 53 (TP53)* gene which plays an important role in gene regulation in response to cellular stress, coordinating cellular processes such as apoptosis.

NECAB2 also plays a role in pain circuits: upon inflammation, NECAB2 KO in mice decreases brain-derived neurotrophic factor (BDNF) and proinflammatory cytokine expression and release and thus facilitates behavioral recovery, while genetic rescue of NECAB2 at the spinal level causes WT-like pain sensitivity (Zhang et al., 2018). Concurrently, Ma et al. (2021) found that NECAB2 interacts with transient receptor potential vanilloid 1 (TRPV1), a sensory ion channel, in chronic constriction injury rat microglia, and that this interaction induces neuropathic pain and inflammation.

2.1.4. NECAB2 structure

The human NECAB gene is localized on chromosome 16q23.3. NECAB2 consists of 389 amino acids (Bernier et al., 2001). In the open reading frame, there are two putative translation initiation codon frames that generate NECAB2 and NECAB2S, respectively. In comparison to NECAB2, NECAB2S lacks 37 amino acids at the N-terminus. Both forms are recognized by a polyclonal NECAB2 antibody, resulting in a 39 kDa and a 43 kDa band in Western blot (Canela et al., 2007). Both forms interact with A2AR (Canela et al., 2007). As previously mentioned, like all three NECAB proteins, NECAB2 contains an N-terminal domain with two EF-hands (Wu et al., 2007) that bind calcium, a highly conserved NHR domain with coiled-coil, and a C-terminal DUF167 or ABM domain. The function of the ABM domain in NECAB2 is still unknown. However, IsdG heme oxygenases containing ABM domains can be found in prokaryotes such as *S. aureus* and *Actinobacteria*; the IsdG family heme oxygenases degrade heme to free iron, staphylobilin, and formaldehyde, and many are expressed under low iron-conditions (Lojek et al., 2017, Lyles and Eichenbaum, 2018). 2Fe-2S cluster proteins play an important role in mitochondria (see chapter [2.7](#), [Figure 1](#)). It is yet unclear whether NECAB2 plays a role in these processes through its ABM domain.

2.2. The striatum

2.2.1. Anatomy of the striatum and connectivity

As reviewed in Bamford and Bamford (2019), the striatum plays an important role in motor and action planning, in decision-making, and in motivational and reward processes. A highly conserved brain region, it is part of the basal ganglia and owes its name to its striped appearance: the capsula interna's crus anterior (white matter) pulls through the nuclei (grey matter) composing the striatum: the caudate nucleus and putamen (Schünke, 2012). The striatum is involved in two main pathways: on one hand, the connection between striatum and subcortical structures such as the thalamus and amygdala leads to automatic and instinctive behavior; on the other hand, the connection between cortex and striatum allows higher-order, slower planned movements. The two pathways converge at the striatum, where they can compete with or complement each other (Bamford and Bamford, 2019).

The striatum is mainly composed of γ -aminobutyric acid (GABA)-ergic spiny projection neurons, also known as medium spiny neurons (MSNs) (Gerfen, 1992).

The dorsal striatum, which comprises the caudate nucleus and the putamen, is connected to the lateral globus pallidus via enkephalinergic MSNs that express enkephalin, D2 and A1 and A2A receptors; the substantia nigra pars compacta (SNc) and reticulata (SNr) and the medial globus pallidus are reached through dynorphinergic MSNs with dynorphin and substance P secretion and via D1 and A1 receptors. In the ventral striatum, which encompasses the nucleus accumbens and the olfactory tubercle, both dynorphinergic and enkephalinergic MSNs are present. Both types of MSNs project to the ventral pallidum, the medial globus pallidus, the substantia nigra (especially the SNc and the ventral tegmental area), the extended amygdala, the lateral hypothalamus and the pedunculo-pontine tegmental nucleus (Ferre et al., 2010).

2.2.2. The basal ganglia and the motor circuit

As reviewed by DeLong and Wichmann (2007), the cerebral cortex projects to the striatum and the subthalamic nucleus, whereas the globus pallidus pars interna (GPi) and SNr supply the basal ganglia's output to the thalamus and brainstem. There are two connections between the striatum and its output structures: a direct pathway and an indirect pathway that includes the globus pallidus pars externa (GPe) and the subthalamic nucleus (STN). The direct pathway is monosynaptic and inhibitory through GABA; by contrast, the indirect pathway is polysynaptic and excitatory. Both path-

ways receive cortical input. In addition, the striatal direct pathway receives input from the intralaminar nuclei of the thalamus. Thalamocortical projection neurons in the brainstem and the thalamus are tonically inhibited through the high discharge rates of GABAergic projections from the GPi and SNr neurons. The activation of striatal neurons involved in the direct pathway inhibits the GPi and SNr, whereas the activation of striatal neurons that partake in the indirect pathway has an excitatory effect on the GPi and SNr. Neurons from the SNc release dopamine in the striatum and thus regulate the balance between the direct and indirect pathway. Through D1 receptors, release of dopamine in the striatum increases activity in the direct pathway; through D2 receptors, activity along the indirect pathway decreases. This leads to a reduction in GPi and SNr activity, enabling the performance of intended movements. Contrarily, a decrease in striatal dopamine release leads to an increase in GPi and SNr activity, thus suppressing involuntary movements (DeLong and Wichmann, 2007).

2.2.3. Clinical significance

Because of its role in processes involving reward, cognition, reinforcement, motor function, stimulus-response learning and executive functions, striatal degeneration plays an important role in several diseases; most notably, Parkinson's disease (PD), which will be discussed in section 2.5.

2.2.3.1. Hyperkinetic disorders and neuropsychiatric diseases

Lesions in the basal ganglia are involved in several hyperkinetic movement disorders. Huntington's disease, for example, is characterized by cell loss and atrophy in the nucleus caudatus and putamen (Walker, 2007). The disease's typical symptoms include cognitive decline, psychiatric symptoms, and motor dysfunction - chorea, incoordination, and dystonia (Walker, 2007). Other hyperkinetic disorders such as dystonia, ballismus, and chorea all result from lesions in the motor circuit, too. Furthermore, motor circuit disturbances are involved in neuropsychiatric conditions such as obsessive-compulsive disorder and Tourette syndrome (DeLong and Wichmann, 2007).

Cortico-striatal circuits play a role in compulsive and impulsive behaviors as well, with the striatum promoting the behavioral patterns and the prefrontal components of the circuit inhibiting them. An imbalance between striatal and cortical activity might thus promote impulsive or compulsive behavior (Fineberg et al., 2010). The striatum is thus involved in the pathogenesis of autism spectrum disorder (in which both com-

pulsive and impulsive behaviors occur), addiction, trichotillomania, and pathological gambling (Fineberg et al., 2010, Brewer and Potenza, 2008).

Because of its high number of MSNs, the striatum is highly dependent on mitochondrial energy production. Mitochondrial quality control and mitochondrial maintenance are of vital importance for the striatum (Damiano et al., 2010).

2.3. Mitochondria

2.3.1. Structure and function of mitochondria

Mitochondria are traditionally viewed as the 'powerhouses' of the cell, have a double membrane, and only appear in eukaryotes (Siekevitz, 1957). According to the endosymbiosis theory, mitochondria derive from a bacterial endosymbiont that established itself in an eukaryotic cell (Gray et al., 1999). This is why they contain their own mitochondrial DNA, mtDNA (Schapira, 2006). A mitochondrion measures approximately 0.75 to 3 μm^2 (Wiemerslage and Lee, 2016). Structurally, the mitochondrion contains an outer mitochondrial membrane (OMM), an intermembrane space, an inner mitochondrial membrane (IMM) which is folded into cristae containing the electron transport chain and adenosine triphosphate (ATP) synthase that enable ATP (and thus, energy) production, and the matrix (Andersson et al., 2003, McBride et al., 2006). By providing ATP, mitochondria play an important role in regulating the cell cycle (Sweet and Singh, 1999).

Besides energy production, mitochondria are involved in several other metabolic processes: the urea cycle, biosynthesis of co-factors and amino acids, and the generation of iron sulphur (Fe-S) clusters which are needed in respiratory complexes in the mitochondria; furthermore, they play a role in calcium signaling and homeostasis and in the formation of reactive oxygen species (ROS) (Lill et al., 1999, Alberts et al., 2017).

Thanks to their fusion and fission processes, mitochondria form a constantly shape-shifting reticulum. Mitochondrial fusion is known to be mediated through three GTPases: Optic Atrophy1 protein (Opa1) in the intermembrane space (Song et al., 2009) and Mitofusin 1 (Mfn1) and Mitofusin 2 (Mfn2) in the OMM (Chen et al., 2003). A different GTPase, Dynamin-related protein 1 (DRP1), mediates mitochondrial fission (Smirnova et al., 2001). When there is an imbalance between fusion and fission

processes, the mitochondria either fragment or become excessively interconnected. Both scenarios result in insufficient mitochondrial distribution to the neuron's periphery, leading to neuronal dysfunction (reviewed in Chen and Chan, 2009, Mullin and Schapira, 2013).

2.3.2. Clinical relevance of mitochondrial impairment

Mitochondrial disruption has been linked to several conditions: neurons are especially dependent on mitochondrial energy production. Likewise, cardiac and skeletal muscle cells demand high energy levels and thus contain many mitochondria. This means that these three tissues are especially susceptible to mitochondrial dysfunction. For example, Leber hereditary optic neuropathy (LHON), Friedreich's ataxia, and amyotrophic lateral sclerosis (ALS) have all been linked to mitochondrial dysfunction (Schapira, 2006, King et al., 2014). In aging individuals and in PD, high levels of mtDNA deletions were found in dopaminergic neurons of the substantia nigra (Gegg et al., 2010). MFN2 mutations cause Charcot-Marie-Tooth type 2A (a peripheral neuropathy), while mutations in OPA1 are associated with autosomal dominant optic atrophy (Rouzier et al., 2012).

The central nervous system is responsible for about a fifth of the body's metabolic demand and the developing brain is particularly susceptible to mitochondrial dysfunction since it depends on aerobic energy. Furthermore, oxidative stress, immune defects, and calcium homeostasis disturbances are all mitochondrial-related disruptors of brain development. This is why mitochondrial disruption has been linked to autism spectrum disorder as well (Griffiths and Levy, 2017).

2.4. Autophagy

Autophagy enables the cell to recycle and rebuild faulty molecules and organelles (Alberts et al., 2017). It is especially important when the cell is under duress, such as starvation or oxidative stress (Alberts et al., 2017). More severe stress, on the other hand, directly leads to uncontrolled or controlled cell death (these processes are called necrosis and apoptosis, respectively) (Alberts et al., 2017). In mammals, three autophagic pathways exist that all converge on lysosomal degradation: macroautophagy, chaperone-mediated autophagy, and microautophagy. In addition, through endocytosis, the cell can internalize proteins/lipids from the plasma membrane and

extracellular material. Endocytosis, like autophagy, can also end in lysosomal degradation (Alberts et al., 2017). I shall focus on macroautophagy and mitophagy in particular, though other specific organelle recycling pathways, such as reticulophagy and aggrephagy (as reviewed in Evans and Holzbaur, 2020), have been described.

2.4.1. Macroautophagy

As reviewed in Navarro-Romero et al. (2020), macroautophagy is commonly referred to just as “autophagy”. It is vital in maintaining cellular homeostasis. Cargo that needs degradation is engulfed in autophagosomes (double membraned vesicles), which subsequently fuse with lysosomes, where the cargo is broken down through acidic hydrolases. Macroautophagy functions under baseline conditions, but it can also be induced through stress such as starvation (Lum et al., 2005) or stress hypoxia (Zhang et al., 2008). Nonspecific cytosolic content, as well as specific proteins and organelles, can be recycled in this manner (Navarro-Romero et al., 2020). In the following passage, I shall briefly present the specific organelle recycling pathway for mitochondria, a process called mitophagy.

2.4.1.1. Mitophagy

Oxidative stress in mitochondrial membranes or abnormal protein synthesis owing to faulty mtDNA cause protein misfolding and aggregation, leading to aqueous pores in the mitochondrial membrane, a process called Mitochondrial Permeability Transition (MPT), which then initiates specific mitochondrial autophagy, also known as mitophagy; ensuring mitochondrial quality control through mitophagy seems to delay the early phase of apoptosis (Mijaljica et al., 2007).

As presented by Twig et al. (2008), mitochondrial fusion triggers fission, which in turn is essential for autophagy. Most commonly, fusion is quickly followed by fission, which produces two daughter mitochondria. Sometimes, one of the daughter mitochondria is depolarized, the other hyperpolarized. The mitochondrion with reduced mitochondrial membrane potential ($\Delta\psi_m$) is less likely to re-fuse with the mitochondrial network and more likely targeted by autophagy. The hyperpolarized mitochondrion, on the other hand, is much more likely to fuse again post-fission. Twig et al. found that depolarization occurred well before autophagy events and that non-fusing and autophagocytosed mitochondria were characterized by reduced $\Delta\psi_m$, decreased OPA1 (a possible reason for their reduced fusion capability) and smaller size. These findings suggest that mitochondrial fusion and fission processes separate less active

mitochondrial units from the mitochondrial network, thereby eliminating dysfunctional units through autophagy (Twig et al., 2008). Upon inhibition of fission, mitochondria accumulate more oxidized protein, but not ROS, since mitochondrial respiratory function is impaired. This suggests that a decrease in fission events decreases mitochondrial turnover, corroborating the thesis that fission is required to ensure mitochondrial quality control (mtQC). Interestingly, inhibition of fission impedes mitochondrial, but not ER autophagy (Twig et al., 2008).

For neurons, which are terminally differentiated and which should survive as long as the organism they form part of, the ability to recycle organelles and proteins is of vital importance (Evans and Holzbaur, 2020). Hence, it is not surprising that a number of selective autophagic degradation processes, in addition to mitophagy, have been discovered and the number is continually growing (reviewed in Evans and Holzbaur, 2020). After receptor recruitment, an autophagosome is formed, which subsequently fuses with a lysosome for degradation of the organelle, organelle fragment or protein aggregate in question (Alberts et al., 2017).

2.4.2. Endocytosis

Through endocytosis, the cell can internalize extracellular material and proteins or lipids from the plasma membrane via so-called early endosomes (Alberts et al., 2017). The cargo is then either directed back to the plasma membrane or the early endosomes mature into late endosomes, which will then fuse to a lysosome for degradation (Alberts et al., 2017). The maturation is achieved through pH changes, changes in phosphatidylinositol lipids, and recruitment of Rab guanosine triphosphates (RAB GTPases). Endocytosis plays a significant role in neurotransmitter uptake and neuronal signaling and is hence particularly important in neurons (Navarro-Romero et al., 2020).

2.5. Parkinson's Disease

Parkinson's disease (PD) is caused by a loss of nigrostriatal dopaminergic neurons (Bernheimer et al., 1973), and is the second most common neurodegenerative disease. Bradykinesia, increased muscle tone, and tremor at rest make up the typical Parkinsonian triad (reviewed in DeLong and Wichmann, 2007, Mullin and Schapira, 2013). It is reported that patients will often experience a loss of olfaction (Hawkes et

al., 1997) and some patients also complain of autonomic dysfunction years before somato-motor dysfunctions appear (Meco et al., 1991). This is due to changes in catecholaminergic systems in the hypothalamus, locus coeruleus, dorsal vagal nuclei, the medulla, and sympathetic ganglia, all of whom are involved in vegetative control (Meco et al., 1991). Lewy bodies, typical markers of neuronal injury in PD, can be found in these structures (Lipkin, 1959, Den Hartog Jager and Bethlem, 1960). Idiopathic PD patients experience further nonmotor issues such as depression, anxiety, sleep disorders, and cognitive impairment (Ceballos-Baumann, 2018). These symptoms are thought to arise from dopamine deficiency in the nonmotor portions of the striatum combined with progressive pathologic changes in the brainstem, thalamus, and, later, the cerebral cortex (DeLong and Wichmann, 2007).

2.6. The PINK1/Parkin pathway

PTEN-induced kinase 1 (PINK1) and Parkin are proteins encoded by two genes linked to familial PD (Lucking et al., 2000, Valente et al., 2004). Parkin mutations, usually homozygous or compound heterozygous, are the most frequent cause of autosomal recessive early-onset PD (Lucking et al., 2000). PINK1 is a putative serine/threonine kinase; Parkin is an E3 ubiquitin ligase. PINK1 and Parkin are involved in mitophagy: after depolarization, PINK1 levels increase in the depolarized mitochondrion, which promotes Parkin's translocation into the mitochondria (it is normally a cytosolic protein) (Matsuda et al., 2010). When mitophagy is induced, several mitochondrial proteins are thus ubiquitinated in a PINK1-/Parkin-dependent manner, including MFN1 and MFN2 (Gegg et al., 2010). Hence, in a Parkin-dependent manner, Sequestosome 1 (p62/SQSTM1, an adaptor protein of selective autophagy) is recruited to poly-ubiquitinated mitochondrial clusters (Geisler et al., 2010). Parkin recruitment thus mediates the mitochondrion's fusion with the autophagosome, resulting in the elimination of damaged mitochondria (Narendra et al., 2008).

Silencing of PINK1 in dopaminergic SH-SY5Y cells leads to mitochondrial dysfunction - reflected in an increase in oxidative stress, a decrease in ATP synthesis and decreased mitophagy (Gegg et al., 2009). By contrast, a rescue through overexpression of Parkin (which is downstream of PINK1) restores ATP synthesis and mitophagy (Gegg et al., 2010). PINK1 seems to furthermore be involved in other autophagy processes by interacting with Beclin-1 (Michiorri et al., 2010), which is a pro-

autophagic protein (Liang et al., 1999). Interestingly, stable knockdown of PINK1 seems to activate autophagy/mitophagy processes (Gegg et al., 2010). Gegg et al. (2010) suggest that this is due to an activation of other compensatory pathways that promote mitophagy through Parkin recruitment. Furthermore, chronic PINK1 knock-down causes significant fragmentation of the mitochondrial network (Gegg et al., 2010). As previously mentioned, fission is an important cause of mitophagy.

In proliferating cells, the damaging effect of dysfunctional mitochondria can be diluted through cell division. By contrast, in neurons – which are post-mitotic – mitophagy plays a major role in the avoidance of oxidative stress and energy deficiency. If mitochondrial quality control is not performed correctly, a vicious circle ensues with mitochondria and other macromolecules causing more energy deficiency and oxidative stress (Gegg et al., 2010, Michiorri et al., 2010), resulting in diseases such as PD.

2.6.1. Alternative quality control pathways

The PINK1/Parkin pathway is the best-known pathway for mtQC. In recent years, however, more and more alternative mtQC pathways have been proposed and the clinical relevance of the “classical” PINK1/Parkin has been increasingly questioned. McWilliams et al. (2018) studied mitophagy in mice and found high levels of it in tyrosine hydroxylase (TH) positive nigral dopaminergic neurons, which correlated with the neurons’ high metabolic activity. In all examined cell populations, the researchers found no differences in basal mitophagy between PINK1 knockout (KO) and wildtype (WT) neurons. The same was true for microglial, neurovascular, and astrocytic basal mitophagy. In other tissues of high metabolic demand, such as the retina, the liver, the heart, and the exocrine pancreas, the researchers also did not find significant differences in PINK1 KO compared to WT. They concluded that PINK1 was not necessary to ensure mtQC in various (but not all) tissues with high energy demand. By contrast, in endocrine islet cells, mitophagy was upregulated in PINK1 KO. This was consistent with the fact that PINK1 deficiency was previously known to cause mitochondrial dysfunction and decrease metabolism in the endocrine pancreas. The authors concluded that different basal and stress-evoked mtQC pathways must exist and that the *in vivo* role of PINK1 remains unclear. They supported their thesis by arguing that if the PINK1/Parkin pathway were the only insurance for mtQC, PINK1/Parkin impairment would lead to a complete loss in mitophagy and thus result in much severer and earlier PD symptoms (McWilliams et al., 2018).

2.6.1.1. Parkin-independent pathways

In line with the group around McWilliams' findings, Koentjoro et al. described an unusual family with Parkin mutations in 2012: the patient had a compound heterozygous mutation and suffered from early onset PD (EOPD), while both parents only presented with unilateral upper limb rigidity (Koentjoro et al., 2012). The father had a single heterozygous Parkin mutation, whereas the mother had homozygous mutations but did not meet PD criteria (Koentjoro et al., 2012). The daughter – who had inherited her mother's mutant allele and her father's different mutation – displayed first EOPD symptoms at 18 years of age. A loss of functional Parkin and a lack of ubiquitination of Mfn2 were found in both the mother and the affected daughter (Koentjoro et al., 2012). The authors later identified Nip3-like protein X (Nix), a mitochondrial autophagy receptor located on the OMM, as the reason for the mother's asymptomaticity (Koentjoro et al., 2017). Nix was previously known to play a role in reticulocyte maturation in mammals (Schweers et al., 2007). In the mother, Nix was upregulated and mediated Parkin-independent mitophagy, ensuring largely normal mtQC – and thus, mitochondrial function (Koentjoro et al., 2017). The authors also found that they could significantly improve mitochondrial function in Parkin- or PINK1-mutated cells derived from other PD patients by inducing the Nix mtQC pathway, making Nix an interesting potential target in PD treatment (Koentjoro et al., 2017).

2.6.1.2. PINK1 can operate without Parkin

Lazarou et al. (2015) found that in the absence of Parkin, PINK1 recruited autophagy receptors like Nuclear domain 10 protein 52 (NDP52) and Optineurin (OPTN) to mitochondria, stimulating Parkin-independent mitophagy in HeLa cells. The authors propose that PINK1 recruits OPTN and NDP52 and induces mitophagy, while Parkin amplifies PINK1's signal by generating more ubiquitin chains on mitochondria which are then phosphorylated by PINK1 (Lazarou et al., 2015). This in turn causes autophagy receptors to recruit autophagy factors such as ULK1, DFCP1 and WIP11 (Lazarou et al., 2015). PINK1 was previously known to be upstream of Parkin. The authors showed that PINK1's kinase activity on its own can recruit the autophagy receptors and upstream autophagy machinery to mitochondria, inducing mitophagy without depending on Parkin (Lazarou et al., 2015).

2.6.1.3. Mitophagy depends on other organelles

As reviewed by Killackey et al. (2020), mitophagy is not an isolated event within the cell, but operates in tandem with and depends on other organelles. On the one hand,

the mitophagy pathways known to date converge, ending with the fusion with the lysosome, so lysosomal efficiency is vital to maintaining healthy mitochondria. On the other hand, the contact sites of ER and mitochondria form mitochondria-associated membranes (MAMs) (Vance, 1990), key for mitophagy (Hamasaki et al., 2013). The ER provides most of the lipids required for the autophagosome; furthermore, following stimulation of autophagy, PINK1-Beclin1 localizes to a subdomain of the ER (Gelmetti et al., 2017), the omegasome (Axe et al., 2008), and Double FYVE-containing protein 1 (DFCP1) translocates to MAMs (Axe et al., 2008). DFCP1 itself is an autophagy-related protein (ATG) and a marker of the omegasome (Axe et al., 2008). Close contact between mitochondria and the ER ensures efficient calcium transfer and balance between the two organelles and hence, efficient energy production and mitophagy initiation (MacVicar et al., 2015, Marchi et al., 2018). Lastly, ER and mitochondrial stress crosstalk has been proposed as a trigger for Parkin expression, activating the PINK1/Parkin “classical” mitophagy pathway (Itakura et al., 2012, Dupont et al., 2017, Killackey et al., 2020). Furthermore, through so-called mitochondrial-derived vesicles, oxidized or damaged proteins can be transported to peroxisomes or lysosomes without needing to degrade the entire mitochondrion (Hsu et al., 2018).

The Endosomal Sorting Complex Required for Transport (ESCRT) consists of four subcomplexes, ESCRT-0 through III. The ESCRT is involved in a multitude of cellular processes, including endosomal protein sorting, synthesis of multivesicular endosomes (MVEs), budding of viruses like HIV-1, cytokinetic abscission, plasma membrane repair, and neuron pruning, i.e., the elimination of synaptic connections without apoptosis (Campsteijn et al., 2016, Remec Pavlin and Hurley, 2020).

Hammerling et al. (2017) described a novel Parkin-mediated mitophagy pathway involving the ESCRT machinery. The authors demonstrated Parkin-mediated mitochondrial clearance in autophagy-deficient mouse embryonic fibroblasts (MEFs) from Atg5 and Atg7 KO mice. The clearance rate was similar in WT MEFs and both KO variants, while MEFs overexpressing control vector or non-functional Parkin were unable to clear mitochondria efficiently in response to exposure to the mitochondrial uncoupler Carbonyl cyanide-4-(trifluoromethoxy) phenylhydrazone (FCCP) (Hammerling et al., 2017). Mitochondrial stress, but not DNA damage, triggered the endosomal pathway. Mitochondria depolarized through either FCCP or valinomycin (which permeabilizes the mitochondrial membrane to K^+) were ubiquitinated through

Parkin. Subsequently, the mitochondria were sequestered in single-membrane Rab5-positive endosomes through the ESCRT machinery. The endosomes matured into Rab7-positive endosomes and then were degraded by lysosomes, thereby ensuring efficient mitochondrial clearance in both Atg5 KO and WT MEFs. Conversely, endosomal pathway inhibition led to increased cell death in both WT and KO MEFs (Hammerling et al., 2017).

Rab5-mediated mitophagy was Beclin-1-dependent, but did not require Ulk1/2 or Rab9 (Hammerling et al., 2017). Ulk1/2 and Rab9 play a role in an autophagy pathway discovered by Nishida et al. (2009). Not only did Hammerling et al. (2017) find colocalization between mitochondria and ESCRT proteins such as Hgs, Tsg1010, Snf8 and Chmp3; they also found that knockdown of either Hgs, Tsg1010, or Snf8 and treatment with FCCP resulted in lower mitochondrial clearance and increased cell death (Hammerling et al., 2017).

Hsu et al. (2018) described a different mechanism implying Rab5. When oxidative stress is induced (through laser, FCCP or H₂O₂), mitochondria undergo OMM permeabilization and change from their usual elongated tubular form to rounded and swollen. Rab5 requires a guanine nucleotide exchange factor (GEF) for activation. Upon release of cytochrome C, the Rab5 GEF ALS protein 2 (ALS2/Alsin) recruits Rabenosyn-5, which causes Rab5 to relocate from early endosomes to mitochondria. The authors showed that this mechanism was reversible, concluding that this was a way of protecting, rather than degrading, mitochondria, and hence promoting cell survival. The authors suggest that the Rab5 machinery is used to bring mitochondria close to the early endosomes (EE) to form membrane contact sites (MCS) between mitochondria and EE. The MCS enable the transfer of lipids and metabolites and the repair of the mitochondrial membrane (MM) through either the ESCRT or other endomembranes that fuse with the MM. Alsin had previously been linked to ALS: the authors propose that defects in Alsin decrease Rab5 recruitment to faulty mitochondria, increasing the effects of ROS and oxidative stress. In ALS patients, motor neurons thus accumulate more and more damaged mitochondria over time. Another link between Rab5 function and mtQC is suggested by a known PD mutation in Leucine-rich repeat serine/threonine-protein kinase (LRRK2) protein, since the mutation leads to hyperphosphorylation of Rab5 and other Rab GTPase substrates (Hsu et al., 2018).

Hammerling et al. (2017) found that in response to FCCP, the number of Rab5-positive endosomes briefly rose, while autophagosomes steadily, but slowly, increased. Since early endosomes are continuously synthesized, whereas autophagosomes are produced on demand, the authors propose that the endosomal pathway is a first response to mitochondrial damage. If and when the damage exceeds endosomal capacity, the autophagy pathway is activated. The authors also showed that upon Rab5 inhibition, autophagy activity increased, demonstrating once more that different, sometimes redundant, mtQC pathways exist and that, at least to some degree, they can compensate for each other. Some proteins, such as Beclin-1, Rab5, and Parkin, also play a role in multiple mtQC pathways and/or are involved in other organelle metabolism processes (Hammerling et al., 2017).

2.7. The CDGSH iron-sulfur domain-containing protein 1

Originally identified as a target of pioglitazone (Colca et al., 2004) – a type 2 diabetes mellitus drug – the CDGSH iron-sulfur domain-containing protein 1 (CISD1), also known as MitoNEET (mNT), is encoded by the *CISD1* gene and named thus because of its Asn-Glu-Glu-Thr (NEET) amino acid sequence (Wiley et al., 2007). mNT plays a role in apoptosis, autophagy, iron and ROS homeostasis in cells (Karmi et al., 2017). The protein is located at the OMM and contains a 2Fe-2S cluster and a CDGSH iron-sulphur domain (CISD) oriented towards the cytoplasm (Wiley et al., 2007). Two more proteins belong to the CISD family: nutrient-deprivation autophagy factor-1 (NAF-1, also known as ERIS, Miner1, CISD2 and Noxp70), and mNT-related 2 (Miner2), encoded by *CISD2* and *CISD3*, respectively (reviewed in Tamir et al., 2015). mNT and NAF-1 both present as homodimers (Paddock et al., 2007, Conlan et al., 2009). NAF-1 is located at MAMs and the ER (Wiley et al., 2013) and, like mNT, has been associated with diabetes, cancer, differentiation and aging processes, neurodegenerative diseases, and neuronal development (Amr et al., 2007, Chen et al., 2009, Darash-Yahana et al., 2016, Colca et al., 2004, Salem et al., 2012).

Interestingly, mNT mRNA was downregulated in tracheobronchial epithelial cells (CFDE) and bronchial epithelial cells (IB3-1) derived from cystic fibrosis (CF) patients (Taminelli et al., 2008). The reduced amount of mNT mRNA may account for the mitochondrial failure associated with CF (Taminelli et al., 2008). A mutation in *CISD2* leads to Wolfram Syndrome 2, a neurodegenerative disease, and overexpression of

NAF-1 in mice delayed aging, while KO led to early aging and symptoms similar to those seen in WFS2 patients (Wu et al., 2012). In breast cancer, mNT and NAF-1 supported cancer cells by enhancing cell proliferation and mitochondrial function, while knockdown of the proteins decreased tumor growth in mice (Sohn et al., 2013). These findings were corroborated by Bai et al. (2015)'s finding that MAD-28, a designed cluvenone (a tumor growth inhibitor) derivative, showed high selectivity toward epithelial cancer cells due to their high levels of NEET proteins. The authors proposed that MAD-28 binds near the NEET proteins' Fe-S clusters and destabilizes them.

In line with these findings, Karmi et al. (2017) postulated that mNT and NAF-1 play a role in cancer cells thanks to their labile 2Fe-2S clusters, which were shown by Sohn et al. (2013) to mitigate iron and ROS accumulation, through redox or cluster transfer reactions (Karmi et al., 2017). mNT is a known interaction partner of anamorsin (Lipper et al., 2015) and cytosolic aconitase (Ferecatu et al., 2014), which both play a role in iron-sulfur biogenesis and iron regulation (Kennedy et al., 1992, Banci et al., 2013); furthermore, mNT interacts with the redox regulator glutathione reductase (Landry et al., 2015) and with glutamate dehydrogenase 1 (Roberts et al., 2013), an insulin regulator (Sener and Malaisse, 1980). NAF-1 was found to interact with BCL-2 (Chang et al., 2010) and CAPN2 (Lu et al., 2014), both proteins implicated in apoptosis (Nakagawa and Yuan, 2000), and anamorsin (Lipper et al., 2015). Karmi et al. (2017) thus propose more of a metabolic/redox role for mNT and more of a regulatory role for NAF-1. By contrast, suppression of either protein resulted in similar effects as suppressing both (Sohn et al., 2013), so Karmi et al. (2017) argue they both act in the same cellular pathway in cancer cells and cannot compensate for each other's loss. Indeed, the authors found a high amount of overlap between transcripts altered in expression in mNT-KO and NAF-1-KO cancer cells (Karmi et al., 2017). While suppression of mNT and NAF-1 leads to iron and ROS accumulation and consequently autophagy and apoptosis, this effect could be suppressed by deferiprone, an iron chelator (Sohn et al., 2013). Concomitantly, overexpression of mNT or NAF-1 prevents oxidative stress (Yuan et al., 2016, Darash-Yahana et al., 2016); mNT also protects cancer cells from ferroptosis² by limiting mitochondrial iron uptake (Yuan et al., 2016), while NAF-1 protects them from apoptosis (Darash-Yahana et al., 2016).

² Ferroptosis is a non-apoptotic form of regulated cell death, which is iron-dependent and is characterized by increased lipid reactive oxygen species (Dixon et al., 2012).

Oxidized mNT was shown to donate its cluster to pre-reduced apo-NAF-1 (Karmi et al., 2017), similarly to how mNT or NAF-1 donate their cluster to anamorsin or ferredoxin (Zuris et al., 2011, Lipper et al., 2015). Karmi et al. (2017) hence propose a model (Figure 1) in which mNT accepts a 2Fe-2S cluster from a mitochondrial donor and transfers it to NAF-1. NAF-1 normally interacts with BCL-2 at the ER and this interaction is thought to be dependent on the presence of the cluster (Karmi et al., 2017); if NAF-1 is suppressed or does not accept the cluster, it cannot interact with BCL-2 and autophagy/apoptosis is initiated. Since mNT and NAF-1 were previously shown to be able to donate their clusters, the authors propose a “cluster transfer relay [...] from the mitochondria to the cytosol” (Karmi et al., 2017, p. 12) which the cell would use to monitor mitochondrial function, iron and ROS levels, and regulate cellular proliferation (probably through the MAPK and PI3K-Akt pathway) and/or apoptosis (via BCL-2) (Karmi et al., 2017).

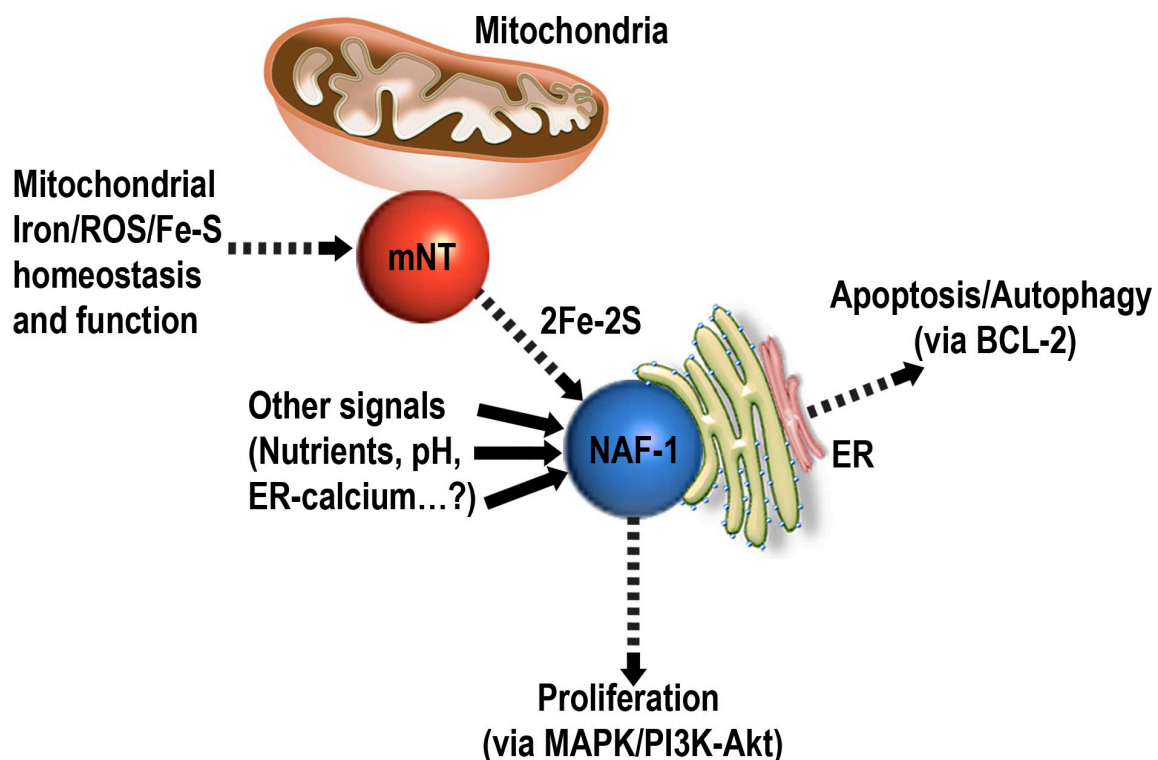


Figure 1: Model of mNT and NAF-1 interaction in cells, from (Karmi et al., 2017): mNT accepts 2Fe-2s clusters from the mitochondria and relays them to NAF-1, thus regulating apoptosis/ autophagy (when the cluster is not relayed, apoptosis/autophagy is activated via BCL-2) and proliferation (via the MAPK and PI3K pathways) by linking these processes to mitochondrial iron, ROS and Fe-S homeostasis.

Interestingly, Geldenhuys et al. (2017) showed an increase in ROS and superoxide levels in mitochondria in mNT KO mice. Striatal mNT KO mitochondria's ability to produce ATP was reduced to 50% and state III respiration was only 70% compared to WT mitochondria (Geldenhuys et al., 2017). Furthermore, the mNT KO striatum

showed iron accumulation – the probable cause for the aforementioned increase in ROS and superoxide – and a significant decrease in TH and dopamine levels (Geldenhuis et al., 2017). Concurrently, KO mice performed far worse on the rotarod and displayed a shortened stride length compared to their WT counterparts. These findings suggest mNT deletion induces many of the characteristics of early neurodegeneration in PD (Geldenhuis et al., 2017).

Mitochondrial dysfunction has long been proposed as the reason for damage caused by traumatic brain injury (TBI) (Singh et al., 2006). Traditionally, this was attributed to direct oxidative damage to mitochondrial enzymes (Singh et al., 2006). However, while studying traumatic brain injury, Yonutas et al. (2020) found that glutamate excitotoxicity following TBI leads to calcium overload in mitochondria, which decreases their respiration. The authors discovered that mNT is an important mediator of calcium-induced mitochondrial dysfunction (Yonutas et al., 2020). Pioglitazone, the T2DM drug that had previously been shown to interact with mNT (Colca et al., 2004), was able to reverse calcium-induced mitochondrial damage in mNT WT mice (Yonutas et al., 2020). In mNT KO, by contrast, pioglitazone had no neuroprotective effects (Yonutas et al., 2020). NL-1, a drug similar to pioglitazone with the same affinity for mNT but no peroxisome proliferator activated receptors (PPAR) binding region, resulted in significant neuroprotection in mice and rats after TBI, demonstrating that mNT's effect is reproducible across different species (Yonutas et al., 2020).

Lazarou et al. (2013) found that mNT is ubiquitinated by Parkin. Based on their studies of mNT in adipocytes and β -cells of the pancreas, Kusminski et al. (2016) found that mNT lowers $\Delta\psi_m$. This loss of $\Delta\psi_m$ in turn recruits the PINK1-Parkin machinery (see [2.7](#)) and induces mitophagy. Lastly, proteomics data from our group showed that mNT was upregulated in PINK1 KO human dopaminergic neurons (unpublished data). Taken together, these findings suggest mNT may play a role in mtQC. For this reason, mNT played a prominent role in my research.

3. Materials

3.1. Cell lines

3.1.1. HT22

HT22 is a mouse neuronal cell line subcloned from the HT4 mouse hippocampal cell line which was immortalized with a temperature-sensitive SV40 T-antigen (Morimoto and Koshland, 1990, Davis and Maher, 1994). HT22 cells provide a simple in vitro model for neuronal processes (Koszla et al., 2020). For experiments with empty vector and full length NECAB2 expressing cells, HT22 cells stably transfected with the plasmid pPB-CAG-BFP2-Relin and HT22 cells stably transfected with the plasmid pPB-CAG-HA-trunc.-Necab2-Ires-BFP2-Dest were used, respectively.

3.1.2. Primary striatal neurons

NECAB2^{+/-} (Necab2tm1a(KOMP)Wtsi) mice were provided by KOMP, UC Davis Mouse Biology Program. The mice have a C57BL/6NCrl background. Animals were exclusively handled by [REDACTED], PhD, my supervisor. Neurons were isolated from the striatum of mouse embryos at gestation age E16-18 and subsequently cultivated. Experiments were performed with homozygous wildtype (WT, NECAB2^{+/+}) and knockout (KO, NECAB2^{-/-}) mouse embryos.

3.1.3. Induced pluripotent stem cells (iPSCs)

Experiments with human iPSC-derived dopaminergic neurons were done in cooperation with the Hertie Institute for Clinical Brain Research in Tübingen under the leadership of [REDACTED], PhD. Briefly, induced pluripotent stem cells (isogenic control, K7.1) were generated from a healthy woman characterized by Reinhardt et al. (2013b). Through Transcription activator-like effector nucleases (TALEN) directed to Exon 1, a homozygous PINK1 deletion was induced. Two distinct clonal iPSC lines with no PINK1 transcripts up- or downstream of the gene edit, Δ8.9 (KO 1) and Δ40.7 (KO 2), were selected (Bus et al., 2020). For my experiments, [REDACTED] and [REDACTED] kindly provided human dopaminergic neurons derived from the Δ8.9 (KO 1), Δ40.7 (KO 2), and K7.1 (isogenic control) iPSC-derived lines.

3.2. Chemicals, buffers, markers

Table 1: Chemicals, buffers, markers

Material	Company name	Number
1M HCl Guanidin HCl 1 kg	Roth	0037.1
25 mM dNTPs	Fisher Scientific	R1121
Accumax	PAN Biotech	P10-21250
Acetic acid	Carl Roth	3738.4
Agarose	AppliChem	A8963
Agarose type II	Sigma-Aldrich	A9918
Antimycin A	Sigma-Aldrich	A8674-25MG
Ascorbic acid	Sigma-Aldrich	A92902
B-27 Serum-free Supplement	Life Technologies	17504-044
B27 supplement	Gibco	17504044
BDNF	Peprtech	450-02
Betain solution	Sigma-Aldrich	B0300-1VL
Carbonyl cyanide 3-chlorophenylhydrazone (CCCP)	Sigma-Aldrich	C2759-100MG
Carbonyl cyanide-4-(trifluoromethoxy) phenylhydrazone (FCCP)	Sigma-Aldrich	C2920-10MG
Chameleon Duo Pre-stained Protein Ladder	LI-COR	928-60000
CHIR99021	Axon Medchem	Axon 1386
Corning® Collagen I, Rat Tail, 100mg	Fisher Scientific	354236
Corning™ MITO+ Serum Extender	Corning	355006
DAPT	Sigma-Aldrich	D5942
dbcAMP	Applichem	A0455
DirectPCR Lysis Reagent (Mouse Tail) 100ml	Viagen Biotech	102-T
DMEM Hams F12	Biochrom	FG4815
DMEM with GlutaMax	Gibco	31966
DMSO 99,5%	Roth	A994.1
DNase	Zymo	E1009
Dulbecco's PBS 14190 (1x) w/o Ca, Mg (500 ml)	Gibco	14190-169
Fetal Bovine Serum	Thermo Scientific	1235-0273
FGF8	Peprtech	100-25
Fluorescence Mounting Medium	Agilent	S3023
gDNA Mini-Prep kit	Zymo Research	D3006
GDNF	Peprtech	450-10
Gene Ruler 50 bp Ladder	Thermo Fisher	SM0373
Glucose	Sigma Aldrich	158968
GlutaMAX	Thermo Scientific	35050061
GoTaq® G2 DNA Polymerase	Promega	M7845
HBSS -/-	Life Technologies	14170-138
Horse serum	Gibco	26050088
Matrigel	Corning	354277

MEM Medium	Life Technologies	31985-047
MG Midori Green Advance (1ml)	Biozym	617004
MG132	Merck/Millipore	474791-1MG
MitoTracker Red	ThermoFisher	M7512
N2 supplement	Gibco	17502048
Neurobasal medium	ThermoFisher	A2477501
Neurobasal® medium	Gibco	21103-049
Nuclease-Free Water (not DEPC-Treated)	Ambion	AM9937
PDL solution	Sigma-Aldrich	P7886-100MG
Penicillin/Streptomycin	Biochrom/Millipore	516106
Penicillin/Streptomycin (100 ml)	Sigma-Aldrich	P0781
PMA	Alexis	ALX-420-045-M005
Proteinase K (RNase free)	Peqlab	04-1075
Roti-Histofix 4 % (500 ml)	Roth	P087.4
Roti®-ImmunoBlock	Roth	T144.1
TGF-β3	Peptotech	100-36E
Thiazolyl Blue Tetrazolium Bromide, 98%	Sigma-Aldrich	M2128
Triton™ X-100 Surfact-Amps™ Detergent Solution	ThermoFisher	28314
Trypsin-EDTA	Sigma-Aldrich	SLBG2832
Trypsin/EDTA 0,05/0,02%	Sigma-Aldrich	T3924

3.3. PCR primers

Table 2: PCR primers

Name	Sequence
Primer 1 N2ttR	AAACAATAACCCTTCCCCTCCTGGG
Primer 2 - NeoF	GGGATCTCATGCTGGAGTTCTTCG
Primer 2 - Necab2F	GTGAGTTGCAGGACACAGAGAAACC

3.4. Plasmids

Table 3: Plasmids

Name	Reference/Supplier
EGFP-Rab5A S34N	Generated by Verena Bender
mKeima-PLVX-Puro	Generated by Verena Bender
pEGFP-C1-Parkin	Generated by Verena Bender

3.5. Antibodies

Table 4: Antibodies

Antibody name	Species	Company	Number	Concentration
Anti-NECAB2, IgG, polyclonal	rabbit	Sigma Aldrich	HPA013998	1:500
Rab5	mouse	Santa Cruz	sc-46692	1:200 - 1:10
CD63	mouse	Santa Cruz	sc-5275	1:250
COX IV	rabbit	Cell Signaling	4844	1:1000
Vinculin	mouse	Sigma Aldrich	V9131	1:1000
MRB251 (mNT)	mouse	Geneva Anti-body Facility	ABCD_RB251	1:10
CISD1 polyclonal anti-body	rabbit	Proteintech	16006-1-AP	1:1000- 1:25
TH-2 clone	mouse	Sigma-Aldrich	T1299	1:200
Anti-TOMM20	rabbit	Sigma-Aldrich	HPA011562	1:200
Goat anti-Mouse IgG (H+L) Secondary Anti-body, Alexa Fluor® 488 conjugate	mouse	ThermoFischer	A-11001	1:1000
Goat anti-Mouse IgG (H+L) Polyclonal Secondary Antibody, Alexa Fluor 568	mouse	ThermoFischer	A-11031	1:1000
Goat anti-Rabbit IgG (H+L) Secondary Anti-body, Alexa Fluor® 488 conjugate	rabbit	ThermoFischer	A-11008	1:1000
Goat anti-Rabbit IgG (H+L) Secondary Anti-body, Alexa Fluor® 568 conjugate	rabbit	ThermoFischer	A-11011	1:1000

3.6. Consumables

Table 5: Consumables

Consumables	Company
Cell scrapers	Greiner bio-one
CELLSTAR Tissue Culture Dish, 60 x 15 mm, Sterile, Vented, 600 Dishes	Greiner bio-one
centrifuge tubes, 15 ml	Corning
Certified 0,2ml 8 Twin Strip StarPCR Tubes	Starlab
Coverslips, Ø 10 and 12 mm	VWR International
Cryo tubes, 2 ml	Biochrom
Culture flasks, tissue culture treated	Greiner Bio-One
Falcon tubes, 50 ml; 15 ml	Sarstedt Biozym and Greiner bio-one
Luna™ cell counting chambers	Logos Biosystems
Microcentrifuge Tubes 0.5 ml; 1.5 ml; 2 ml	Sarstedt
Microscope slides	VWR International
Microseal® B PCR plate sealing film	Bio-Rad
Mini-PROTEAN® TGX™ Stain Free Precast Gels 4-15% and 4-20%	Bio-Rad
Multiplate™ 96-well PCR plate	Bio-Rad
Pipette 2,5;10;100;1000 µl	Eppendorf
Pipette tips	Starlab
Scalpels	Fine Science Tools
Serological pipettes, sterile 5;10;25 ml	Greiner Bio-One
Tissue plates 6 well; 12-well; 24-well; 96-well	Greiner Bio-One
Trans-Blot Turbo Midi, Mini PVDF, or Nitrocellulose Transfer Pack	Bio-Rad
TubeOne® Microcentrifuge Tubes, 1.5 ml	Starlab
µ-Slide 8-well glass bottom	ibidi

3.7. Devices

Table 6: Devices

Device	Company name
Accu-jet® pro	Brand
Centrifuge 5430	Eppendorf
CFX Connect™ Real-Time PCR Detection System	Biorad
CO2-Incubator MCO-20AIC	SANYO
Electrophoresis Power Supply	Peqlab
FlexStation 3 Multi-Mode Microplate Reader	Molecular Devices
Freezer, -80°C	Sanyo
Fresco 21 Centrifuge Heraeus	Thermo Scientific
Heratherm Incubator	Thermo Scientific
Ice machine	Ziegra
iBlot	Thermo Scientific
Luna Automated Cell Counter	Logos Biosystems
Magnet stirrer and heating plate MR Hei-Standard	Heidolph
Micro Scale CPA 10035	Sartorius
Microscope Motic AE20 Series	Motic
Micro-Star 17R	VWR
Milli-Q Plus-System	Millipore
Mini PROTEAN Tetra System	Bio-Rad
Mini-Sub® Cell GT Horizontal Electrophoresis System	Bio-Rad
MSC-Advantage Laminar Flow Hood	Thermo Scientific
Multifuge 3 L-R Centrifuge Heraeus	Thermo Scientific
Multifuge X1 Centrifuge Heraeus	Thermo Scientific
Multifuge X1R Centrifuge Heraeus	Thermo Scientific
Odyssey® Infrared Imaging System Sa	LI-COR Biosciences
Orbital Shaker	Heidolph
pH-Meter Education Line	Mettler Toledo
Pipettes	Eppendorf
PowerPac™ Basic Power Supply	Bio-Rad
Rocking Platform	VWR
Scale ALC-810.2	Acculab Sartorius Group
TCS SP5 confocal microscope	Leica Microsystems
Tecan Reader, Infinite M200 Pro	Tecan
TGradient Thermocycler	Biometra
Thermomixer F 1,5	Eppendorf
Trans-Blot Turbo Transfer System	Bio-Rad
Tube rotator	VWR
Vacunsafe Vacuum Pump	Integra Biosciences
Vortex-Genie 2	Scientific Industries
Water bath Aqualine AL 12	LAUDA
XCell SureLock™ Electrophoresis Cell	Novex® Life Technologies

3.8. Software

Table 7: Software

Software Name	Company
Adobe Illustrator CS6	Adobe
Adobe Photoshop CS6	Adobe
GraphPad Prism 8	GraphPad Software
Image J (Fiji)	Wayne Rasband, NIH
Image Studio Lite	LI-COR Biosciences
Imaris	Bitplane
Inkscape	Inkscape
Leica Application Suite Advanced Fluorescence	Leica Microsystems
Microsoft Excel	Microsoft Corporation
Microsoft PowerPoint	Microsoft Corporation
Microsoft Word	Microsoft Corporation

4. Methods

4.1. Cell culture – neuronal striatal primary cultures

All steps involving the handling of animals were exclusively performed by [REDACTED], PhD, my supervisor. E16-18 mouse embryos from two heterozygous (NECAB2^{+/-}) parents were used in order to compare paired WT and KO neuronal populations. First, the mother was sacrificed by cervical dislocation by Dr. Dey. After disinfection of the mother's abdomen, the embryos were removed and placed on a petri dish with HBSS ^{-/-}. The head of each embryo was removed, the skull cut open and the brain removed and placed into HBSS ^{-/-}. Under a Leica 56D binocular microscope, the striatum was retrieved and put in an epi with HBSS ^{-/-} on ice. The instruments were sterilized between each embryonic dissection to avoid contamination. After all embryos had been dissected, the supernatant was removed with filter tips and the samples were washed with 5 ml HBSS ^{-/-} carefully, gently shaking. The medium was then removed and another 5 ml HBSS ^{-/-}, 120 µl trypsin and 10 µl DNase were added with filter tips, then everything was incubated for 12-14 minutes at 37°C. The supernatant was then removed and 3 ml of plating medium were added. The medium and cells were re-suspended carefully about 50 times in order to disconnect the tissue. After 5 minutes' rest, the supernatant cell concentration was measured using a cell counter. Cells were then seeded onto coverslips³: 450,000 cells with 2 ml of plating medium per well in 6-well plates, or 300,000 cells with 1 ml of plating medium per well in 12-well plates. After 3-4 hours, the plating medium was removed, the wells were washed with PBS to remove dead cells, and cultivation medium was added to the plates. Every 3-4 days, the cultivation medium was replaced.

Table 8: Plating and cultivation medium

Plating medium, filtered sterilely		Cultivation medium, filtered sterilely	
Reagent	Dose	Reagent	Dose
20% Glucose	3 ml	B27	1 ml
10% Horse serum	10 ml	L-glutamine	125 µl
P/S	1 ml	P/S	0,5 ml
MEM Medium	86 ml	Neurobasal medium	48.375 ml

³The coverslips had previously been sterilized with 1M HCl, coated with PLL, rinsed thrice with sterile MilliQ water, then twice with 70% ethanol and once in 100% ethanol, then placed into 6-well or 12-well plates and airdried in a sterile vertical laminar flow hood.

4.2. Cell culture – HT22

4.2.1. Defrosting HT22

Cryotubes containing frozen HT22 were first removed from the N₂ tank and placed in a freezer at -80°C. Subsequently, they were moved to a -20°C freezer while DMEM was warmed up in a hot water bath. Plates were then labelled and 20 ml DMEM added. The cryotubes were then heated in the water bath and gently rocked until the clump of cells came loose. The cells were then slid into the labelled plates and placed in the incubator.

4.2.2. Splitting HT22

HT22 cells were split 1:10 twice a week, typically on Mondays and Thursdays. To split the cells, the medium was removed from each plate. Between plates, the pipette tip was changed to avoid contamination. The plates were washed with 6 ml PBS, which was subsequently removed. 1 ml trypsin was added; in the meantime, new plates were labeled and 9 ml medium were added to each plate. Cells were dislodged from the plate with the trypsin, then 9 ml of fresh medium were added and resuspended several times to achieve a uniform 10 ml cell suspension. 1 ml of the cell suspension was then added to the new plate with 9 ml fresh medium and the rest of the suspension discarded.

4.2.3. Transfection of HT22 cells

On day one, cells were split from the stock plates into either 8-well ibidi slides or 6-well plates at a concentration of 40'000 cells/well for the ibidi slides or approximately 200'000 cells/well for the 6-well plates. On day 2, transfection was performed. A plasmid concentration of 1 µg/µl was used for all experiments. For 6-well plates, 100 µl Optimem medium and 1,5 µg plasmid per well were added to an eppi, briefly vortexed and shaken. 4,8 µl Attractene per well were added to the eppis. For 8-well ibidi slides, the same procedure was followed, but with 0,4 µg plasmid, 1,5 µl Attractene and 40 µl Optimem. The eppis were briefly vortexed and the transfection solution was left to incubate at RT for 15 minutes. In the meantime, cells were taken out of the incubator and their medium was changed. After 15 minutes the transfection solution was added to each well, the plates shaken 5 times front to back and 5 times left to right, and the cells were put back into the incubator. On day 4, the cells from 6-well plates were collected for Western blotting (see [4.5.1](#), [4.5.2](#), [4.5.3](#)), whereas cells from the 8-well ibidi slides were imaged using an SP5 microscope.

4.3. Cell culture – iPSCs

This protocol is based on Reinhardt et al. (2013a)'s method for derivation and expansion of human neural progenitors using small molecules. [REDACTED] from the Hertie Institute for Clinical Brain Research in Tübingen kindly prepared human iPSC-derived dopaminergic neurons for me according to this protocol. On day 1, embryoid bodies (EBs) were prepared by scraping colonies from iPSC culture and putting them in day 1-3 medium. On day 4, the medium was changed and NPC growth medium added. On day 7, the EBs were plated in a Matrigel-coated plate. Prior to each splitting step, APOI was always added to the medium in question. On day 9, the EBs were split with accutase and plated in a new Matrigel-coated plate with NPC growth medium and APOI 1:1000. After reaching enough confluency, the EBs were split again with accutase. The previous passages were frozen. The NPC growth medium was changed every second day and the neuronal progenitor cells (NPCs) split 1:10 once a week. Typically, after 5-6 passages, the NPCs' differentiation into neurons could be started. For this, NPCs were split 1:10 and plated on a Matrigel-coated plate. At 80% confluency, the medium was replaced with differentiation medium for differentiation for 7 days. After 4-5 days in differentiation medium, depending on cell confluency, cells were split with accumax 1:2 or 1:3 and plated in a Matrigel-coated plate. On day 8, the medium was replaced with maturation medium + APOI 1:1000. The medium was changed every second day. Neurons were kept in maturation medium for 2 weeks before experiments. 21 days after first adding differentiation medium, neurons were generally ready for experiments.

Table 9: Differentiation media for iPSCs

50:50 medium	NPC growth medium	Differentiation medium	Maturation medium
250 ml DMEM/Ham's F12	50:50 medium	50:50 medium	50:50 medium
250 ml neurobasal medium	200 µM ascorbic acid	20 ng/ml BDNF	10 ng/ml BDNF
5 ml Penicillin/streptomycin	3 µM CHIR	10 ng/ml FGF8	10 ng/ml GDNF
5 ml L-Glutamine	0.5 µM PMA	1 µM PMA	1 ng/ml TGF-β3
5 ml B27 supplement		200 µM ascorbic acid	200 µM ascorbic acid
2.5 ml N2 supplement			500 µM dbcAMP
			10 µM DAPT

4.4. Molecular biology

4.4.1. Genotyping

Overnight PCR

A mastermix of 200 μ l direct lysis reagent and 3 μ l Proteinase K was prepared and added to each sample. The samples were then put in the water bath overnight at 55°C. The following morning, the water bath temperature was raised to 85°C for an hour in order to deactivate the Proteinase K. For NECAB2 polymerase chain reactions (PCRs), two mastermixes were prepared, a KO and a WT one, consisting of 7.05 μ l sterile nuclease-free water, 6.5 μ l Betain, 5 μ l GoTaq® G2 DNA Polymerase, 2 μ l 2.5mM dNTPs, 0.325 μ l DMSO and 1 μ l of Primer 1 and 1 μ l of Primer 2 for each sample. Primer 1 was N2ttR in both cases; for the KO mastermix, NeoF was used as primer 2, while for the WT mastermix, Necab2F was used as primer 2. 300 μ l sterile water were added to each lysed sample and each sample was then pipetted into two PCR tubes. The KO mastermix was added to one of the PCR tubes of each sample, the WT mastermix to the other PCR tubes. In addition, two negative controls with sterile water and just the mastermix were pipetted. While the PCR ran, a 1.5% agarose gel, usually 4.5 g agarose basic with 300 ml 1X Tris-acetate-EDTA (TAE buffer: 40 mM Tris, 20 mM acetic acid and 1 mM ethylenediaminetetraacetic acid (EDTA), pH 8) and 7.5 μ l Midori Green with 40 wells was prepared. After the PCR was completed, agarose gel electrophoresis was performed in a horizontal running chamber filled with 1x TAE buffer. A Gene Ruler 50 bp Ladder was pipetted into the first well, followed by the samples with the KO and WT mastermixes. The gel was run for half an hour at 120 V and then detected.

Fast genotyping

When my supervisor and I needed to determine the embryos' genotype while harvesting the neurons, we did a fast genotyping, for which the quick gDNA Mini-Prep kit from Zymo Research was used. For this, each of the embryos' tails was put in a tube. Subsequently, 200 μ l Genomic Lysis Buffer were added to each tube and the tails mashed with pestles, then the samples were vortexed for 4 seconds and left at room temperature for 5-10 minutes. The mixture was then transferred to a ZymoSpin column in a collection tube and centrifuged for 1 minute at 16,000xg. The collection tube and flowthrough were discarded and the column was transferred to a new collection tube. 200 μ l DNA Pre-Wash Buffer were added to the column and the samples were centrifuged for 1 minute at 16,000xg. 500 μ l gDNA Wash Buffer were then added to

each column and the samples were centrifuged for 1 minute at 16,000xg. The spin column was then transferred to a clean microcentrifuge tube and 50 μ l sterile water were added; everything was incubated for 2-5 minutes and then centrifuged for 30 seconds at 16,000xg. Then, the same procedure as with a normal genotyping (see above) was followed.

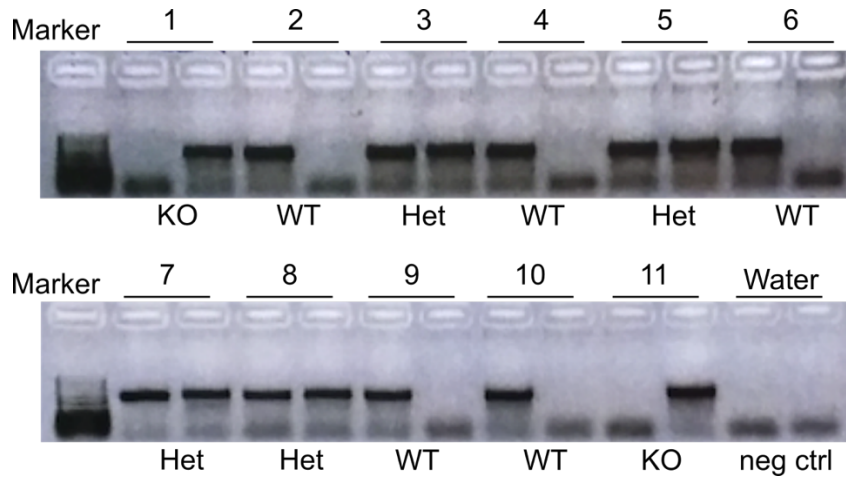


Figure 2: Example of genotyping PCR.

Each number represents an animal from which a tail was collected and genotyped. KO: NECAB2 knockout animal. WT: NECAB2 wildtype animal. Het: heterozygous, i.e., NECAB2^{+/-} animal. Water was used as negative control.

4.5. Protein biochemistry

4.5.1. Protein isolation from cells

First, the medium was removed from the plates. Then, the plates were carefully washed with PBS. 350 µl radioimmunoprecipitation assay buffer (RIPA buffer), supplemented with protease inhibitors and phosphatase inhibitors, was added to the plates to lyse the cells and cells were removed from the wells with a cell scraper. The cells were then transferred to eppis on ice. The eppis were vortexed and left on ice for 30 minutes. After that, the eppis were centrifuged at 21,000xg for 30 min at 4°C. The supernatant was either directly processed or frozen for later use. The pellet was discarded.

4.5.2. BCA protein assay

To determine the protein concentration of samples, a bicinchoninic acid (BCA) protein assay was performed using Interchim's BC Assay Protein Quantification Kit according to manufacturers' instructions. If the lysates had been frozen, they were thawed on ice prior to the BCA.

Cell lysates were diluted with sterile MilliQ in eppis at a 1:10 and a 1:25 concentration. 15 µl of each sample were pipetted in technical triplicates: a bovine serum albumin (BSA) standard series with known concentrations (0, 6.25, 12.5, 25, 50, 100 and 200 µg/ml) in ascending concentration order and the testing samples. 200 µl reagent A and 1:50 reagent B were added to every well and the plate was incubated for 30 min at 37°C. Cu^{2+} ions in the BCA solution are reduced to Cu^+ ions by the protein in the samples. Cu^+ and BCA form purple-blueish complexes which can be detected photometrically (Smith et al., 1985) at a wavelength (λ) of 562 nm in an Infinite M200 PRO microplate reader (Tecan). Protein concentrations were then calculated with Microsoft Excel.

4.5.3. SDS-PAGE

Sodium Dodecyl Sulfate Polyacrylamide Gel Electrophoresis (SDS-PAGE) enables the separation of proteins by size, independently of their charge. Western blot samples were prepared according to the concentrations of lysate previously determined with the BCA assay and the needed amounts of protein buffer and water calculated with Microsoft Excel. Samples were heated at 95°C for 5-10 minutes and pipetted onto 4-15 % Mini PROTEAN Membrane Stain Free precast gels in a Mini PROTEAN

Tetra System chamber. Gels were run at 300 V for approximately 15 minutes with a Chameleon Duo Pre-stained Protein Ladder. Gels were then transblotted onto nitrocellulose membranes with a Trans-Blot Turbo Transfer System. The blots were blocked in a 3,5% milk solution with either TBST or PBST for one hour and then incubated with primary antibody overnight. The next morning, they were washed thrice with TBST/PBST and then incubated with secondary antibody for 1 hour in the dark. Then they were washed thrice and stored in either TBS or PBS and detected in an Odyssey® Infrared Imaging System.

Table 10: Protein buffer composition

Protein buffer
5 ml Glycerol
2.5 ml 1M Tris pH 6.8
1 g SDS
0.77g Dithiothreitol (reduces inter- and intramolecular disulfide bonds)
2.5 ml MilliQ
20 mg Thiazolyl Blue Tetrazolium Bromide, 98%

Western blots at the Hertie Institute for Clinical Brain Research in Tübingen were made as described in the preceding paragraph, with the exception that rather than using precast gels, I prepared my own gels there. First, the running gel was prepared by mixing all ingredients (Table 11) except APS and TEMED, which were subsequently added. The running gel was pipetted into the cast and after hardening the stacking gel was prepared and added to the cast in a similar fashion.

Table 11: Running and stacking gel composition

Running gel	Stacking gel
Acrylamide	Acrylamide
1.5 M Tris	0.5 M Tris
10% SDS	10% SDS
10% APS	10% APS
TEMED	TEMED
MilliQ	MilliQ

4.5.4. CCCP treatment

Three different iPSC-derived human dopaminergic neuronal cell lines were used: two PINK1 KOs, $\Delta 8.9$ (KO 1) and $\Delta 40.7$ (KO 2), and their isogenic control, K7.1. All three were treated with 10 μM of the mitochondrial uncoupler Carbonyl cyanide 3-chlorophenylhydrazone (CCCP). A test series of 0hrs, 2hrs, 6hrs, 6hrs plus 10 μM MG132, and 24hrs 10 μM CCCP treatment was performed with two wells per condition and treatment time excepting 0hrs: here, sample from 4 wells for each condition was collected. After completion of the CCCP treatment, the medium was removed, then the plates were carefully washed with PBS once. Afterwards, RIPA buffer was added. The next steps were performed on ice. The samples were scraped down and put into eppis. They were then homogenized by needling: ten times through a 20G needle, then every sample was supersonized 5x twice and then passed them 10 times through a 29G needle. The samples were then left on ice for 20 min and centrifuged at 14,000xg for 10 min at 4°C. The supernatant was subsequently collected and either directly used as described in [4.5.2](#) and [4.5.3](#) or frozen for later use.

4.6. Immunocytochemistry

4.6.1. Murine primary striatal neurons

If MitoTracker Red was used in the staining, live neurons were incubated with pre-warmed serum-free medium (neurobasal medium, NBM) with MitoTracker Red 1:5000. After incubating for 15 minutes, the NBM with MitoTracker was removed and replaced with prewarmed NBM. If MitoTracker was used, the plates were from here on covered in aluminum foil. After the optional MitoTracker staining and before incubation with antibodies to stain them, cells were fixed with histofix 4% by removal and replacement of the medium with 500 μ l histofix per well for 24-well plates or 1 ml histofix per well for 6-well plates. The cells were incubated at room temperature on a shaker for 15-20 minutes, then the histofix was removed and the coverslips washed with 1-2ml PBS thrice in five-minute intervals. The coverslips were then either directly used for immunocytochemistry (ICC) or stored at 4°C for up to 4 weeks.

For ICC, first the neurons were permeabilized with 500 μ l (24-well plate) or 1ml (6-well plate) 0.25% TritonX100 in PBS for 10 minutes at room temperature on the shaker, then washed 3 times with 1-2 ml PBS in five-minute intervals. Then the neurons were blocked with RotiBlock 1x for at least 30 minutes. Meanwhile, primary antibodies were diluted in different concentrations (see [Table 4](#)) in RotiBlock with 0.1 % TritonX100. For small coverslips in 24 well-plates, 250 μ l of primary antibody solutions were prepared and pipetted into the well after removal of the RotiBlock with 0.1% TritonX100. Alternatively for 10mm coverslips and always for 12mm coverslips, 20-30 μ l (10 mm coverslips) or 200-300 μ l (12 mm coverslips) of primary antibody solution were prepared and pipetted onto a glass plate covered in parafilm in a wet incubation chamber. Then, the coverslips were carefully retrieved from the well-plates and placed on the antibody solution drop with the neurons facing the antibody. Coverslips were incubated at 4°C overnight in the dark. The following day, the primary antibody was recovered from the 24 well plates or the coverslips were retrieved from the incubation chamber and placed back into well plates. The coverslips were washed with PBS at 5-minute intervals thrice. In the meantime, the secondary antibody was prepared in RotiBlock with 0.1% Triton. AlexaFluor antibodies in 488 (green), 568 (red) and far red (647) raised in goat were used at a concentration of 1:1000; the coverslips were incubated the same way as described for the primary antibody for an hour in the dark (covered in aluminum foil from this point onwards if they had not already been due to MitoTracker staining) at 4°C. Then, the neurons

were incubated for 5 min with 250-500 μ l DAPI per well for 24-well plates or 1 ml DAPI per well for 6-well plates to achieve nuclear staining, after which the coverslips were washed thrice with PBS at five-minute intervals. Coverslips were mounted on specimen slides with 6-7 μ l DAKO mounting medium for 10mm or 15 μ l for 12 mm coverslips. The specimen slides were left to dry overnight in a folder and 4°C and were stored under the same conditions and/or imaged using a SP5 confocal microscope.

4.6.2. Human iPSC-derived dopaminergic neurons

After washing coverslips with PBS to remove as much medium as possible, human iPSC-derived dopaminergic neurons were fixated with 4% paraformaldehyde (PFA, 250 μ l per well) for 20 minutes at RT. The plates were then washed twice with PBS with 0.01% Triton. If the staining was completed the following day, coverslips were washed and stored in pure PBS. Blocking was performed with 10% Normal Goat Serum (NGS) in PBS+0.01% Triton for 60 min at RT (150 μ l/well), then the first antibody was diluted in 5% NGS in PBS+0.01% Triton. Coverslips were placed on a glass plate covered in parafilm with drops of 30 μ l antibody solution and either incubated overnight at 4°C or 1-2hrs at 37°C. The coverslips were then washed with PBS+0.01% Triton thrice. The secondary antibody was diluted in 10% NGS in PBS+0.01% Triton and incubated 1 hour at RT (30 μ l per well) in the dark. Then, coverslips were washed once more with PBS+0.01% Triton. Afterwards, a DAPI solution (1: 50,000 in PBS) was applied for 5 min (150 μ l/well) for nuclear staining. The coverslips were then washed twice with PBS+0.01% Triton, then once with MilliQ and then mounted on specimen slides with DAKO.

4.7. Image analysis

4.7.1. Imaris analysis of z-stacks

Original .lif files were imported into the Imaris analysis software by Bitplane. Under the coloc menu, the two channels of interest (green and magenta; the third channel, blue, only displayed nuclear staining and was not of interest for the analysis) were selected. Under threshold options, the “Polygon” option was pressed and the appropriate threshold manually selected, after which the “build coloc channel” command was hit. Next, a background subtraction of 1 μm and a smoothing through Gaussian filter of 0.1 μm was applied. Then, a surface encompassing the neuron was manually drawn; two masks, one for the green and one for the colocalization channel, were built. Now, within the masked channels, spots could be counted automatically by the program. Data was then copied into GraphPad Prism for statistical analysis (see [4.8](#)).

4.7.2. ImageJ Deconvolution and Pearson’s Coefficient

Before analyzing images with the JACoP plugin in Image J (Fiji), image quality was improved by deconvolution through Fiji’s Iterative Deconvolve 3D plugin. Briefly, original .lif files were opened in ImageJ and each image was split into its three channels (blue, green, magenta). When analyzing z-stacks, each channel was collapsed into a single image through the Z Project tool (MAX intensity). Then, the Iterative Deconvolve 3D plugin was launched and each channel deconvolved 10x. Files were saved as 8-bit Tiffs. Next, colocalization was studied by calculating the Pearson’s Coefficient with Fiji’s Just Another Colocalization plugin (JACoP). Data was then copied into GraphPad Prism for statistical analysis (see [4.8](#)).

4.8. Statistical analysis

Statistical analysis was performed with GraphPad Prism 8 (GraphPad). Outliers were removed with the ROUT method. The Shapiro-Wilk test was used to determine data’s normal distribution. Normally distributed data was analyzed with one-way ANOVA followed by Tukey’s multiple comparisons test. Not normally distributed data was analyzed with the Mann-Whitney test. P-values <0.05 were considered significant. Data are displayed as Tukey’s box and whiskers plot.

5. Results

5.1. NECAB2 is present at mitochondria and potentially at endosomes

To verify NECAB2's localization in cells, I performed immunocytochemistry (ICC) in murine primary striatal cultures from NECAB2 wildtype (WT) and knockout (KO) mice, investigating colocalization between NECAB2 and mitochondria ([Figure 3](#)). Mitochondria were stained with MitoRed (mtRed) before neuronal fixation. Striatal neurons from NECAB2 KO mice did not display any immunoreactivity to the NECAB2 antibody ([Figure 3A](#)). As delineated in chapter [6](#), the Pearson's coefficient is not an ideal colocalization tool, and due to inexperience initial microscopical images taken

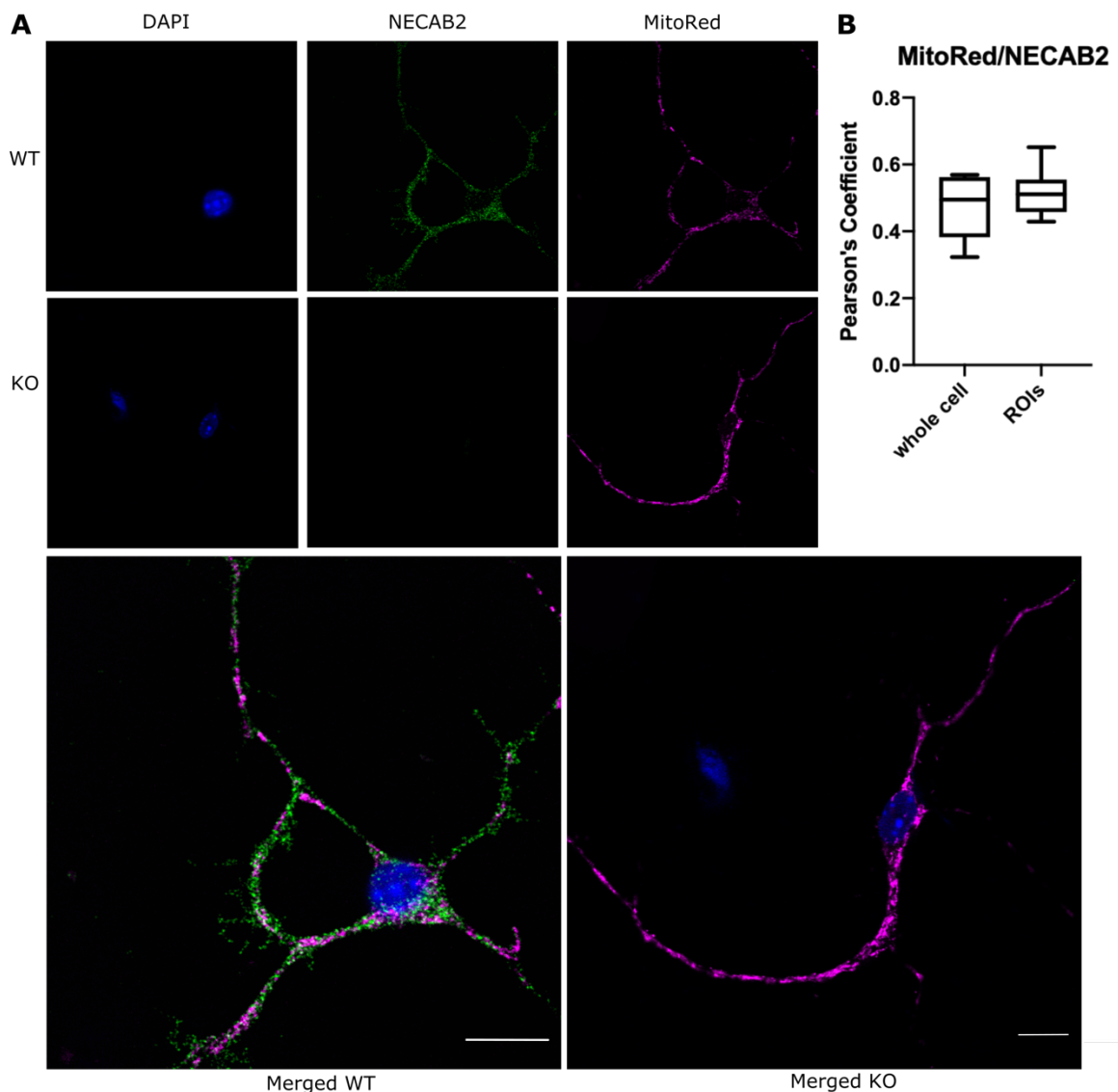


Figure 3: MitoRed and NECAB2 may colocalize in WT in striatal neurons.

A) NECAB2 (N2) and MitoRed, a mitochondrial dye, may colocalize in mouse WT primary striatal neurons. Note that NECAB2 KO cells show no NECAB2 reactivity. MitoRed 1:5000, Necab2/rb 1:500. Scale bars: 10 μ m.

B) Pearson's coefficient for colocalization between N2 and MitoRed in WT whole cell and ROIs. Images were deconvolved 10x using the Iterative Deconvolve Plugin in ImageJ and colocalization studies were performed using the JACoP plugin in ImageJ. Data are presented as Tukey plots.

by me were suboptimal. Hence, with a PC of about 0,55, [Figure 3B](#) shows mitochondria and NECAB2 may colocalize in WT striatal murine neurons.

However, through Western blot, I was able to confirm NECAB2's presence at crude mitochondria and membrane-associated mitochondria (MAMs) in the brain of N2 WT mice ([Figure 4](#)).

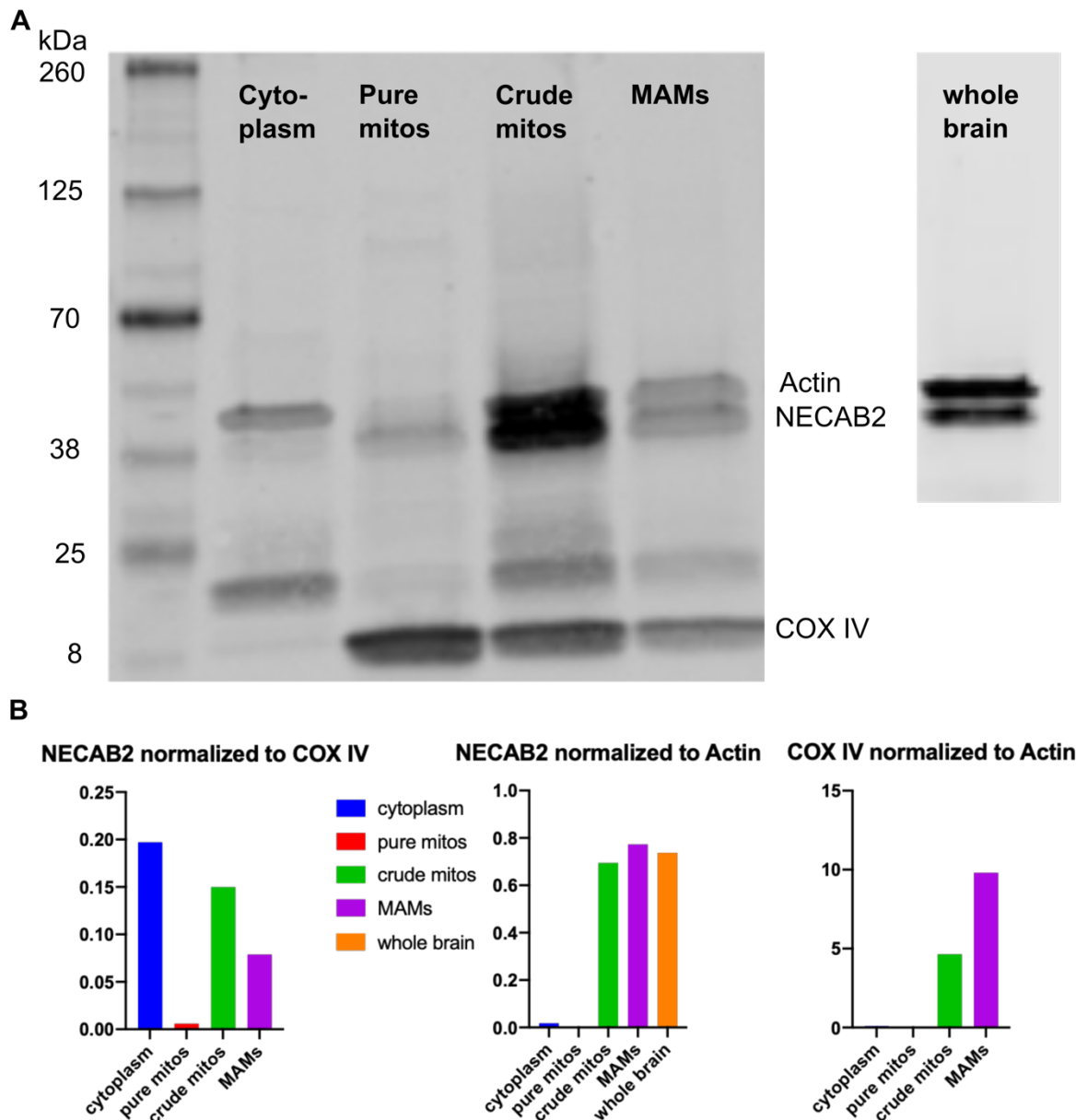


Figure 4: NECAB2 is predominantly present at crude mitochondria in WT mouse brain.

A) Western blot demonstrating NECAB2 is present in brain tissue (right) and particularly at crude mitochondria and membrane-associated mitochondria (MAMs). **B)** When normalizing to COX IV, a mitochondrial marker, N2 is especially present in MAMs and crude mitochondria; when normalizing to Actin, N2 again is present especially in MAMs, crude mitochondria, and the whole brain. Since the cytoplasm does not contain much COX IV (far right), the ratio of N2/COX IV (left, blue bar) is high in the cytoplasm.

I next wanted to find out whether NECAB2 is also present at endosomes. Therefore, I performed ICC in murine primary striatal cultures from N2 WT mice with antibodies against two distinct endosomal markers, CD63 (Figure 5A) and Rab5 (Figure 5B), and NECAB2, to study colocalization between endosomes and NECAB2.

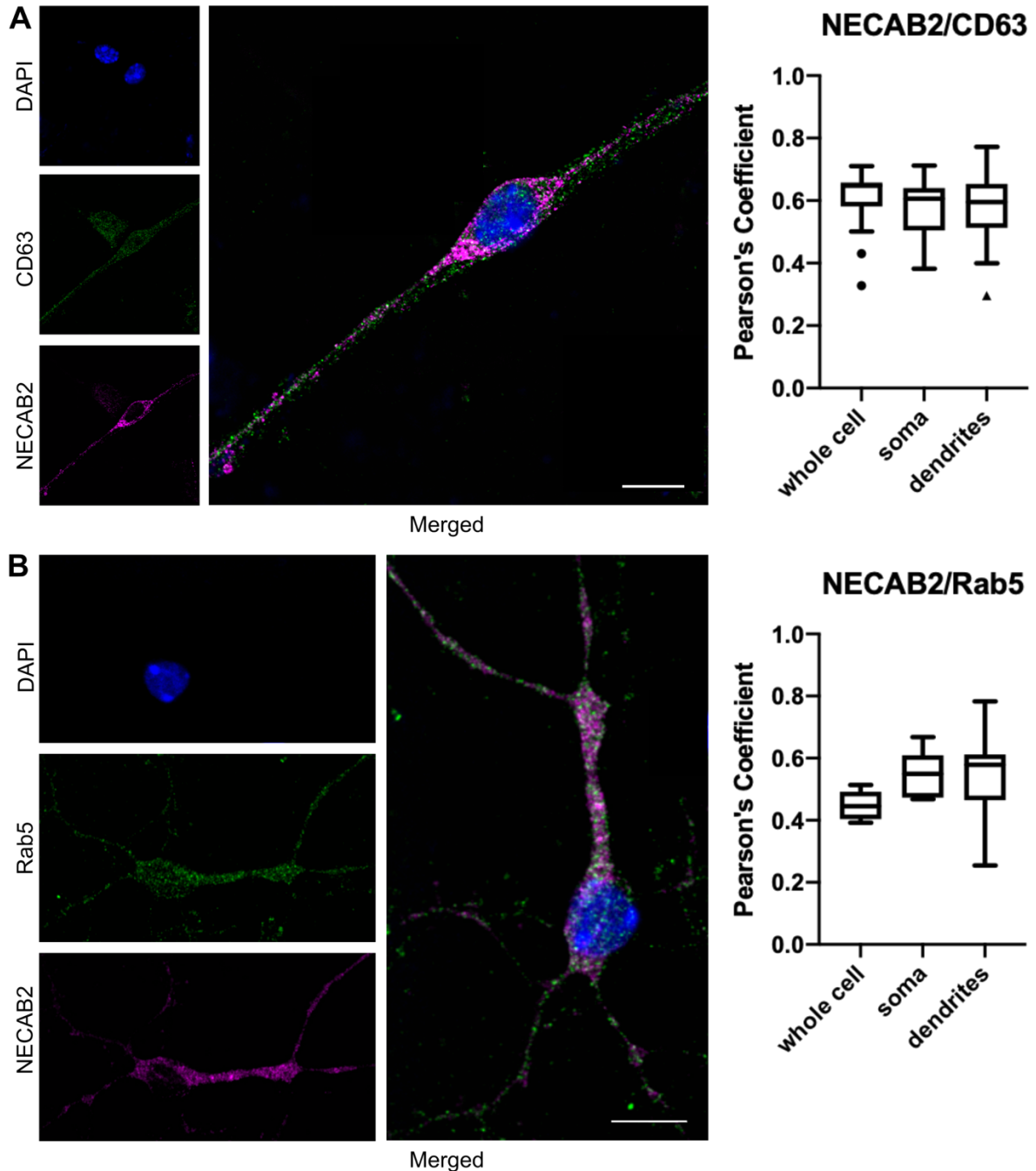


Figure 5: NECAB2 may colocalize with endosomal markers.

A) NECAB2 (N2) and CD63, an endosomal marker, colocalize in mouse WT primary striatal neurons. Right: Pearson's coefficient for N2/CD63 in WT whole cell, soma, and dendrites. **B)** N2 and Rab5, a marker for early endosomes, colocalize in mouse WT primary striatal neurons. Right: Pearson's coefficient for N2/Rab5 in WT whole cell, soma, and dendrites. CD63/Mo 1:250, Rab5/Mo 1:200, Necab2/rb 1:500. Scale bars: 10 μ m. Images were deconvolved 10x using the Iterative Deconvolve Plugin in ImageJ and colocalization studies were performed using the JACoP plugin in ImageJ. Data are presented as Tukey plots.

With a PC of about 0,67, [Figure 5A](#) indicates CD63 and N2 may colocalize when considering the whole cell, as well as when considering only the soma or dendrites. With Rab5 and N2: colocalization seems higher in the dendrites ([Figure 5B](#)). [Figures 3 and 5](#) thus show NECAB2's potential presence at mitochondria and endosomes.

5.2. Mitophagy is significantly lower in N2-expressing cells

Next, I wanted to find out whether NECAB2 expression had any effect on mitophagy. For this reason, I transiently transfected hippocampal HT22 blue fluorescent probe 2 (BFP2) empty vector (EV) cells, which do not express NECAB2 ([Figure 9](#)), and HT22 BFP2 cells expressing full-length NECAB2 (N2) with the mitophagy probe mtKeima ([Figure 6](#)). mtKeima is a fluorescent protein resistant to lysosomal degradation (Sun et al., 2017). At mitochondrial pH (pH 8.0), the short-wavelength excitation dominates, while after mitophagy, given the lysosome's acidic pH of 4.5, the excitation veers towards longer-wavelength (Sun et al., 2017). Mitophagy was significantly increased in HT22 BFP2 EV cells compared to HT22 BFP2 N2 cells ([Figure 6](#)), suggesting NECAB2 plays a role in mtQC.

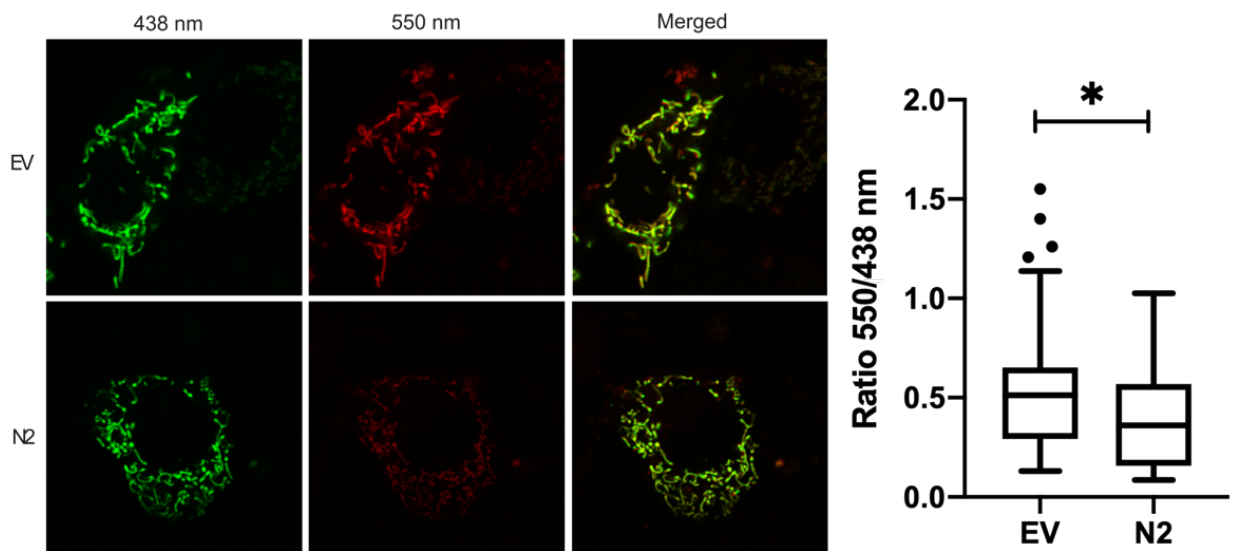


Figure 6: Mitophagy is significantly increased in HT22 BFP2 EV cells.

The mitophagy marker mtKeima was transiently transfected into HT22 BFP2 cells expressing no NECAB2 (EV, top) and full-length NECAB2 (N2, bottom). Images were recorded sequentially with an Argon laser at 12%, a 438 nm excitation of 20% (PMT1 565-633 nm) and a 561 excitation of 20% (PMT1 571-663 nm). Scale bars, 1 μ m. Data are presented as Tukey plots, * <0.05 Mann Whitney test.

5.3. Parkin and MitoRed colocalization increases with FCCP

Parkin is selectively recruited to faulty mitochondria and promotes mitophagy (Narendra et al., 2008). To further study NECAB2's effect on mtQC, I transiently transfected HT22 BFP EV and N2 cells with Parkin-GFP (green fluorescent protein) and stained them with MitoRed, a mitochondrial dye. Both cell types were then treated with 10 μ M of the mitochondrial uncoupler FCCP for two hours (Figure 7).

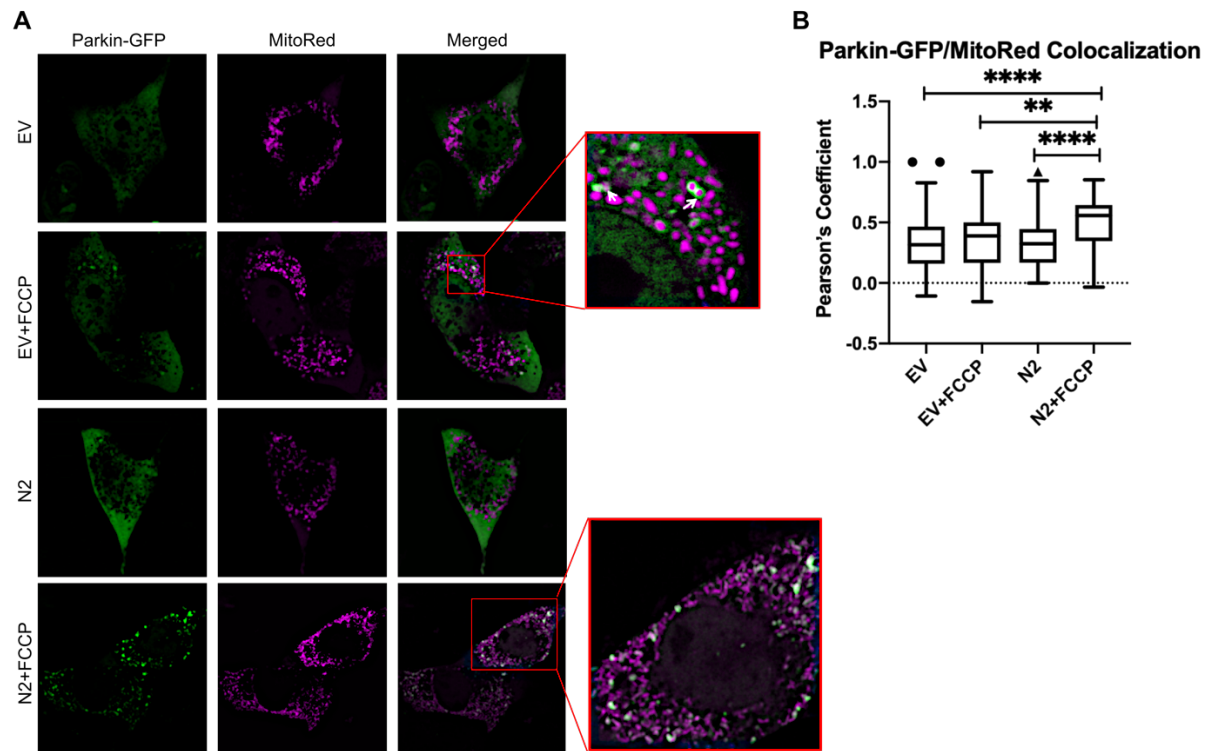


Figure 7: Parkin and MitoRed colocalization increases in HT22 BFP2 N2 cell lines transiently transfected with Parkin-GFP treated with FCCP.

A) Parkin and MitoRed signals in HT22 BFP cells. From top to bottom: empty vector (EV), EV treated with 10 μ M of the mitochondrial uncoupler FCCP for 2hrs (EV+FCCP), NECAB2 (N2), and N2 treated with FCCP (N2+FCCP). **B)** Pearson's coefficients for colocalization in each condition. Data are presented as Tukey plots, * <0.05 Mann Whitney test. Images were deconvolved 10x using the Iterative Deconvolve Plugin in ImageJ and colocalization studies were performed using the JACoP plugin in ImageJ.

At baseline, Parkin and mitochondrial colocalization was similar in EV and N2 cells; however, upon FCCP treatment, there was significantly more colocalization in N2 cells treated with FCCP compared to EV. Hence, like Figure 6, Figure 7 again indicates NECAB2 is involved in mtQC.

5.4. NECAB2 and MitoNEET may colocalize

As presented in section 2.7, the CDGSH iron-sulfur domain-containing protein 1 (CISD1), also known as MitoNEET (mNT) is present at the OMM and has been implicated in mtQC due to its labile 2Fe-2S cluster, its ability to donate the cluster to other proteins (Karmi et al., 2017, Lipper et al., 2015, Zuris et al., 2011), and the fact that it can be ubiquitinated by Parkin (Lazarou et al., 2013). Furthermore, mNT overexpression reduces mitochondrial abundance (Kusminski et al., 2016). Experiments from our group found that NECAB2 dimerizes through its ABM domain similarly to prokaryotic ABM-containing proteins (Dey et al., 2021). In prokaryotes, the ABM domain represents a heme oxygenase and functions as a homodimer (Lyles and Eichenbaum, 2018). Therefore, NECAB2 could exert its mtQC function by interacting through its ABM domain with mNT's 2Fe-2S cluster and Rab5 in a similar pathway to the one described by Hammerling et al. (2017). The fact that mNT is present at the OMM (Wiley et al., 2007) makes it an accessible potential target for N2; indeed, proteomics experiments from our group (unpublished data) found mNT was upregulated in N2 KO mice.

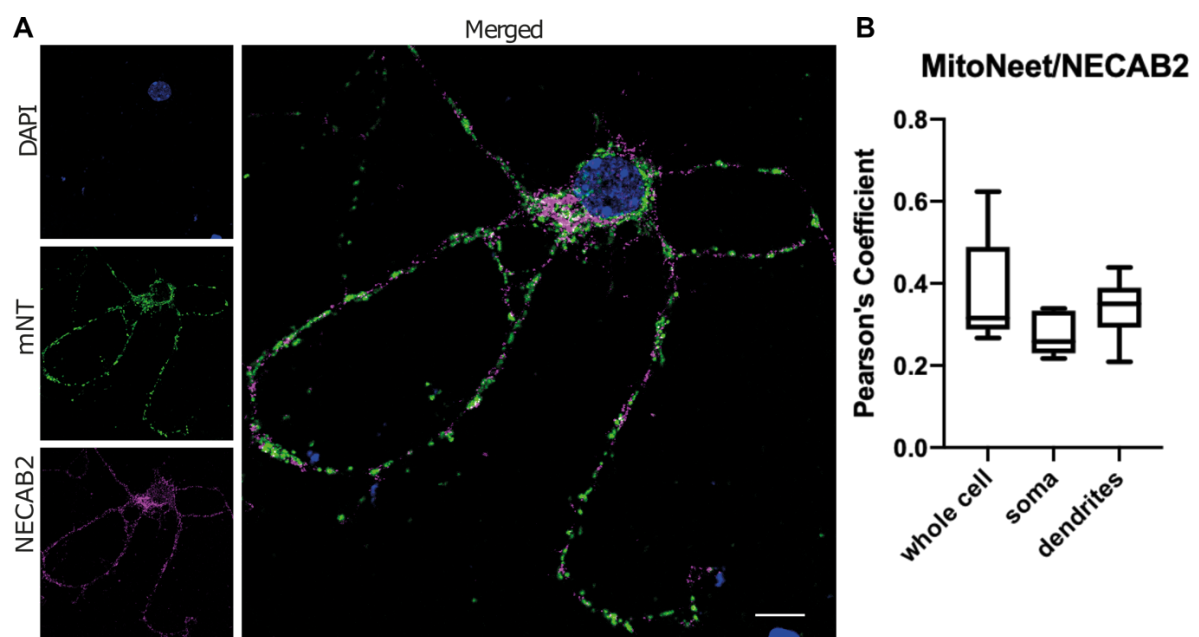


Figure 8: NECAB2 may colocalize with MitoNEET in mouse WT primary striatal neurons.

A) NECAB2 (N2) and MitoNEET (mNT) colocalization in mouse WT primary striatal neurons. mNT/mo: 1:10, Necab2/rb 1:500. Scale bar: 10 μ m. **B)** Pearson's coefficient for colocalization between N2 and mNT in WT primary striatal neurons: whole cell, soma and dendrites. Images were deconvolved 10x using the Iterative Deconvolve Plugin in ImageJ and colocalization studies were performed using the JACoP plugin in ImageJ. Data are presented as Tukey plots.

For this reason, I investigated whether mNT and NECAB2 (Figure 8) and Rab5 and mNT colocalize (Figure 10). The Pearson's Coefficient presents some challenges as

a colocalization analysis tool (Bolte and Cordelieres, 2006) (see [chapter 6](#)). With a Pearson's coefficient of about 0.37, [Figure 8A/B](#) does not allow any conclusions.

5.5. HT22 N2 cells express higher amounts of mNT when compared to EV

As mentioned in the previous section, colocalization studies between NECAB2 and mNT in mouse WT primary striatal neurons were inconclusive. However, in Western blot comparing HT22 BFP N2 to HT22 BFP EV cells, I was able to demonstrate much higher amounts of mNT in N2 cells than in EV. This does not show increased colocalization between mNT and NECAB2, but the result was consistent in all three experiments ([Figure 9](#)), indicating the two proteins could potentially be interaction partners. mNT WT/KO MEF were used as positive/negative mNT control and negative control for NECAB2.

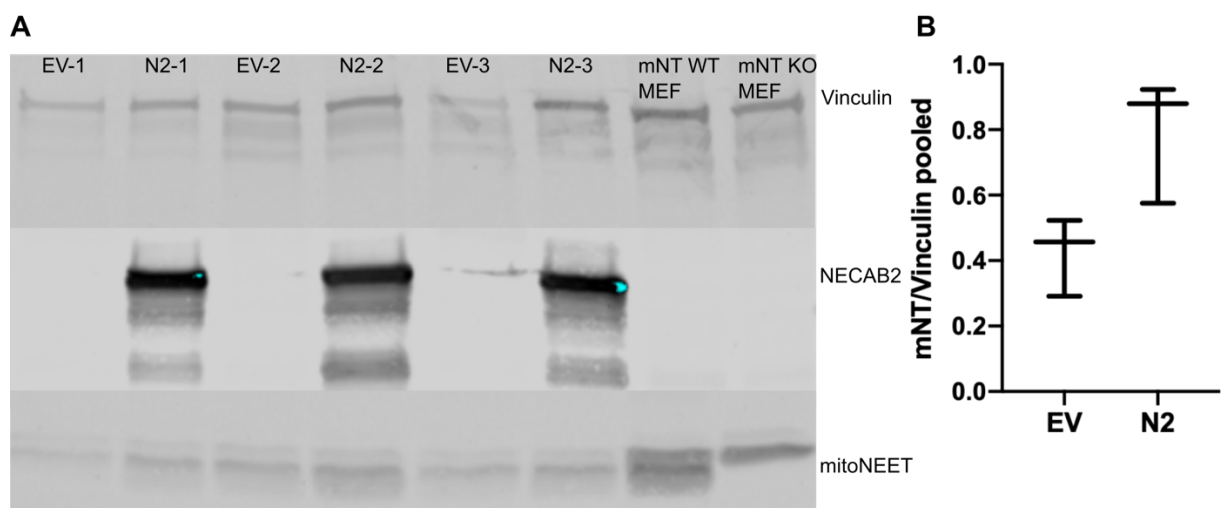


Figure 9: Western blot showing increased mNT expression in N2 HT22 cells.

A) Middle band: NECAB2 is clearly expressed in N2, but not in EV, HT22 BFP fluorescent cells. Lysates from three distinct passages were used for both N2 and EV. mNT WT and KO MEFs were used as control. NECAB2 is not expressed in either. Lower band: mNT. Upper band: Vinculin (used for normalization). **B)** mNT expression in EV and N2 HT22 cells normalized to Vinculin, all three experiments pooled.

5.6. MitoNEET and Rab5 colocalize

As previously mentioned, Pearson's Coefficient is not the ideal colocalization analysis tool (see [chapter 6](#)). At this timepoint in my thesis, however, the Bitplane Imaris analysis software became available to me thanks to the Institute for Molecular Biology (IMB) Mainz and the Paul-Klein-Zentrum für Immunintervention (PKZI). For this reason, I decided to study mNT and Rab5 colocalization in N2 WT and KO murine striatal primary cultures ([Figure 10](#)) using the Imaris software in z-stacks, rather than the Pearson's Coefficient in 2D images as I had hitherto. I also wanted to see whether the mitochondrial uncoupler FCCP had any impact on Rab5/mNT colocalization and whether there were differences between KO and WT neurons.

When comparing Rab5-positive endosomes in primary striatal cultures ([Figure 10](#)), in both NECAB2 WT and KO mice the number increased upon 2-hour 10 μ M FCCP treatment compared to baseline, but only significantly so in WT neurons.

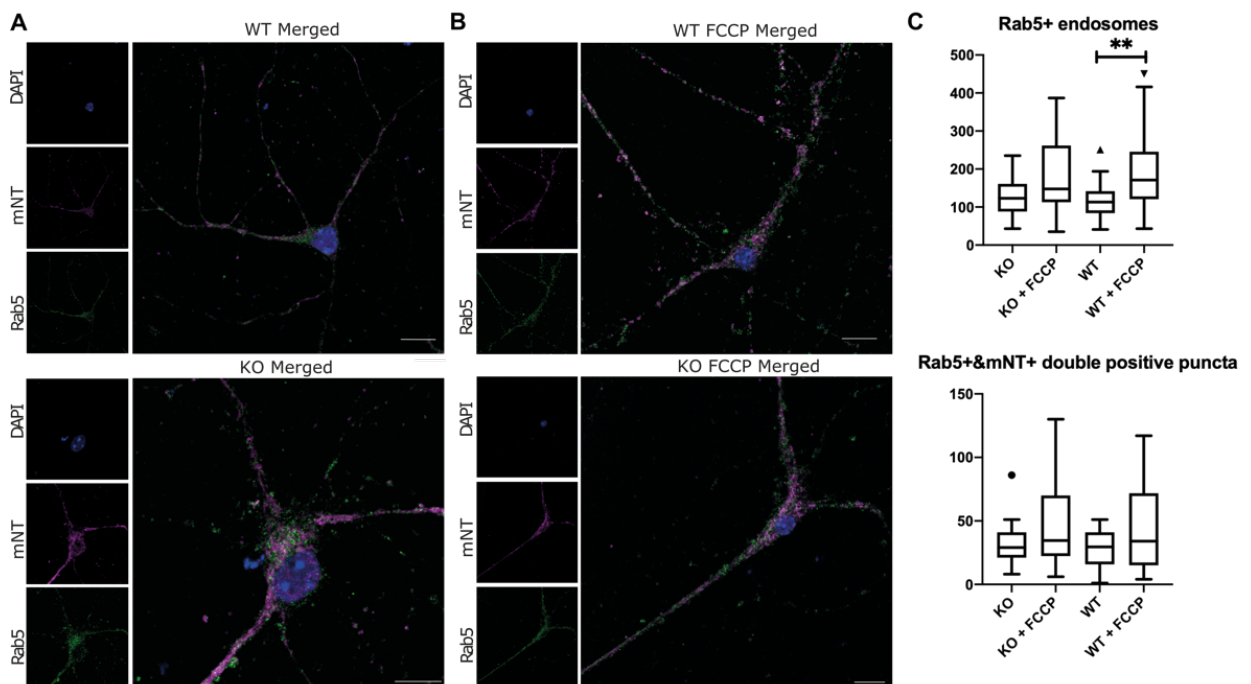


Figure 10: Rab5 colocalizes with MitoNEET (mNT) in striatal neurons.

A) Rab5 and mNT immunostaining in WT and N2 KO primary striatal neurons. **B)** Rab5 and mNT immunostaining in WT and N2 KO primary striatal neurons after 2hrs 10 μ M FCCP treatment. mNT/rb: 1:25, Rab5/mo: 1:10. Scale bars: 10 μ m. **C)** Imaris analysis: Rab5+ puncta per cell and Rab5+/mNT+ puncta per cell. Data are presented as Tukey plots, * <0.05 Mann Whitney test.

The fact that Rab5+ endosomes significantly increased in WT+FCCP suggests NECAB2 may interact with Rab5 particularly when the cell is under duress in order to clear faulty mitochondria. Rab5 and mNT colocalize ([Figure 10C](#)); however, the structures positive for both Rab5 and mNT were similar in KO and WT condition at base-

line and increased slightly, but not significantly, in both KO and WT treated with FCCP. Hence, it seems FCCP had little impact on Rab5/mtNT colocalization; furthermore, there was almost no difference in Rab5/mtNT colocalization between KO and WT.

5.7. Endosomal and mitochondrial overlap increases upon Antimycin A treatment and decreases upon FCCP treatment in HT22 cells

I next wanted to test endosomal – i.e., Rab5 – and mitochondrial (mtRed) colocalization in HT22 cells at baseline, after a 2-hour treatment with 10 μ M of the mitochondrial uncoupler FCCP (Figure 11A), and after a 2-hour treatment with 50 μ M Antimycin A (AMA) (Figure 11B). AMA is an inhibitor of the mitochondrial respiratory chain complex III (Ahmad et al., 1950).

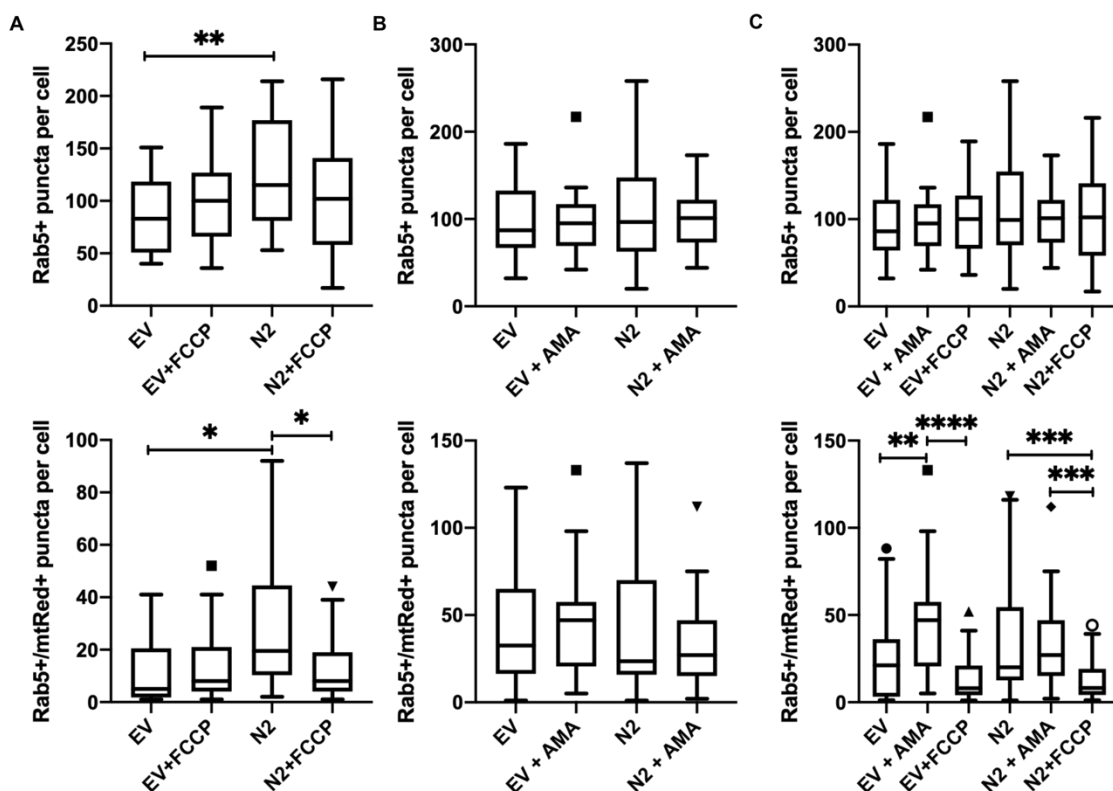


Figure 11: Rab5 and MitoRed colocalization increases upon AMA treatment, decreases upon FCCP treatment in HT22 BFP2 cell lines transiently transfected with Rab5.

A) Top: quantification of endosomal structures (marked by Rab5) in HT22 BFP2 EV and N2 cells at baseline, and after 2hrs treatment with 10 μ M FCCP; bottom: quantification of structures positive for both Rab5 (endosomes) and mitochondria (mtRed). **B)** Top: quantification of endosomal structures in HT22 BFP2 EV and N2 cells at baseline, and after 2hrs treatment with 50 μ M Antimycin A; bottom: quantification of structures positive for both Rab5 and mitochondria. **C)** Pooled data from all six conditions: EV and N2 no treatment, EV and N2 2hrs 50 μ M Antimycin A treatment, EV and N2 2hrs 10 μ M FCCP treatment. Data are presented as Tukey plots, * $<$ 0.05 Mann Whitney test.

In [Figure 11C](#), when considering the pooled data from the three experiments with 50 μM AMA and 10 μM FCCP compared to baseline in EV and N2 cells, the number of Rab5-positive puncta was slightly, but not significantly, higher in N2 cells than EV cells. Upon FCCP treatment, Rab5-positive puncta slightly increased in the EV but remained the same in the N2 cells, while upon AMA treatment, Rab5-positive puncta slightly rose in both N2 and EV. The number of double positive (Rab5/mtRed) puncta was slightly lower in N2 compared to EV at baseline and significantly increased in EV with 50 μM AMA treatment. The number also rose in N2 with 50 μM AMA treatment, but not at a significant level. Upon 10 μM FCCP treatment, the number of double positive (Rab5/mtRed) puncta decreased in both conditions.

5.8. TOM20 and Rab5 colocalization increases upon AMA treatment in HT22 cells

Since our assumptions are strongly based on Hammerling et al. (2017)'s findings, I next transfected HT22 BFP EV and N2 cells with Rab5 and studied colocalization with the same protein used by Hammerling et al., namely translocase of outer membrane 20 (TOM20), an OMM protein (Figure 12) at baseline, with 5 μ M AMA, 50 μ M AMA, and FCCP.

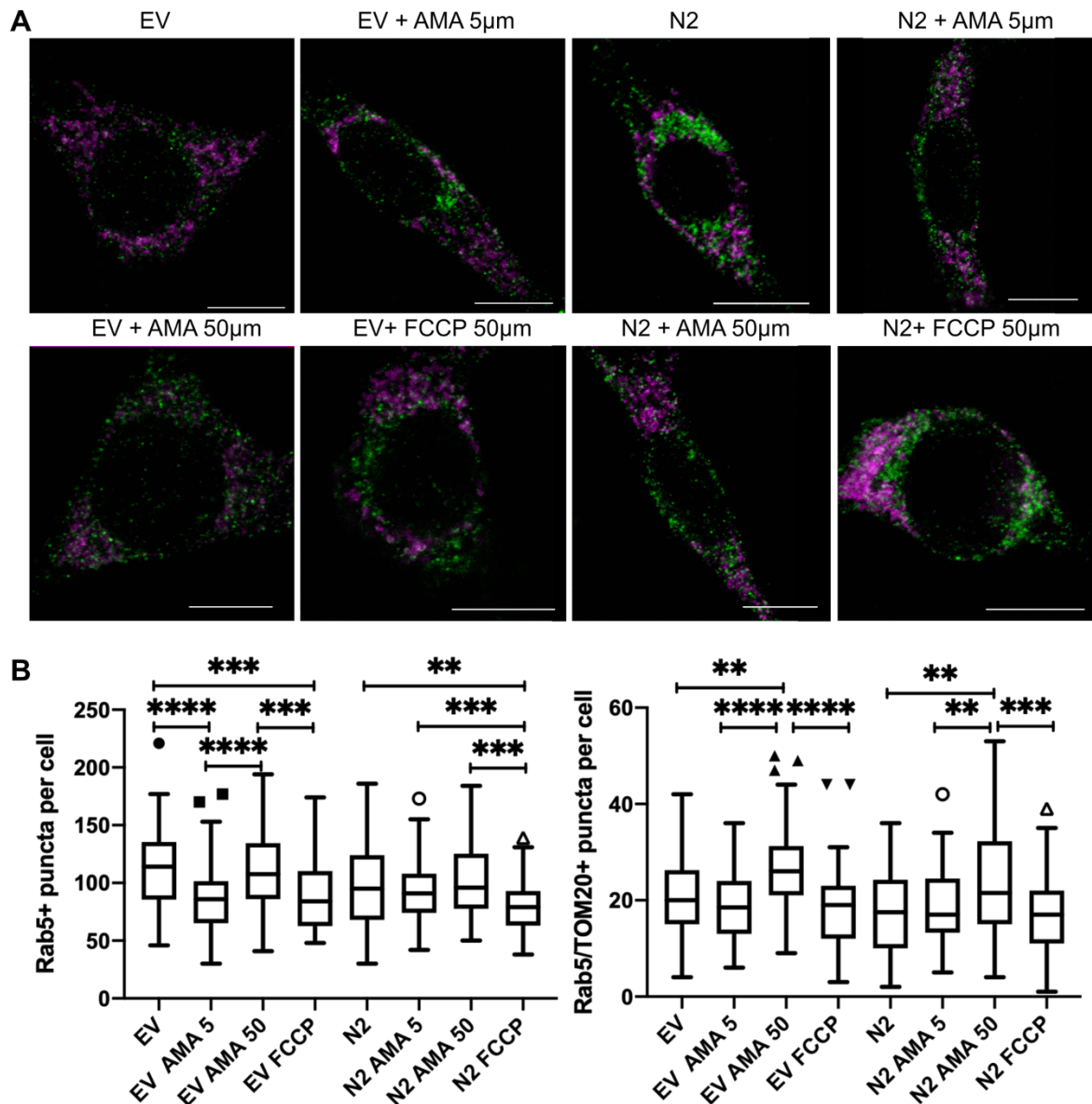


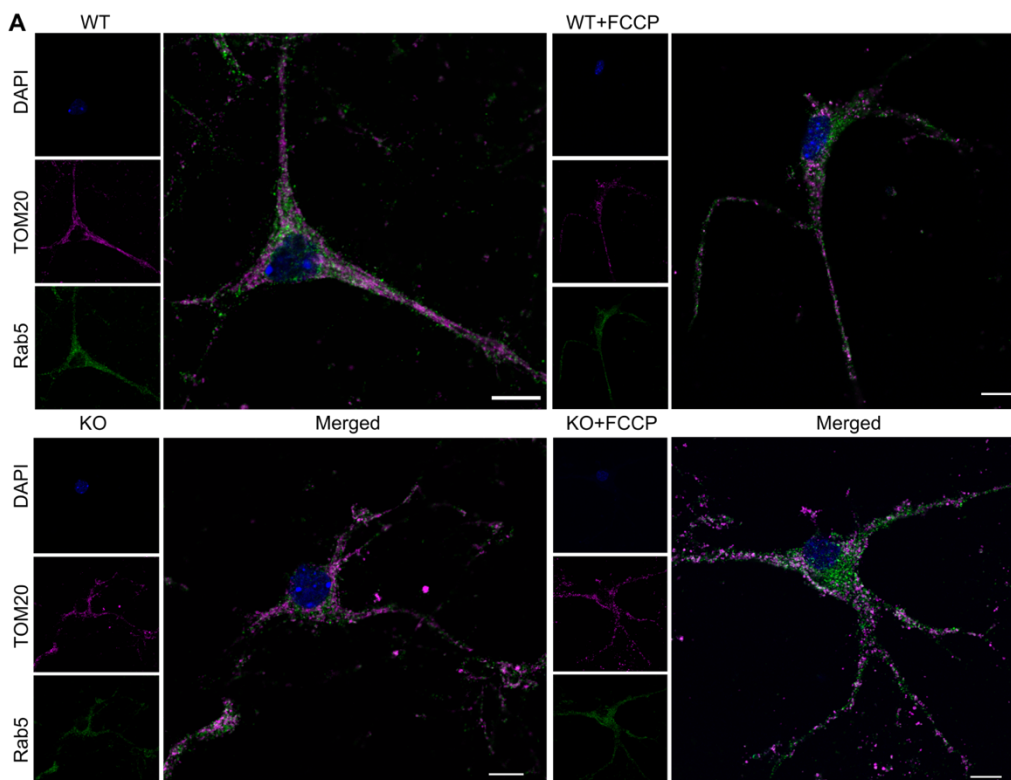
Figure 12: Rab5 and TOM20 colocalization increases upon AMA treatment in HT22 BFP2 cell lines transiently transfected with Rab5.

(A) Endosomal structures (marked by Rab5, green channel) and mitochondria (marked by TOM20, magenta channel) in HT22 BFP2 EV and N2 cells at baseline and after 2hrs treatment with 5 μ M Antimycin A (AMA), 50 μ M AMA, and 10 μ M FCCP, respectively. (B) Pooled data from all six conditions: EV and N2 no treatment, EV and N2 2hrs 5 μ M AMA treatment, EV and N2 2hrs 50 μ M AMA treatment, EV and N2 2hrs 10 μ M FCCP treatment. Data are presented as Tukey plots, * <0.05 Mann Whitney test.

Contrarily to the previous experiment, the number of Rab5-positive puncta was slightly (not significantly) higher in EV cells than in N2 cells. Upon FCCP treatment, Rab5-positive puncta significantly decreased in EV and N2 cells, while the number of double positive (Rab5/TOM20) stayed about the same. Upon 5 μ M AMA treatment, Rab5-positive puncta and double positive (Rab5/TOM20) puncta slightly decreased in both N2 and EV. Upon 50 μ M AMA treatment, by contrast, Rab5-positive puncta stayed about the same, while double positive (Rab5/TOM20) puncta significantly increased in both N2 and EV.

5.9. TOM20 and Rab5 colocalization increases upon FCCP treatment in KO primary striatal neurons

I next studied TOM20 and Rab5 colocalization at baseline and following 2-hr 10 μ M FCCP treatment in primary striatal neurons derived from NECAB2 KO and WT mice (Figure 13). The number of Rab5-positive puncta was about the same in WT and KO at baseline, increasing significantly in both WT and KO neurons after a two-hour 10 μ M FCCP treatment. Like in Figure 10, the fact that Rab5+ endosomes significantly increased in WT+FCCP (Figure 13) suggests NECAB2 may interact with Rab5 particularly when the cell is under duress in order to clear faulty mitochondria. However, in discordance with results from Figure 10, Rab5+ increased even more significantly



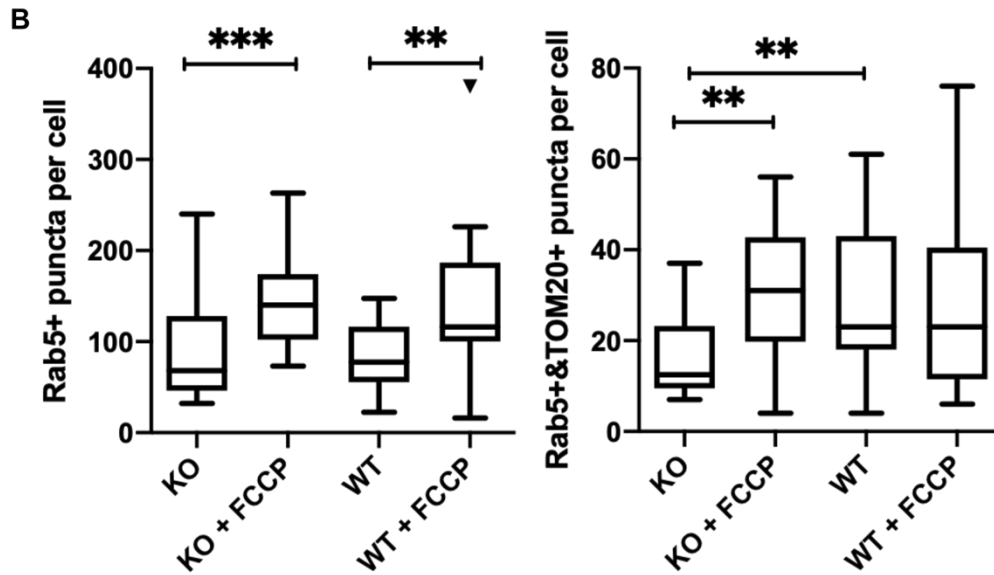


Figure 13: Rab5 increasingly colocalizes with TOM20 in KO mouse primary striatal neurons upon FCCP treatment.

A) Rab5 and TOM20 in WT and N2 KO mouse primary striatal neurons. Left: WT and KO at baseline. Right: WT and KO after 2hrs treatment with 10 μ M FCCP. TOM20/rb 1:200, Rab5/mo: 1:10. Scale bars: 10 μ m. Images were deconvolved 10x using the Iterative Deconvolve Plugin in ImageJ. **B)** Imaris analysis: Rab5+ puncta per cell and Rab5+/TOM20+ puncta per cell. Data are presented as Tukey plots, * <0.05 Mann Whitney test.

in KO upon FCCP treatment in [Figure 13](#). When considering colocalization between Rab5 and TOM20, the number of double positive puncta was higher in WT compared to KO at baseline and stayed about the same in WT while significantly increasing in KO with FCCP treatment.

5.10. NECAB2 is upregulated in human iPSC-derived dopaminergic neurons with PD mutations

Thanks to [REDACTED], I had the opportunity to work at the Department of Neurodegenerative Diseases of the Center of Neurology of the Hertie Institute for Clinical Brain Research in Tübingen. With a TALEN directed towards Exon 1, the group around [REDACTED] obtained two PINK1 knockouts: $\Delta 8.9$ and $\Delta 40.7$ from an isogenic control, K7.1, in human iPSC-derived dopaminergic neurons (Figure 14D, courtesy of [REDACTED], MSc). Figure 14D shows that both $\Delta 8.9$ and $\Delta 40.7$ are successful PINK1 knockouts, while K7.1 is an isogenic control since it expresses PINK1. Immunocytochemistry against tyrosine hydroxylase (TH), a marker for dopaminergic neurons, which are mainly affected in PD (Bernheimer et al., 1973),

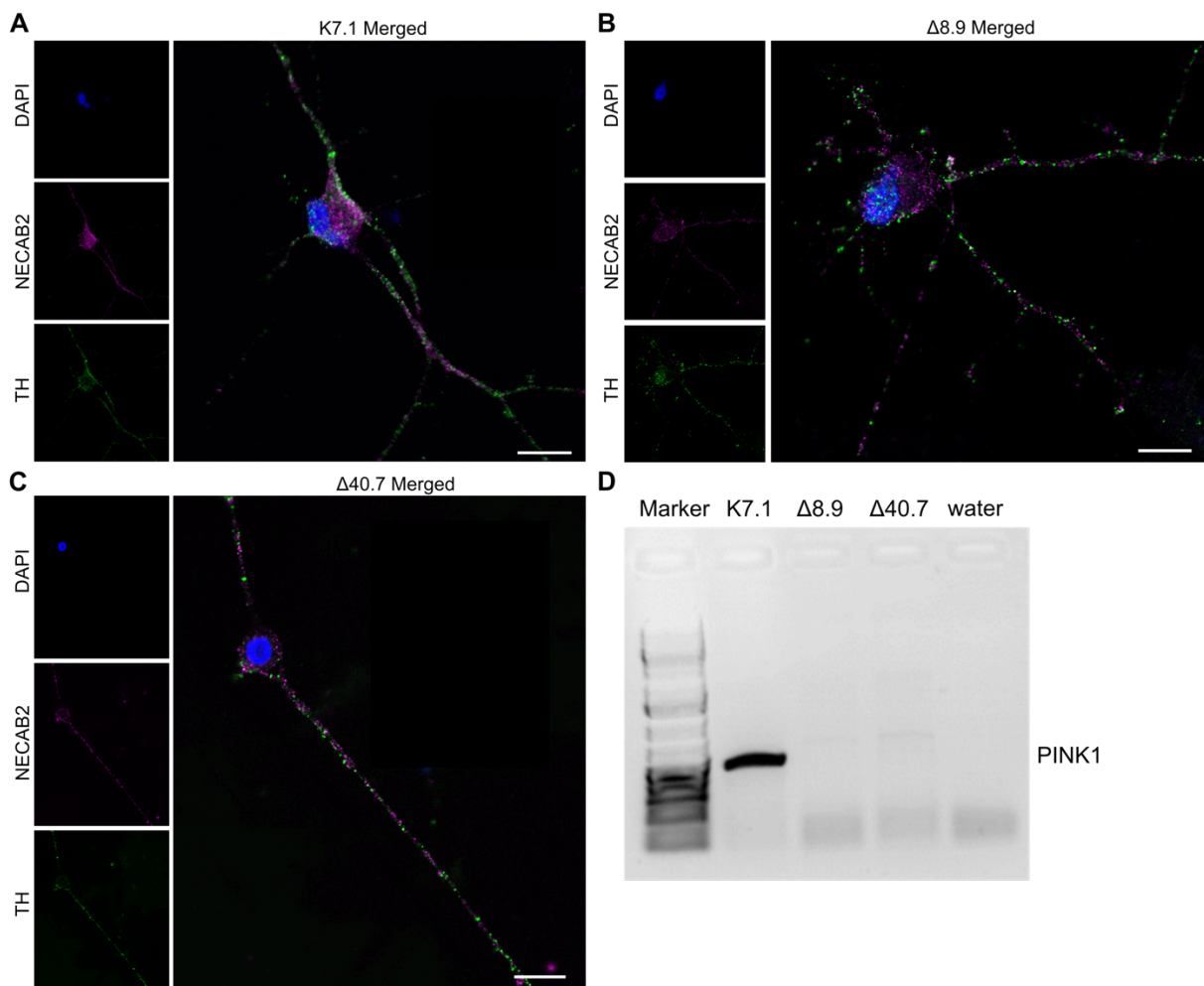


Figure 14: NECAB2 and tyrosine hydroxylase are present in iPSC-derived dopaminergic neurons.

Two iPSC-derived dopaminergic neuronal cell lines with distinct PINK1 knockouts, $\Delta 8.9$ and $\Delta 40.7$, and their isogenic control, K7.1, were obtained through a TALEN directed towards Exon 1 and used for experiments. Tyrosine hydroxylase (TH) is a marker for dopaminergic neurons. ICC shows dopaminergic differentiation of the iPSC-derived neurons and NECAB2 expression. ICC was performed on neurons from differentiation 66. TH-2 clone/mo 1:200, Necab2/rb 1:500. Scale bars: 10 μ m. **A)** NECAB2 (N2) and TH in the isogenic control, K7.1. **B)** N2 and TH in PINK1 KO#1, also known as $\Delta 8.9$. **C)** N2 and TH in PINK1 KO#2, also known as $\Delta 40.7$. **D)** PCR demonstrating successful PINK1 knockout in human iPSC-derived dopaminergic neurons. K7.1, the isogenic control, clearly shows a PINK1 band, while $\Delta 8.9$ and $\Delta 40.7$, the two PINK1 knockouts, do not display a band. Water was used as control. Image **D)** courtesy of [REDACTED], MSc, Hertie Institute for Clinical Brain Research in Tübingen.

showed specific staining in all three conditions against TH (Figure 14A-C), indicating dopaminergic differentiation. In both knockouts and K7.1, NECAB2 was present (Figure 14A-C).

Next, I wanted to assess whether there were any differences in NECAB2 expression in the three cell lines. In Western blot (Figure 15), NECAB2 was significantly more present in both $\Delta 8.9$ and $\Delta 40.7$ compared to the control, K7.1, both in differentiation 54 and several differentiations later, namely in differentiation 68. mNT was also upregulated in differentiation 68 in both $\Delta 8.9$ and $\Delta 40.7$ compared to K7.1, but only significantly so in $\Delta 8.9$ compared to K7.1. The upregulation of NECAB2 and mNT further support their potential role in a mtQC pathway.

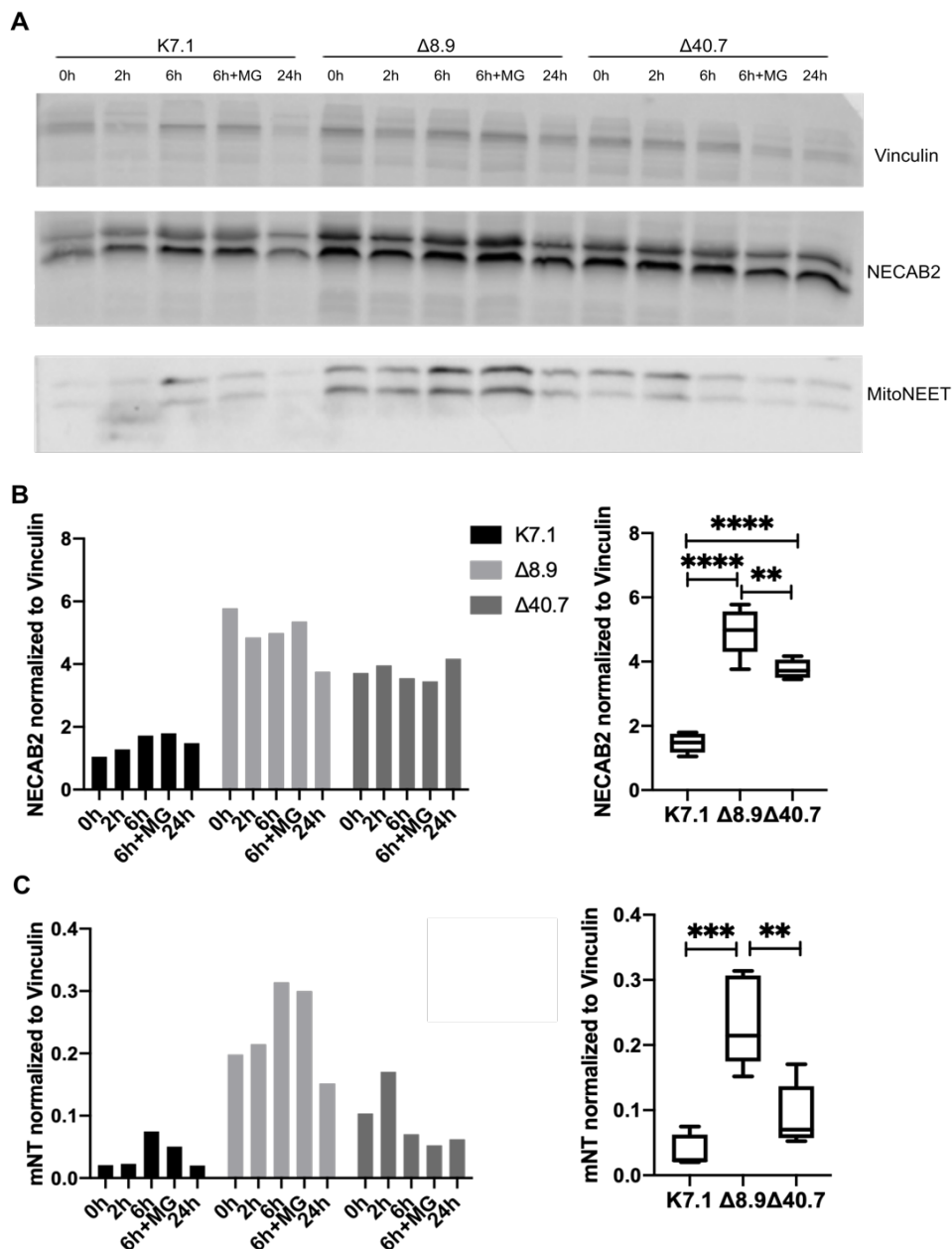


Figure 15: NECAB2 and MitoNEET are upregulated in human iPSC-derived dopaminergic neurons with PD mutations compared to isogenic control.

Two iPSC-derived dopaminergic neuronal cell lines with distinct PINK1 knockouts, $\Delta 8.9$ and $\Delta 40.7$, and their isogenic control, K7.1, were used for experiments. All three cell types were analyzed at baseline and after treatment with the mitochondrial uncoupler CCCP (10 μM) for 2h, 6h, 6h with the addition of 10 μM MG132, and 24h. **A)** Vinculin, NECAB2 and MitoNEET (mNT) in exemplary Western blot from differentiation 68. **B)** NECAB2 normalized to Vinculin, pooled data from differentiations 54 and 68. NECAB2 is significantly increased in both KOs compared to isogenic control. **C)** mNT normalized to Vinculin from differentiation 68. mNT is significantly increased in $\Delta 8.9$ compared to K7.1. Data are presented as Tukey plots, $* < 0.05$ one-way ANOVA.

5.11. NECAB2 colocalizes more with Rab5 in isogenic control

Lastly, I investigated colocalization through Pearson's coefficient between MitoNEET and NECAB2 and Rab5 and mNT ([Figure 16](#)). mNT and N2 colocalization was significantly higher in K7.1 compared to $\Delta 40.7$ and higher, but not significantly so, in K7.1 compared to $\Delta 8.9$. Rab5/NECAB2 colocalization was significantly more prominent in K7.1 compared to both $\Delta 40.7$ and $\Delta 8.9$. This could be interpreted as either a product

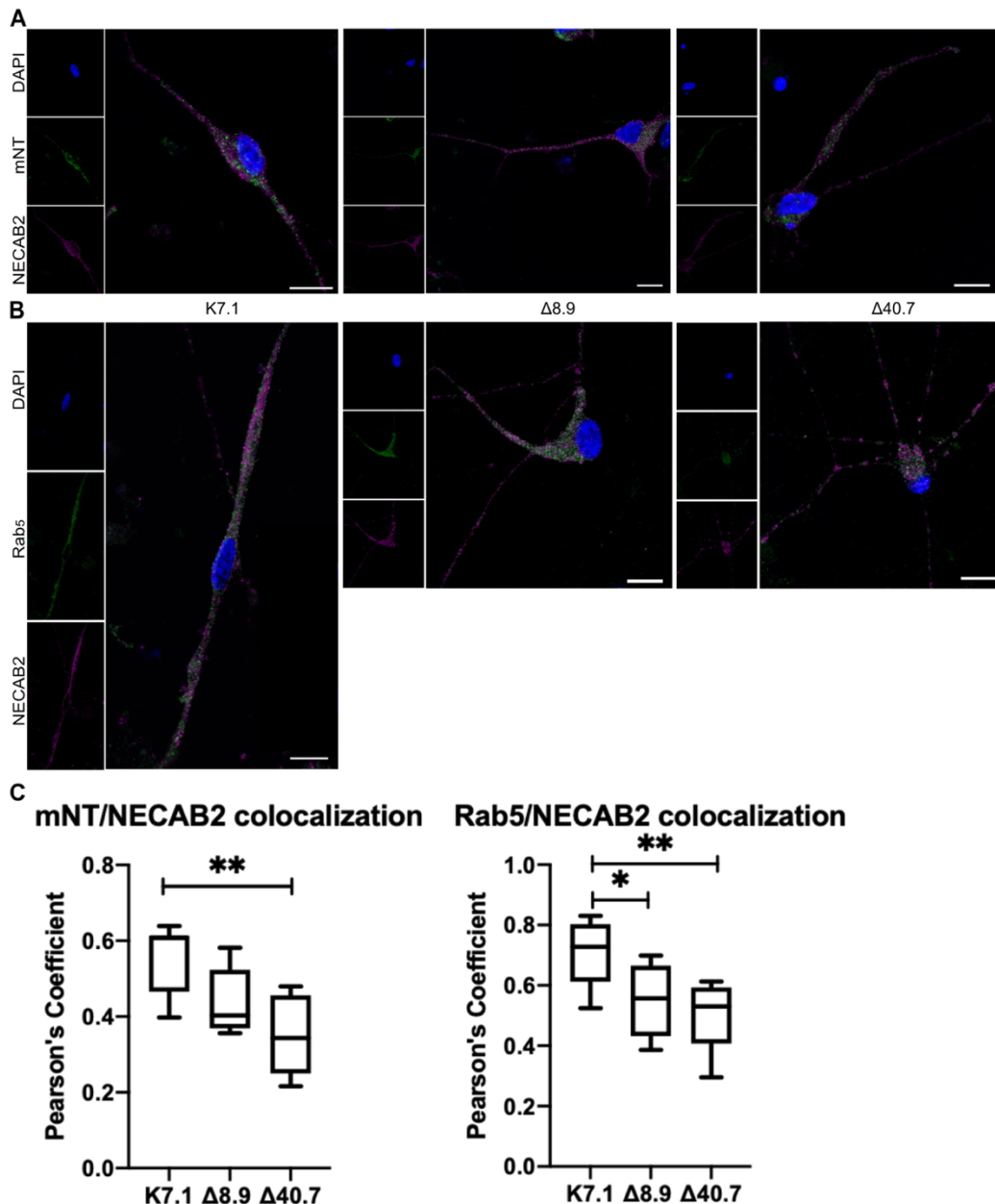


Figure 16: MitoNEET/NECAB2 and Rab5/NECAB2 colocalize in human iPSC-derived dopaminergic neurons.

A) MitoNEET (mNT, green) and NECAB2 (N2, magenta) colocalization and **B)** Rab5 (green) and N2 (magenta) colocalization in human iPSC-derived dopaminergic neurons from differentiation 66. From left to right: isogenic control (K7.1), PINK1 KO#1 ($\Delta 8.9$) and PINK1 KO#2 ($\Delta 40.7$). mNT/mo: 1:10, Rab5/mo: 1:10; NECAB2/rb: 1:500. Scale bars: 10 μ m. **C)** Pearson's coefficient for colocalization between mNT/N2 and Rab5/N2. Z-stacks were collapsed into one image using Z Project (Max Intensity) and subsequently deconvolved 10x using the Iterative Deconvolve Plugin in ImageJ. Colocalization studies were performed using the JACoP plugin in ImageJ. Data are presented as Tukey plots, * <0.05 one-way ANOVA test.

of lower NECAB2 levels in the isogenic control, or it could be yet another sign that the many different mtQC pathways work better in healthy cells (see [chapter 6.8](#)).

6. Discussion

The aim of this thesis was to explore NECAB2's function. The experiments I performed in HT22 cells with the mitophagy probe mtKeima and with Parkin indicate NECAB2 is involved in mitochondrial quality control (mtQC). First, I showed NECAB2 is present at mitochondria. I hypothesized NECAB2 acts on mtQC through endosomes and mNT; for this reason, I investigated mNT and NECAB2, and Rab5 and mNT colocalization in primary striatal mouse neurons and HT22 cells. mNT and N2 studies were inconclusive, but I was able to show an increase in Western blot of mNT in N2 HT22 cells. Unfortunately, mNT/Rab5 and Rab5/TOM20 in HT22 colocalization studies were discrepant. Lastly, to investigate NECAB2's potential implications in disease, I worked with iPSC-derived human dopaminergic neurons. Here, I found NECAB2 was upregulated in neurons with PD mutations compared to their isogenic control. Interestingly, NECAB2 colocalized more with Rab5 and mNT in the isogenic control compared to the two PINK1 KOs.

Much of the data presented here is based on ICC and colocalization studies. To study colocalization, I initially calculated Pearson's coefficient (PC) with ImageJ's JACoP. The rate of association of two fluorochromes is described by linear approximation and PC estimates the goodness of this approximation (Bolte and Cordelieres, 2006). A PC of 1 means complete positive correlation, 0 no correlation, and -1 negative correlation (Bolte and Cordelieres, 2006). However, PC poses several problems: it is influenced by noise and bleed-through (Bolte and Cordelieres, 2006). To minimize this effect, I used the Iterative Deconvolve Plugin in ImageJ. Regardless, in many of my analyses I still obtained mid-range PC, which do not allow colocalization conclusions. Another problem with PC is its sensitivity to variation in fluorescence intensities (Bolte and Cordelieres, 2006). Furthermore, some of the images (obtained through confocal microscopy) I took at the beginning of my lab work do not have optimal resolution. Lastly, reducing such complex cells as neurons to a single 2D image very likely omitted some colocalization events, which is why I changed my methods to study colocalization through Imaris. When Imaris became available to me, I started taking z-stack images to have 3D rendering and counting puncta (either positive for one marker, usually Rab5, or for two for colocalization studies) through the software. However, this type of analysis is very laborious and time-consuming, which is why I was not able to perform Imaris analyses in all experiments presented here.

6.1. NECAB2 is present at mitochondria and in endosomes

I started my experiments by determining NECAB2's location and potential overlap with proteins involved in autophagic pathways. Immunocytochemistry (ICC) in primary striatal mouse culture showed specific NECAB2 staining in WT mice and no NECAB2 staining in KO animals ([Figure 3](#)).

As presented in [2.6.1.3](#), both Hammerling et al. (2017) and Hsu et al. (2018) proposed two mtQC pathways involving Rab5 and the ESCRT machinery distinct from "canonical" Parkin/PINK1-dependent mitophagy.

To test whether NECAB2 could be involved in mtQC and whether this pathway could be mediated via endosomes, I first studied NECAB2 colocalization with mitochondria ([Figure 3](#)) and with endosomes ([Figure 5A&B](#)). The PC was inconclusive because of the aforementioned problems. However, I was able to confirm via Western blot that NECAB2 is enriched at mitochondria ([Figure 4C&D](#)). Also, colleagues from our group were able to show NECAB2 is indeed present at endosomes (Dey et al., 2021).

6.2. NECAB2 is involved in mitochondrial quality control

Given that the striatum receives input from the cortex, the thalamus, and the rest of the basal ganglia, mitochondrial efficiency – and therefore, mitochondrial quality control (mtQC) – is of paramount importance in the striatum (Damiano et al., 2010).

Concurrently, in my experiments mitophagy was significantly increased in HT22 BFP2 EV cells – which do not express NECAB2 – compared to HT22 BFP2 N2 cells expressing full-length NECAB2 ([Figure 6](#)). I next studied Parkin – which is involved in canonical mtQC – and mitochondrial colocalization in HT22 EV and N2 cells ([Figure 7](#)). At baseline, Parkin and mitochondrial colocalization was similar in EV and N2 cells; however, upon two-hour treatment with the mitochondrial uncoupler FCCP, there was significantly more colocalization in N2 cells treated with FCCP compared to EV. Taken together, these results strongly support NECAB2's involvement in mtQC.

6.3. NECAB2 could act on mtQC through endosomes

In erythroid cells, Hamdi et al. (2016) described a mechanism by which endosomes associate with mitochondria in order to deliver iron to mitochondria. Furthermore, both Hammerling et al. (2017) and Hsu et al. (2018) (see section [2.6.1.3](#)) proposed two mtQC pathways involving Rab5 and the ESCRT machinery. I hypothesize NECAB2 also acts on mtQC via endosomes, which is why I investigated differences in endosomal and mitochondrial colocalization in HT22 EV and N2 cells ([Figure 11](#), [Figure 12](#)) transiently transfected with Rab5 and in primary striatal neurons from NECAB2 WT and KO mice ([Figure 13](#)) under mitochondrial stressors, namely Antimycin A (AMA) and Carbonyl cyanide-4-(trifluoromethoxy) phenylhydrazone (FCCP). AMA is an inhibitor of the mitochondrial respiratory chain complex III (Ahmad et al., 1950), while FCCP is a mitochondrial uncoupler (Heytler and Prichard, 1962).

[Figure 11](#) shows no significant difference between HT22 EV and N2 at baseline in Rab5+ puncta and Rab5+/MitoRed puncta. Upon 2-hour 50 μ M AMA and 10 μ M FCCP treatment, there was no significant difference in Rab5+ puncta, but Rab5+/MitoRed puncta increased significantly in EV upon AMA treatment and slightly rose in N2 as well, while double positive (Rab5/mtRed) puncta decreased in both conditions upon FCCP treatment.

In my next experiment ([Figure 12](#)), I studied TOM20 and Rab5 colocalization in HT22 EV and N2 cells transfected with Rab5. I chose TOM20 as a mitochondrial marker because it was used by Hammerling et al. (2017)'s paper, which our assumptions are based on. I also tested 5 μ M AMA to have a dose comparison. In contrast to the previous experiment, the number of Rab5-positive puncta was slightly higher in EV compared to N2 at baseline. Upon FCCP treatment, Rab5-positive puncta significantly decreased in EV and N2 cells, while the number of double positive puncta (Rab5/TOM20) stayed about the same. Upon 5 μ M AMA treatment, Rab5-positive puncta and double positive (Rab5/TOM20) puncta slightly decreased in both N2 and EV. Upon 50 μ M AMA treatment, by contrast, Rab5-positive puncta stayed about the same, while double positive (Rab5/TOM20) puncta significantly increased in both N2 and EV.

The fact that Rab5+ puncta in the experiments with HT22 cells showed no difference in [Figure 11](#) and showed a marked decrease in [Figure 12](#) upon 2 hours 10 μ M FCCP treatment may be attributable to the fact that Rab5 was transiently transfected. Given

the fact that the two sets of experiments were performed at markedly different timepoints with different generations of HT22 cells, the transient Rab5 transfection may have worked to a varying degree. Double positive (Rab5/mtRed) puncta decreased in N2 and EV upon FCCP treatment in [Figure 11](#), while in [Figure 12](#), the number of double positive puncta (Rab5/TOM20) stayed about the same upon FCCP treatment. In both sets of experiments, 2-hour 50 μ M AMA treatment caused an increase in double positive (Rab5/mtRed and Rab5/TOM20) puncta in both N2 and EV. No significant differences between N2 and EV were measurable for any condition. Overall, the HT22 experiments regarding endosomal and mitochondrial colocalization were, unfortunately, inconclusive.

In hopes of finding more conclusive results in neurons, I next studied TOM20 and Rab5 colocalization at baseline and following 2-hours 10 μ M FCCP treatment in primary striatal neurons derived from NECAB2 KO and WT mice ([Figure 13](#)). The number of Rab5-positive puncta was about the same in WT and KO at baseline. Rab5-positive puncta increased significantly in both WT and KO neurons after a two-hour 10 μ M FCCP treatment, more strongly so in KO. This Rab5+ increase in both WT and KO may be attributable to the activation of the endosomes/ESCRT machinery. At baseline, WT had significantly more TOM20+/Rab5+ puncta compared to KO. The number of TOM20+/Rab5+ puncta increased significantly in KO while staying about the same in WT. I hypothesize that NECAB2 WT cells have better mtQC (and hence more TOM20/Rab5 colocalization at baseline) and are thus less susceptible to FCCP treatment – the cell is able to repair damaged mitochondria. KO, on the other hand, represents a handicap for the cell, resulting in less mtQC (less TOM20/Rab5 colocalization at baseline). Adding FCCP to KO results in greater mitochondrial distress, (over-) activating other mtQC pathways involving Rab5, enabling less mitochondria to be salvaged. The findings from [Figure 13](#) are in line with my mtKeima mitophagy experiments in HT22 cells ([Figure 6](#)) and with our group's findings that KO mitochondria had higher but less efficient mitochondrial activity compared to WT (Dey et al., 2021).

6.4. NECAB2 could interact with MitoNEET

If indeed NECAB2 is a sensor for increased calcium levels and ergo plays a role in mtQC, what could its target be?

In chapter [2.7](#) and [Figure 1](#), the CDGSH iron-sulfur domain-containing protein 1 (CISD1), also known as MitoNEET (mNT), and its potential implications in mtQC were explored. Briefly, mNT is located at the OMM and contains a 2Fe-2S cluster (Wiley et al., 2007). In cancer cells, its labile 2Fe-2S cluster mitigates iron and ROS accumulation (Sohn et al., 2013). Karmi et al. (2017) proposed that mNT's ability to donate its cluster and relay it to NAF-1 plays a role in apoptosis and autophagy regulation. NAF-1 usually interacts with BCL-2 at the ER (Chang et al., 2010); if NAF-1 is suppressed or does not accept the cluster, it cannot interact with BCL-2 and autophagy/apoptosis is initiated (Karmi et al., 2017). Geldenhuys et al. (2017) showed that mNT's correct function is especially important in the striatum: the mNT KO striatum showed iron accumulation and mNT KO mitochondria had increased ROS and superoxide levels (Geldenhuys et al., 2017). Striatal mNT KO mitochondria's ATP production and state III respiration were significantly reduced compared to WT mitochondria (Geldenhuys et al., 2017). Furthermore, the mNT KO striatum displayed a significant decrease in TH and dopamine levels and mNT KO mice had impaired motor skills; overall, mNT deletion induces many traits of early neurodegeneration in PD (Geldenhuys et al., 2017). Furthermore, Yonutas et al. (2020) found that mNT is an important mediator of calcium-induced mitochondrial dysfunction. Taken together, these findings suggest mNT may play a role in mtQC. Indeed, Lazarou et al. (2013) found that mNT is ubiquitinated by Parkin. This is probably due to the fact that mNT lowers $\Delta\psi_m$ (Kusminski et al., 2016). This loss of $\Delta\psi_m$ recruits the PINK1-Parkin machinery (see [2.6](#)) and induces mitophagy. Furthermore, proteomics data from our group showed that mNT was upregulated in PINK1 KO human dopaminergic neurons (unpublished data).

For these reasons, I hypothesized that mNT could be involved in NECAB2's mtQC pathway and hence studied mNT and NECAB2 colocalization ([Figure 8](#)) and mNT and Rab5 colocalization (see next section).

Colocalization studies between NECAB2 and MitoNEET ([Figure 8 A/B](#)) in primary striatal mouse neurons from NECAB2 WT mice were not very conclusive due to suboptimal imaging and PC limitations (see beginning of chapter [6](#)). However, in

Western blot comparing HT22 cells expressing NECAB2 (N2) to non-NECAB2 expressing HT22 cells (EV), I compared the amount of mNT in N2 cells to that in EV. mNT WT/KO MEF were used as positive/negative mNT control and negative control for NECAB2 ([Figure 8C/D](#)). Consistently across all three experiments, N2 cells expressed more mNT than EV cells, suggesting mNT's function could be linked to NECAB2's.

6.5. MitoNEET and Rab5 colocalization increases upon FCCP treatment

As previously mentioned, the Imaris analysis software became available to me at this timepoint in my thesis. Given its ability to count puncta in 3D images, it appears a tool better suited to colocalization studies, albeit a very time-consuming one.

Since NECAB2 is present at mitochondria and endosomes (Dey et al., 2021) (chapters [5.1](#), [6.1](#)) and appears to play a role in mtQC via the Rab5/ESCRT machinery, I next studied mNT and Rab5 colocalization ([Figure 10](#)) in primary striatal cultures from NECAB2 WT and KO mice. I also wanted to find out whether FCCP could have an effect on either cell type. When comparing Rab5-positive endosomes, at baseline Rab5+ endosomes were about the same in both WT and KO mice, just as in [Figure 13](#). Upon 2-hour 10 μ M FCCP treatment, the number of Rab5+ puncta increased in both WT and KO compared to baseline, like in [Figure 13](#). However, while in [Figure 13](#), the increase in Rab5+ puncta was significant in both WT and KO at baseline compared to WT/KO treated with FCCP, in [Figure 10](#), the increase was only significant in WT+FCCP compared to WT at baseline. The structures positive for both Rab5 and mNT were similar in KO and WT condition at baseline and increased slightly, but not significantly, in both KO and WT treated with FCCP.

In [Figure 13](#), at baseline, WT had significantly more TOM20+/Rab5+ puncta compared to KO and the number of TOM20+/Rab5+ puncta increased significantly in KO while staying about the same in WT. By contrast, in [Figure 10](#), Rab5+/mNT were about the same at baseline and slightly, but not significantly, increased in both WT and KO with FCCP treatment. A reason for the discrepancies in Rab5+ puncta between Figures 8 and 11 may be found in the different timepoints in which experiments were performed. With n=22-27 cells total from 3 different coverslips per condition, the sample number may simply have been too small to be conclusive.

6.6. NECAB2 and MitoNEET represent a novel mtQC mechanism

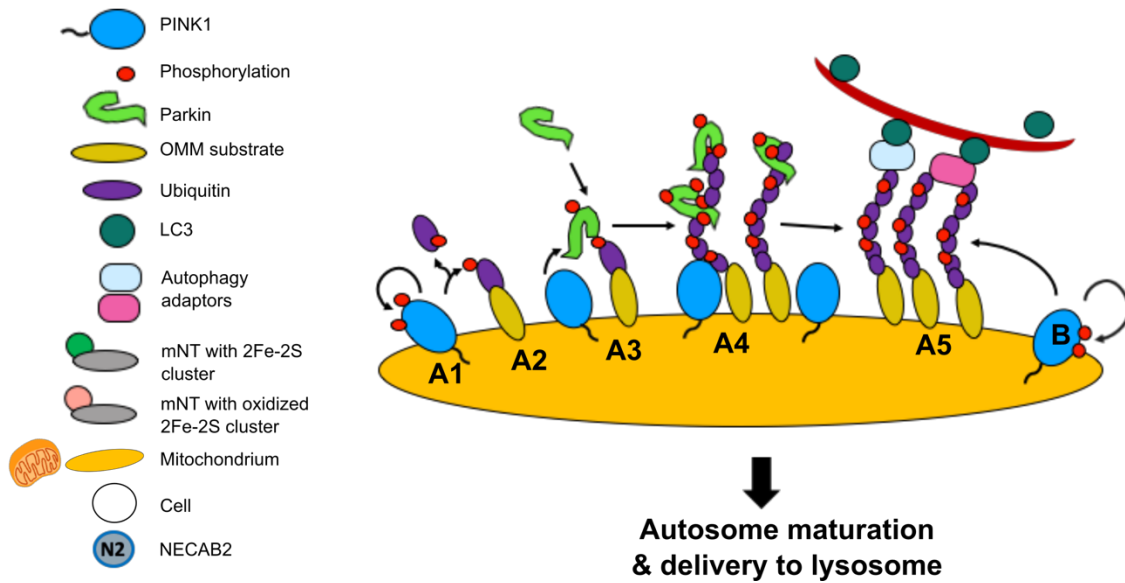


Figure 17: Canonical mitophagy.

Model of canonical mitophagy, based on Figure 2 in McWilliams and Muqit (2017, p. 85). **A1**) PINK1 is activated and autophosphorylates. **A2**) After PINK1-dependent ubiquitin phosphorylation, **A3**) Parkin is recruited and E3 activated, **A4**) which leads to OMM substrate ubiquitylation. **A5**) Polyubiquitination results in recruitment of autophagy adaptors, formation of autophagosomes and mitophagy. **B**) PINK1 can also directly activate mitophagy independently of Parkin, albeit at a lower rate. Figure representing mitochondrion: Sakowski (2016).

NECAB2/mitoNEET model

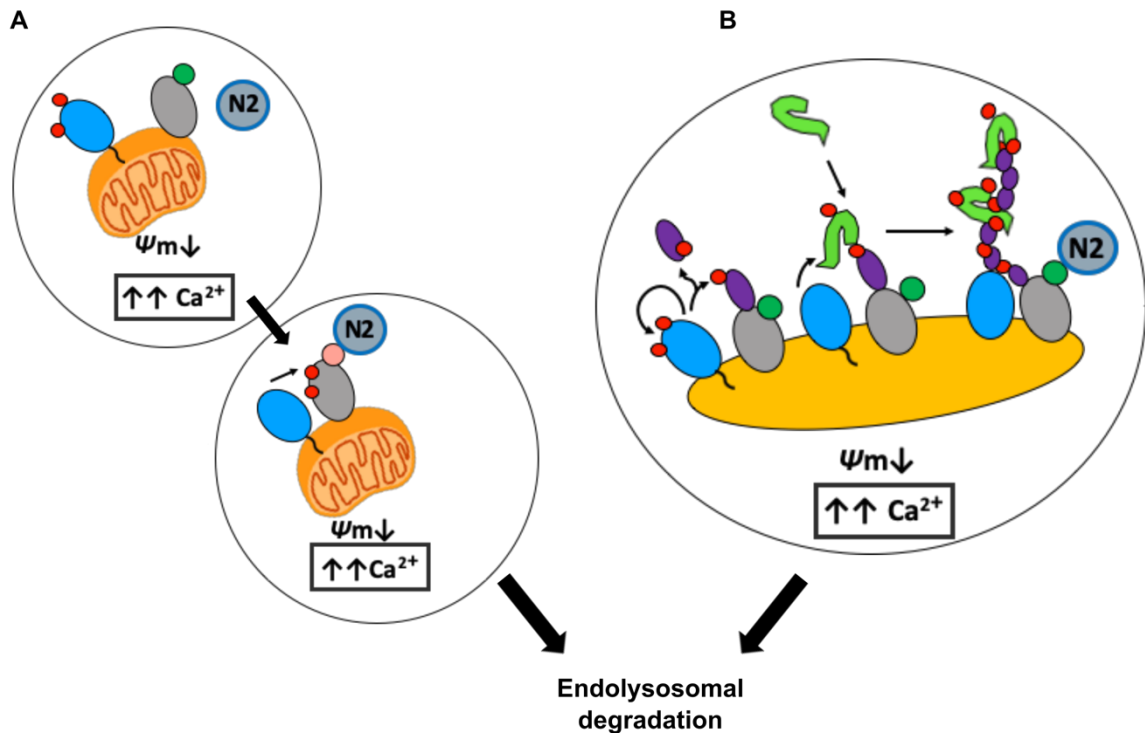


Figure 18: Proposed model of NECAB2 and MitoNEET-dependent mitophagy.

Proposed model of NECAB2 (N2) and MitoNEET (mNT)-triggered mitophagy, based on own experiments and findings from Dey et al. (2021): high calcium levels and low $\Delta\psi_m$ cause NECAB2 to shift to faulty mitochondria, where it binds to phosphorylated (A) or ubiquitinated (B) mNT and degrades mNT's 2Fe-2S cluster, marking faulty mitochondria for endolysosomal degradation.

The experiments performed thus far, combined with findings from our group, lead me to a model of NECAB2's involvement in mtQC ([Figure 18](#)), as opposed to canonical mtQC ([Figure 17](#)).

In canonical mitophagy, PINK1 activation and Parkin recruitment causes ubiquitin phosphorylation at the OMM. Polyubiquitination results in autophagy adaptors recruitment, autosome maturation, delivery to autophagosomes, and lastly, mitophagy. By contrast, in the model presented in [Figure 18](#), as suggested by Dey et al. (2021), high calcium levels, as a signal of mitochondrial distress, would cause NECAB2 to localize to faulty mitochondria. Here, NECAB2 binds to mNT, but only if mNT has previously been marked. This marking could be represented by PINK1-dependent phosphorylation or Parkin-dependent ubiquitination. Lazarou et al. (2013) have previously shown that mNT is ubiquitinated by Parkin. Furthermore, mNT lowers $\Delta\psi_m$ (Kusminski et al., 2016). High calcium levels combined with low $\Delta\psi_m$ would be a “double-hit”, i.e. an activity trigger that induces mitophagy. If like in prokaryotes, NECAB2's ABM domain were indeed a hemoxygenase, it could degrade mNT's 2Fe-2S cluster at mitochondria, thus tagging them for endolysosomal degradation. Karmi et al. (2017)'s model, presented in [chapter 2.7](#), demonstrates mNT's potential involvement in traditional autophagy. By contrast, the model proposed here follows Hammerling et al. (2017)'s findings that early endosomes are continually present in cells, making them a more suitable first-line defense mechanism for mtQC. When the damage exceeds endosomal capacity, canonical autophagy is initiated. I hence propose NECAB2 and mNT represent an alternative activity-triggered⁴ mitochondrial quality control system.

⁴ The activity being high calcium levels and low $\Delta\psi_m$

6.7. NECAB2's potential implications in disease

As reviewed in chapter [2.2.3](#), the striatum, where NECAB2 is mainly expressed, is affected in hyperkinetic disorders, Parkinson's disease (PD), and neuropsychiatric diseases. Given its role in mtQC, it is therefore feasible to think NECAB2 is implicated in neurodegeneration and disease. Indeed, Dey et al. (2021) found motor symptoms in NECAB2 KO mice: decreased motivation and sensory gating and increased catalepsy compared to WT animals.

As shown by Dey et al. (2021), NECAB2 is expressed in the substantia nigra, where degeneration of dopaminergic neurons causes PD. NECAB2 was upregulated in sporadic PD and patients with Leucine-rich repeat serine/threonine-protein kinase 2 (LRRK2) or acid β -glucocerebrosidase (GBA1) mutations (Fernandez-Santiago et al., 2015, Schondorf et al., 2014). Both GBA1 and LRRK2 mutations cause PD, and both GBA1 and LRRK2 are involved in endomembrane trafficking (Biskup et al., 2006, Magalhaes et al., 2016). For this reason, Dey et al. (2021) argue NECAB2 overexpression can somewhat alleviate the effect of PD-linked mutations. Given the redundancy of mtQC pathways, Dey et al. (2021) hypothesize loss of NECAB2 function results in upregulation of the Parkin-dependent ESCRT mtQC pathway described by Hammerling et al. (2017) (also refer to chapter [2.6.1.3](#)).

Furthermore, due to NECAB2's expression in peripheral α -motoneurons in the ventral horn of the spinal cord (Zhang et al., 2014), and NECAB2's recruitment of Rab5 and the endosomal machinery in MSNs, Dey et al. (2021) suggest NECAB2 could be involved in ALS' etiology.

6.8. NECAB2 is upregulated in human dopaminergic neurons with PD mutations but colocalizes more with Rab5 in isogenic control

As briefly touched on in the previous chapter, NECAB2 was upregulated in sporadic PD and in cells from patients harboring PD-associated mutations in LRRK2 or in GBA1 (Fernandez-Santiago et al., 2015, Schondorf et al., 2014). Concurrently, I was able to show NECAB2 and mNT upregulation in iPSC-derived dopaminergic neurons in two distinct PINK1 knockouts when compared to their isogenic control ([Figure 15](#)). Unfortunately, due to technical difficulties I was able to perform Western blot for NE-

CAB2 only in samples from two distinct differentiations and for mNT only in samples from a single differentiation. However, repeated Western blots with the same samples consistently showed higher amounts of NECAB2 and mNT in the two PINK1 KOs. Interestingly, ICC showed more colocalization between Rab5 and NECAB2 in the isogenic control than in either PINK1 KO ([Figure 16](#)).

mNT and NECAB2 colocalization was also seemingly stronger in K7.1; however, with a PC of 0,55 it is difficult to establish whether this is due to real colocalization events. A caveat: ICC studies were performed in only one differentiation (differentiation 66), because the neurons from differentiation 67 and 68 did not grow as planned. Furthermore, due to time constraints I was not able to perform Imaris analysis on these images but again used PC. However, this time I took z-stacks at better resolution and collapsed them for analysis in ImageJ, making the results, especially Rab5/NECAB2 colocalization, more feasible in my opinion.

The fact that NECAB2 and mNT were upregulated in both PINK1 KOs could be explained by two different mechanisms. In the first case, NECAB2/mNT is PINK1/Parkin-dependent (e.g., for phosphorylation/ubiquitination)⁵. If PINK1/Parkin are missing, less mitochondria are degraded and hence more NECAB2 and mNT remain in the cell. In this case, the higher colocalization between Rab5 and NECAB2 in the isogenic control could either be a product of lower NECAB2 levels in the isogenic control, or yet another sign that the many different mtQC pathways⁶ simply work better and more in tandem in healthy cells. In the second case, NECAB2/mNT can be activated by a kinase other than PINK1/Parkin and hence activate mitophagy – probably at a slower rate than the canonical pathway – and somewhat compensate PINK1/Parkin loss. In this case, however, I would have expected higher Rab5/NECAB2 colocalization in the PINK1 KO cells. To settle which of the two hypotheses is correct, experiments with PINK1 and NECAB2 KO compared to KO of only PINK1 and only NECAB2 would need to be performed. If, as I suspect, hypothesis one was correct, double KO should not affect the cell more than KO of either PINK1 or NECAB2 by itself. By contrast, if hypothesis two was correct, double KO should result in less mitophagy and a more severe phenotype than either single KO.

⁵ As reviewed in chapter [2.7](#), Lazarou et al. found mNT is indeed a substrate of Parkin ubiquitination. (Lazarou et al., 2013)

⁶ Presented in chapter [2.6](#).

7. Summary

In recent years, more and more mitochondrial quality control (mtQC) pathways, sometimes overlapping, have been discovered. Neurons cannot proliferate and, at the same time, have high energy demands, requiring carefully orchestrated mtQC to ensure mitochondrial health. The mtQC pathways can, to some degree, compensate for each other (Hammerling et al., 2017); the impact of each one remains to be measured. This may help explain why most neurodegenerative diseases, whether sporadic or caused by gene mutations, usually manifest at an advanced age. In this thesis I propose a novel activity-triggered mitochondrial quality control (mtQC) mechanism actuated by neuronal calcium-binding protein 2 (NECAB2) and MitoNEET (mNT). NECAB2 is a protein primarily found in the striatum and was first described by Bernier et al. in 2001, while mNT was first described as a target of the type 2 diabetes drug pioglitazone by Colca et al. (2004).

In my experiments, I was able to demonstrate that NECAB2, which was originally described as a cytosolic protein (Canela et al., 2009), is present at mitochondria and involved in mtQC. My mNT and NECAB2 colocalization studies were inconclusive, but mNT expression was increased in cells expressing NECAB2 compared to cells with no NECAB2 expression. I hence here propose a model for NECAB2-mediated mitochondrial quality control: high calcium levels caused by damaged mitochondria combined with low mitochondrial membrane potential ($\Delta\psi_m$) represent a mitophagy-inducing “double-hit”. As speculated by Dey et al. (2021), high calcium levels would cause NECAB2’s localization to defective mitochondria. I hypothesize that NECAB2 then binds to phosphorylated or ubiquitinated mNT. Here, thanks to its ABM domain, NECAB2 degrades mNT’s 2Fe-2S cluster, thus tagging mitochondria for degradation. Concurrently, Karmi et al. (2017) proposed mNT plays a role in traditional autophagy. Furthermore, mNT is a Parkin ubiquitination substrate (Lazarou et al., 2013) and lowers the mitochondrial membrane potential ($\Delta\psi_m$) (Kusminski et al., 2016). The ABM domain’s function in NECAB2 has not been uncovered yet, but analogous monooxygenases in prokaryotes degrade heme to ferrous iron (Lojek et al., 2017, Lyles and Eichenbaum, 2018).

mNT KO in mice results in a Parkinson’s disease (PD) phenotype (Geldenhuys et al., 2017). NECAB2 KO in mice results in motor symptoms (Dey et al., 2021) and the expression of NECAB2 is upregulated in patients with sporadic PD and genetic PD

mutations (Fernandez-Santiago et al., 2015, Schondorf et al., 2014). Along with Dey et al. (2021), I speculate NECAB2 could thus be involved in the etiology of PD, but also in amyotrophic lateral syndrome (ALS). Congruently, in human iPSCs-derived dopaminergic neurons, I was able to demonstrate NECAB2 and mNT upregulation in two different PINK1 KOs compared to their isogenic control.

Given early endosomes' continuous presence in the cell, Hammerling et al. (2017) propose they are a first-line defense against malfunctioning mitochondria. If the damage exceeds endosomal capacity, canonical autophagy is initiated. The results from my experiments lead me to conclude that NECAB2/mNT-dependent mtQC is also a first-line defense mechanism and therefore tags mitochondria for endolysosomal degradation, rather than traditional autophagy. Indeed, mitochondrial and endosomal colocalization in primary striatal neurons from NECAB2 WT and KO mice was about the same at baseline and dramatically increased in KO after treatment with the mitochondrial uncoupler FCCP. This is probably because mitochondrial distress caused by FCCP and KO (over-) activates other mtQC pathways involving Rab5 (an endosomal marker). The rest of my experiments to study Rab5's implication in the NECAB2/mNT mtQC mechanism were inconclusive. However, in healthy human iPSCs-derived dopaminergic neurons, NECAB2 and Rab5 colocalization was significantly increased compared to the two PINK1 KOs. This has two potential explanations: if the NECAB2/mNT pathway is PINK1/Parkin-dependent, NECAB2 and mNT would not be degraded in PINK1 KO, explaining their higher levels in Western blot. Higher colocalization between Rab5 and NECAB2 in healthy cells could be a product of lower NECAB2 levels or it could be an indicator for better mtQC orchestration. On the other hand, if NECAB2/mNT can be phosphorylated by a kinase other than PINK1/Parkin, it could activate mitophagy in PINK1 KO cells while somewhat compensating PINK1/Parkin loss. In this case, however, I would have expected higher Rab5/NECAB2 colocalization in the PINK1 KO cells. To settle which of the two hypotheses is correct, more experiments need to be performed comparing single NECAB2 and PINK1 KO to double KO. In any case, NECAB2's involvement in mtQC and upregulation in cells derived from PD patients make it an interesting potential therapeutic target in PD, but further experimental work is required.

8. Zusammenfassung

In den vergangenen Jahren wurden immer mehr Signalwege der mitochondrialen Qualitätskontrolle (mtQK) entdeckt, die sich zum Teil überschneiden. Neuronen sind nicht teilungsfähig und haben gleichzeitig einen hohen Energiebedarf, weswegen hier die mtQK eine besondere Rolle spielt. Die mtQK-Signalwege können sich in gewisser Hinsicht gegenseitig kompensieren (Hammerling et al., 2017); die Bedeutung der einzelnen Signalwege ist noch nicht abschließend geklärt. Dies erklärt ansatzweise, warum die meisten neurodegenerativen Erkrankungen – sowohl sporadisch auftretend als auch durch Genmutationen bedingt – eher im höheren Alter auftreten. In dieser Dissertation schlage ich einen neuen, durch Aktivität ausgelösten Signalweg der mitochondrialen Qualitätskontrolle vor, der durch das Neuronale Kalziumbindende Protein 2 (NECAB2) und MitoNEET (mNT) vermittelt wird. NECAB2 ist ein vor allem im Striatum vorkommendes Protein und wurde zuerst von Bernier et al. 2001 beschrieben, während mNT als erstes von Colca et al. (2004) als Zielstruktur von Pioglitazon (ein Antidiabetikum) beschrieben wurde.

In meinen Experimenten konnte ich zeigen, dass das ursprünglich als zytosolisch vorkommend beschriebene NECAB2 (Canela et al., 2009) auch an Mitochondrien vorkommt und in der mtQK eine Rolle spielt. Meine Experimente zur Kollokalisierung von NECAB2 und mNT waren nicht eindeutig. Die Expression von mNT in NECAB2-exprimierenden Zellen war jedoch im Vergleich zu Zellen ohne NECAB2-Expression deutlich erhöht. Daher schlage ich folgendes Modell für die NECAB2-vermittelte mtQK vor: erhöhte Kalziumkonzentrationen (durch geschädigte Mitochondrien hervorgerufen), kombiniert mit niedrigem mitochondrialen Membranpotential ($\Delta\psi_m$), stellen einen Mitophagie-induzierenden „Doppelschlag“ dar. Wie von Dey et al. (2021) vorgeschlagen, würden erhöhte Kalziumkonzentrationen NECAB2s Verlagerung an beschädigte Mitochondrien veranlassen. Ich stelle die Hypothese auf, dass NECAB2 dort an phosphoryliertes oder ubiquitiniertes mNT bindet. Dank seiner ABM-Domäne degradiert NECAB2 mNTs Eisen-Schwefel-Cluster und markiert somit Mitochondrien für den Abbau. Tatsächlich wurde mNT bereits von Karmi et al. (2017) als Interaktionspartner der traditionellen Autophagie vorgeschlagen. Zudem zeigten Lazarou et al. (2013), dass mNT von Parkin ubiquitiniert wird und Kusminski et al. (2016) bewiesen, dass mNT das mitochondriale Membranpotential ($\Delta\psi_m$) vermindert. Die Funktion von NECAB2s ABM-Domäne ist noch nicht geklärt, ähnliche Monooxygenasen

degradieren in Prokaryoten jedoch Häm zu Eisen (Lojek et al., 2017, Lyles and Eichenbaum, 2018).

Knockout (KO) von mNT in Mäusen verursachte einen Parkinson-typischen Phänotyp (Geldenhuys et al., 2017). NECAB2-KO verursacht in Mäusen ebenso motorische Symptome (Dey et al., 2021). Des Weiteren ist NECAB2 sowohl bei Patienten mit sporadisch auftretendem als auch mit genetisch bedingtem Parkinson hochreguliert (Fernandez-Santiago et al., 2015, Schondorf et al., 2014). NECAB2 könnte daher in die Ätiologie von Parkinson, aber auch von amyotropher Lateralsklerose verwickelt sein (Dey et al., 2021). Erwartungsgemäß konnte ich in humanen, aus iPSC gewonnenen, dopaminergischen Neuronen eine Erhöhung von NECAB2 und mNT in zwei unterschiedlichen PINK1-KOs zeigen.

Da sie kontinuierlich in der Zelle präsent sind, schlagen Hammerling et al. (2017) frühe Endosomen als erste Abwehr gegen geschädigte Mitochondrien vor. Ist die endosomale Kapazität überstiegen, wird die kanonische Autophagie initiiert. Ich vermute, dass NECAB2/mNT ebenso eine erste Abwehr darstellt und Mitochondrien für den endolysosomalen Abbau markiert. Tatsächlich stieg die anfangs in NECAB2-Wildtyp (WT) und -KO ungefähr gleiche mitochondriale-endosomale Kolokalisation nach Behandlung mit dem mitochondrialen Entkoppler FCCP stark in den KO-Zellen. Der durch FCCP und KO bedingte mitochondriale Stress (über-)aktiviert wahrscheinlich andere mtQK-Mechanismen, in denen der endosomale Marker Rab5 eine Rolle spielt. Die restlichen Experimente zu Rab5s Rolle im NECAB2/mNT-Signalweg waren unschlüssig. Interessanterweise war jedoch die Kolokalisation zwischen NECAB2 und Rab5 in gesunden humanen dopaminergischen Neuronen deutlich erhöht im Vergleich zu den zwei PINK1 KOs. Zwei Ansätze könnten dies erklären: falls der NECAB2/mNT-Signalweg PINK1/Parkin-abhängig ist, würden NECAB2 und mNT in PINK1 KO-Zellen nicht degradiert werden, was ihre höhere Konzentration im Western Blot erklären würde. Die höhere Kolokalisation von NECAB2 und mNT in gesunden Zellen könnte demnach eine Folge der niedrigeren NECAB2-Konzentration oder ein Zeichen der besser funktionierenden mtQK sein. Sollte hingegen eine andere Kinase mNT phosphorylieren, könnten NECAB2 und mNT die Mitophagie in PINK1 KO-Zellen aktivieren und den PINK1/Parkin-Verlust ansatzweise kompensieren. In diesem Falle hätte ich jedoch eine erhöhte Rab5/NECAB2-Kolokalisation in den PINK1 KO-Zellen erwartet. Um herauszufinden, welche der Hypothesen korrekt ist, müssten Experimente mit NECAB2-, PINK1- und doppeltem KO durchgeführt wer-

den. In jedem Fall machen seine Beteiligung an der mtQK und seine Hochregulierung in Zellen von Parkinsonpatienten NECAB2 zu einem interessanten potentiellen therapeutischen Angriffspunkt. Um an diesen Punkt zu kommen, wären jedoch weitere Experimente notwendig.

Literature

AHMAD, K., SCHNEIDER, H. G. & STRONG, F. M. 1950. Studies on the biological action of antimycin A. *Arch Biochem*, 28, 281-94.

ALBERTS, B., LEWIS, J., MORGAN, D., RAFF, M., ROBERTS, K., WALTER, P., JOHNSON, A. D., SCHMIFER, U. & HORSTMANN, C. 2017. *Molekularbiologie der Zelle*, Weinheim, GERMANY, John Wiley & Sons, Incorporated.

AMR, S., HEISEY, C., ZHANG, M., XIA, X. J., SHOWS, K. H., AJLOUNI, K., PANDYA, A., SATIN, L. S., EL-SHANTI, H. & SHIANG, R. 2007. A homozygous mutation in a novel zinc-finger protein, ERIS, is responsible for Wolfram syndrome 2. *Am J Hum Genet*, 81, 673-83.

ANDERSSON, S. G., KARLBERG, O., CANBACK, B. & KURLAND, C. G. 2003. On the origin of mitochondria: a genomics perspective. *Philos Trans R Soc Lond B Biol Sci*, 358, 165-77; discussion 177-9.

AXE, E. L., WALKER, S. A., MANIFAVA, M., CHANDRA, P., RODERICK, H. L., HABERMANN, A., GRIFFITHS, G. & KTISTAKIS, N. T. 2008. Autophagosome formation from membrane compartments enriched in phosphatidylinositol 3-phosphate and dynamically connected to the endoplasmic reticulum. *J Cell Biol*, 182, 685-701.

BAI, F., MORCOS, F., SOHN, Y. S., DARASH-YAHANA, M., REZENDE, C. O., LIPPER, C. H., PADDOCK, M. L., SONG, L., LUO, Y., HOLT, S. H., TAMIR, S., THEODORAKIS, E. A., JENNINGS, P. A., ONUCHIC, J. N., MITTLER, R. & NECHUSHTAI, R. 2015. The Fe-S cluster-containing NEET proteins mitoNEET and NAF-1 as chemotherapeutic targets in breast cancer. *Proc Natl Acad Sci U S A*, 112, 3698-703.

BAMFORD, I. J. & BAMFORD, N. S. 2019. The Striatum's Role in Executing Rational and Irrational Economic Behaviors. *Neuroscientist*, 25, 475-490.

BANCI, L., BERTINI, I., CALDERONE, V., CIOFI-BAFFONI, S., GIACHETTI, A., JAISWAL, D., MIKOLAJCZYK, M., PICCIOLI, M. & WINKELMANN, J. 2013. Molecular view of an electron transfer process essential for iron-sulfur protein biogenesis. *Proc Natl Acad Sci U S A*, 110, 7136-41.

BATTAGLIA, A. M., CHIRILLO, R., AVERSA, I., SACCO, A., COSTANZO, F. & BIAMONTE, F. 2020. Ferroptosis and Cancer: Mitochondria Meet the "Iron Maiden" Cell Death. *Cells*, 9.

BERNHEIMER, H., BIRKMAYER, W., HORNYKIEWICZ, O., JELLINGER, K. & SEITELBERGER, F. 1973. Brain dopamine and the syndromes of Parkinson and Huntington. Clinical, morphological and neurochemical correlations. *J Neurol Sci*, 20, 415-55.

BERNIER, G., VUKOVICH, W., NEIDHARDT, L., HERRMANN, B. G. & GRUSS, P. 2001. Isolation and characterization of a downstream target of Pax6 in the mammalian retinal primordium. *Development*, 128, 3987-94.

BISKUP, S., MOORE, D. J., CELSI, F., HIGASHI, S., WEST, A. B., ANDRABI, S. A., KURKINEN, K., YU, S. W., SAVITT, J. M., WALDVOGEL, H. J., FAULL, R. L., EMSON, P. C., TORP, R., OTTERSEN, O. P., DAWSON, T. M. & DAWSON, V. L. 2006. Localization of LRRK2 to membranous and vesicular structures in mammalian brain. *Ann Neurol*, 60, 557-69.

|

- BOLTE, S. & CORDELIERES, F. P. 2006. A guided tour into subcellular colocalization analysis in light microscopy. *J Microsc*, 224, 213-32.
- BREWER, J. A. & POTENZA, M. N. 2008. The neurobiology and genetics of impulse control disorders: relationships to drug addictions. *Biochem Pharmacol*, 75, 63-75.
- BUS, C., ZIZMARE, L., FELDKAEMPER, M., GEISLER, S., ZARANI, M., SCHAEGLER, A., KLOSE, F., ADMARD, J., MAGEEAN, C. J., ARENA, G., FALLIER-BECKER, P., UGUN-KLUSEK, A., MARUSZCZAK, K. K., KAPOLOU, K., SCHMID, B., RAPAPORT, D., UEFFING, M., CASADEI, N., KRUGER, R., GASSER, T., VOGT WEISENHORN, D. M., KAHLE, P. J., TRAUTWEIN, C., GLOECKNER, C. J. & FITZGERALD, J. C. 2020. Human Dopaminergic Neurons Lacking PINK1 Exhibit Disrupted Dopamine Metabolism Related to Vitamin B6 Co-Factors. *iScience*, 23, 101797.
- CAMPSTEIJN, C., VIETRI, M. & STENMARK, H. 2016. Novel ESCRT functions in cell biology: spiraling out of control? *Curr Opin Cell Biol*, 41, 1-8.
- CANELA, L., FERNÁNDEZ-DUEÑAS, V., ALBERGARIA, C., WATANABE, M., LLUÍS, C., MALLOL, J., CANELA, E. I., FRANCO, R., LUJÁN, R. & CIRUELA, F. 2009. The association of metabotropic glutamate receptor type 5 with the neuronal Ca²⁺-binding protein 2 modulates receptor function. *J Neurochem*, 111, 555-67.
- CANELA, L., LUJAN, R., LLUIS, C., BURGUENO, J., MALLOL, J., CANELA, E. I., FRANCO, R. & CIRUELA, F. 2007. The neuronal Ca(2+) -binding protein 2 (NECAB2) interacts with the adenosine A(2A) receptor and modulates the cell surface expression and function of the receptor. *Mol Cell Neurosci*, 36, 1-12.
- CEBALLOS-BAUMANN, A. 2018. *Idiopathisches Parkinson-Syndrom (IPS)*. In: Berlit P. (eds) *Klinische Neurologie*. Springer Reference Medizin. .
- CHANG, N. C., NGUYEN, M., GERMAIN, M. & SHORE, G. C. 2010. Antagonism of Beclin 1-dependent autophagy by BCL-2 at the endoplasmic reticulum requires NAF-1. *EMBO J*, 29, 606-18.
- CHEN, H. & CHAN, D. C. 2009. Mitochondrial dynamics--fusion, fission, movement, and mitophagy--in neurodegenerative diseases. *Hum Mol Genet*, 18, R169-76.
- CHEN, H., DETMER, S. A., EWALD, A. J., GRIFFIN, E. E., FRASER, S. E. & CHAN, D. C. 2003. Mitofusins Mfn1 and Mfn2 coordinately regulate mitochondrial fusion and are essential for embryonic development. *J Cell Biol*, 160, 189-200.
- CHEN, P. L., CHEN, Y. M., BOOKSTEIN, R. & LEE, W. H. 1990. Genetic mechanisms of tumor suppression by the human p53 gene. *Science*, 250, 1576-80.
- CHEN, Y. F., KAO, C. H., CHEN, Y. T., WANG, C. H., WU, C. Y., TSAI, C. Y., LIU, F. C., YANG, C. W., WEI, Y. H., HSU, M. T., TSAI, S. F. & TSAI, T. F. 2009. Cisd2 deficiency drives premature aging and causes mitochondria-mediated defects in mice. *Genes Dev*, 23, 1183-94.
- COLCA, J. R., MCDONALD, W. G., WALDON, D. J., LEONE, J. W., LULL, J. M., BANNOW, C. A., LUND, E. T. & MATHEWS, W. R. 2004. Identification of a novel mitochondrial protein ("mitoNEET") cross-linked specifically by a thiazolidinedione photoprobe. *Am J Physiol Endocrinol Metab*, 286, E252-60.

CONLAN, A. R., AXELROD, H. L., COHEN, A. E., ABRESCH, E. C., ZURIS, J., YEE, D., NECHUSHTAI, R., JENNINGS, P. A. & PADDOCK, M. L. 2009. Crystal structure of Miner1: The redox-active 2Fe-2S protein causative in Wolfram Syndrome 2. *J Mol Biol*, 392, 143-53.

DAMIANO, M., GALVAN, L., DEGLON, N. & BROUILLET, E. 2010. Mitochondria in Huntington's disease. *Biochim Biophys Acta*, 1802, 52-61.

DARASH-YAHANA, M., POZNIAK, Y., LU, M., SOHN, Y. S., KARMI, O., TAMIR, S., BAI, F., SONG, L., JENNINGS, P. A., PIKARSKY, E., GEIGER, T., ONUCHIC, J. N., MITTLER, R. & NECHUSHTAI, R. 2016. Breast cancer tumorigenicity is dependent on high expression levels of NAF-1 and the lability of its Fe-S clusters. *Proc Natl Acad Sci U S A*, 113, 10890-5.

DAVIS, J. B. & MAHER, P. 1994. Protein kinase C activation inhibits glutamate-induced cytotoxicity in a neuronal cell line. *Brain Res*, 652, 169-73.

DELONG, M. R. & WICHMANN, T. 2007. Circuits and circuit disorders of the basal ganglia. *Arch Neurol*, 64, 20-4.

DEN HARTOG JAGER, W. & BETHLEM, J. 1960. The distribution of Lewy bodies in the central and autonomic nervous systems in idiopathic paralysis agitans. *J Neurol Neurosurg Psychiatry*, 23, 283-90.

DEY, P. N., BUENO, D., SCHACHT, T., WOLF, C., WÜLLNER, V., MORPURGO, E., ROJAS-CHARRY, L., SESSINGHAUS, L., LEUKEL, P., SOMMER, C., RADYUSHKIN, K., SCHÄFER, M. K. E., FLORIN, L., TENZER, S., BAUMGART, J., STAMM, P., DAIBER, A., HORTA, G., NARDI, L., VASIC, V., SCHMEISSER, M. J., HELLWIG, A., OSKAMP, A., BAUER, A., ANAND, R., REICHERT, A. S., RITZ, S., SILIES, M., FRAUENKNECHT, K. B. M. & METHNER, A. 2021. NECAB2 orchestrates an endosomal pathway of mitochondrial quality control at striatal synapses. *bioRxiv*, 2021.02.15.431234.

DIXON, S. J., LEMBERG, K. M., LAMPRECHT, M. R., SKOUTA, R., ZAITSEV, E. M., GLEASON, C. E., PATEL, D. N., BAUER, A. J., CANTLEY, A. M., YANG, W. S., MORRISON, B., 3RD & STOCKWELL, B. R. 2012. Ferroptosis: an iron-dependent form of nonapoptotic cell death. *Cell*, 149, 1060-72.

DUPONT, N., NASCIMBENI, A. C., MOREL, E. & CODOGNO, P. 2017. Molecular Mechanisms of Noncanonical Autophagy. *Int Rev Cell Mol Biol*, 328, 1-23.

EVANS, C. S. & HOLZBAUR, E. L. F. 2020. Quality Control in Neurons: Mitophagy and Other Selective Autophagy Mechanisms. *J Mol Biol*, 432, 240-260.

FERECATU, I., GONCALVES, S., GOLINELLI-COHEN, M. P., CLEMANCEY, M., MARTELLI, A., RIQUIER, S., GUITTET, E., LATOUR, J. M., PUCCIO, H., DRAPIER, J. C., LESCOP, E. & BOUTON, C. 2014. The diabetes drug target MitoNEET governs a novel trafficking pathway to rebuild an Fe-S cluster into cytosolic aconitase/iron regulatory protein 1. *J Biol Chem*, 289, 28070-86.

FERNANDEZ-SANTIAGO, R., CARBALLO-CARBAJAL, I., CASTELLANO, G., TORRENT, R., RICHAUD, Y., SANCHEZ-DANES, A., VILARRASA-BLASI, R., SANCHEZ-PLA, A., MOSQUERA, J. L., SORIANO, J., LOPEZ-BARNEO, J., CANALS, J. M., ALBERCH, J., RAYA, A., VILA, M., CONSIGLIO, A., MARTIN-SUBERO, J. I., EZQUERRA, M. & TOLOSA, E. 2015. Aberrant epigenome in iPSC-derived dopaminergic neurons from Parkinson's disease patients. *EMBO Mol Med*, 7, 1529-46.

FERRE, S., LLUIS, C., JUSTINOVA, Z., QUIROZ, C., ORRU, M., NAVARRO, G., CANELA, E. I., FRANCO, R. & GOLDBERG, S. R. 2010. Adenosine-cannabinoid receptor interactions. Implications for striatal function. *Br J Pharmacol*, 160, 443-53.

FINEBERG, N. A., POTENZA, M. N., CHAMBERLAIN, S. R., BERLIN, H. A., MENZIES, L., BECHARA, A., SAHAKIAN, B. J., ROBBINS, T. W., BULLMORE, E. T. & HOLLANDER, E. 2010. Probing compulsive and impulsive behaviors, from animal models to endophenotypes: a narrative review. *Neuropsychopharmacology*, 35, 591-604.

GEGG, M. E., COOPER, J. M., CHAU, K. Y., ROJO, M., SCHAPIRA, A. H. & TAANMAN, J. W. 2010. Mitofusin 1 and mitofusin 2 are ubiquitinated in a PINK1/parkin-dependent manner upon induction of mitophagy. *Hum Mol Genet*, 19, 4861-70.

GEGG, M. E., COOPER, J. M., SCHAPIRA, A. H. & TAANMAN, J. W. 2009. Silencing of PINK1 expression affects mitochondrial DNA and oxidative phosphorylation in dopaminergic cells. *PLoS One*, 4, e4756.

GEISLER, S., HOLMSTROM, K. M., SKUJAT, D., FIESEL, F. C., ROTHFUSS, O. C., KAHLE, P. J. & SPRINGER, W. 2010. PINK1/Parkin-mediated mitophagy is dependent on VDAC1 and p62/SQSTM1. *Nat Cell Biol*, 12, 119-31.

GELDENHUYS, W. J., BENKOVIC, S. A., LIN, L., YONUTAS, H. M., CRISH, S. D., SULLIVAN, P. G., DARVESH, A. S., BROWN, C. M. & RICHARDSON, J. R. 2017. MitoNEET (CISD1) Knockout Mice Show Signs of Striatal Mitochondrial Dysfunction and a Parkinson's Disease Phenotype. *ACS Chem Neurosci*, 8, 2759-2765.

GELMETTI, V., DE ROSA, P., TOROSANTUCCI, L., MARINI, E. S., ROMAGNOLI, A., DI RIENZO, M., ARENA, G., VIGNONE, D., FIMIA, G. M. & VALENTE, E. M. 2017. PINK1 and BECN1 relocalize at mitochondria-associated membranes during mitophagy and promote ER-mitochondria tethering and autophagosome formation. *Autophagy*, 13, 654-669.

GERBER, K. J., DAMMER, E. B., DUONG, D. M., DENG, Q., DUDEK, S. M., SEYFRIED, N. T. & HEPLER, J. R. 2019. Specific Proteomes of Hippocampal Regions CA2 and CA1 Reveal Proteins Linked to the Unique Physiology of Area CA2. *J Proteome Res*, 18, 2571-2584.

GERFEN, C. R. 1992. The neostriatal mosaic: multiple levels of compartmental organization. *Trends Neurosci*, 15, 133-9.

GRAY, M. W., BURGER, G. & LANG, B. F. 1999. Mitochondrial evolution. *Science*, 283, 1476-81.

GRIFFITHS, K. K. & LEVY, R. J. 2017. Evidence of Mitochondrial Dysfunction in Autism: Biochemical Links, Genetic-Based Associations, and Non-Energy-Related Mechanisms. *Oxid Med Cell Longev*, 2017, 4314025.

HAMASAKI, M., FURUTA, N., MATSUDA, A., NEZU, A., YAMAMOTO, A., FUJITA, N., OOMORI, H., NODA, T., HARAGUCHI, T., HIRAOKA, Y., AMANO, A. & YOSHIMORI, T. 2013. Autophagosomes form at ER-mitochondria contact sites. *Nature*, 495, 389-93.

HAMDI, A., ROSHAN, T. M., KAHAWITA, T. M., MASON, A. B., SHEFTEL, A. D. & PONKA, P. 2016. Erythroid cell mitochondria receive endosomal iron by a "kiss-and-run" mechanism. *Biochim Biophys Acta*, 1863, 2859-2867.

HAMMERLING, B. C., NAJOR, R. H., CORTEZ, M. Q., SHIRES, S. E., LEON, L. J., GONZALEZ, E. R., BOASSA, D., PHAN, S., THOR, A., JIMENEZ, R. E., LI, H., KITSIS, R. N., DORN, G. W., II, SADOSHIMA, J., ELLISMAN, M. H. & GUSTAFSSON, A. B. 2017. A Rab5 endosomal pathway mediates Parkin-dependent mitochondrial clearance. *Nat Commun*, 8, 14050.

HAWKES, C. H., SHEPHARD, B. C. & DANIEL, S. E. 1997. Olfactory dysfunction in Parkinson's disease. *J Neurol Neurosurg Psychiatry*, 62, 436-46.

HEYTLER, P. G. & PRICHARD, W. W. 1962. A new class of uncoupling agents--carbonyl cyanide phenylhydrazones. *Biochem Biophys Res Commun*, 7, 272-5.

HSU, F., SPANNL, S., FERGUSON, C., HYMAN, A. A., PARTON, R. G. & ZERIAL, M. 2018. Rab5 and Alsin regulate stress-activated cytoprotective signaling on mitochondria. *Elife*, 7.

IKAWA, F., TANAKA, S., HARADA, K., HIDE, I., MARUYAMA, H. & SAKAI, N. 2020. Detailed neuronal distribution of GPR3 and its co-expression with EF-hand calcium-binding proteins in the mouse central nervous system. *Brain Res*, 1750, 147166.

ITAKURA, E., KISHI-ITAKURA, C., KOYAMA-HONDA, I. & MIZUSHIMA, N. 2012. Structures containing Atg9A and the ULK1 complex independently target depolarized mitochondria at initial stages of Parkin-mediated mitophagy. *J Cell Sci*, 125, 1488-99.

KARMI, O., HOLT, S. H., SONG, L., TAMIR, S., LUO, Y., BAI, F., ADENWALLA, A., DARASH-YAHANA, M., SOHN, Y. S., JENNINGS, P. A., AZAD, R. K., ONUCHIC, J. N., MORCOS, F., NECHUSHTAI, R. & MITTLER, R. 2017. Interactions between mitoNEET and NAF-1 in cells. *PLoS One*, 12, e0175796.

KENNEDY, M. C., MENDE-MUELLER, L., BLONDIN, G. A. & BEINERT, H. 1992. Purification and characterization of cytosolic aconitase from beef liver and its relationship to the iron-responsive element binding protein. *Proc Natl Acad Sci U S A*, 89, 11730-4.

KILLACKEY, S. A., PHILPOTT, D. J. & GIRARDIN, S. E. 2020. Mitophagy pathways in health and disease. *J Cell Biol*, 219.

KING, J. V., LIANG, W. G., SCHERPELZ, K. P., SCHILLING, A. B., MEREDITH, S. C. & TANG, W. J. 2014. Molecular basis of substrate recognition and degradation by human presequence protease. *Structure*, 22, 996-1007.

KOENTJORO, B., PARK, J. S., HA, A. D. & SUE, C. M. 2012. Phenotypic variability of parkin mutations in single kindred. *Mov Disord*, 27, 1299-303.

KOENTJORO, B., PARK, J. S. & SUE, C. M. 2017. Nix restores mitophagy and mitochondrial function to protect against PINK1/Parkin-related Parkinson's disease. *Sci Rep*, 7, 44373.

KOSZLA, O., TARGOWSKA-DUDA, K. M., KEDZIERSKA, E. & KACZOR, A. A. 2020. In Vitro and In Vivo Models for the Investigation of Potential Drugs Against Schizophrenia. *Biomolecules*, 10.

KUSMINSKI, C. M., CHEN, S., YE, R., SUN, K., WANG, Q. A., SPURGIN, S. B., SANDERS, P. E., BROZINICK, J. T., GELDENHUYS, W. J., LI, W. H., UNGER, R. H. & SCHERER, P. E. 2016. MitoNEET-Parkin Effects in Pancreatic alpha- and beta-Cells, Cellular Survival, and Intra-islet Cross Talk. *Diabetes*, 65, 1534-55.

- LANDRY, A. P., CHENG, Z. & DING, H. 2015. Reduction of mitochondrial protein mitoNEET [2Fe-2S] clusters by human glutathione reductase. *Free Radic Biol Med*, 81, 119-27.
- LAZAROU, M., NARENDRA, D. P., JIN, S. M., TEKLE, E., BANERJEE, S. & YOULE, R. J. 2013. PINK1 drives Parkin self-association and HECT-like E3 activity upstream of mitochondrial binding. *J Cell Biol*, 200, 163-72.
- LAZAROU, M., SLITER, D. A., KANE, L. A., SARRAF, S. A., WANG, C., BURMAN, J. L., SIDERIS, D. P., FOGEL, A. I. & YOULE, R. J. 2015. The ubiquitin kinase PINK1 recruits autophagy receptors to induce mitophagy. *Nature*, 524, 309-314.
- LEE, D. S., TOMITA, S., KIRINO, Y. & SUZUKI, T. 2000. Regulation of X11L-dependent amyloid precursor protein metabolism by XB51, a novel X11L-binding protein. *J Biol Chem*, 275, 23134-8.
- LIANG, X. H., JACKSON, S., SEAMAN, M., BROWN, K., KEMPKES, B., HIBSHOOSH, H. & LEVINE, B. 1999. Induction of autophagy and inhibition of tumorigenesis by beclin 1. *Nature*, 402, 672-6.
- LILL, R., DIEKERT, K., KAUT, A., LANGE, H., PELZER, W., PROHL, C. & KISPAL, G. 1999. The essential role of mitochondria in the biogenesis of cellular iron-sulfur proteins. *Biol Chem*, 380, 1157-66.
- LIPKIN, L. E. 1959. Cytoplasmic inclusions in ganglion cells associated with parkinsonian states: a neurocellular change studied in 53 cases and 206 controls. *Am J Pathol*, 35, 1117-33.
- LIPPER, C. H., PADDOCK, M. L., ONUCHIC, J. N., MITTLER, R., NECHUSHTAI, R. & JENNINGS, P. A. 2015. Cancer-Related NEET Proteins Transfer 2Fe-2S Clusters to Anamorsin, a Protein Required for Cytosolic Iron-Sulfur Cluster Biogenesis. *PLoS One*, 10, e0139699.
- LOJEK, L. J., FARRAND, A. J., WISECAVER, J. H., BLABY-HAAS, C. E., MICHEL, B. W., MERCHANT, S. S., ROKAS, A. & SKAAR, E. P. 2017. *Chlamydomonas reinhardtii* LFO1 Is an IsdG Family Heme Oxygenase. *mSphere*, 2.
- LU, S., KANEKURA, K., HARA, T., MAHADEVAN, J., SPEARS, L. D., OSLOWSKI, C. M., MARTINEZ, R., YAMAZAKI-INOUE, M., TOYODA, M., NEILSON, A., BLANNER, P., BROWN, C. M., SEMENKOVICH, C. F., MARSHALL, B. A., HERSHEY, T., UMEZAWA, A., GREER, P. A. & URANO, F. 2014. A calcium-dependent protease as a potential therapeutic target for Wolfram syndrome. *Proc Natl Acad Sci U S A*, 111, E5292-301.
- LUCKING, C. B., DURR, A., BONIFATI, V., VAUGHAN, J., DE MICHELE, G., GASSER, T., HARHANGI, B. S., MECO, G., DENEFLÉ, P., WOOD, N. W., AGID, Y., BRICE, A., FRENCH PARKINSON'S DISEASE GENETICS STUDY, G. & EUROPEAN CONSORTIUM ON GENETIC SUSCEPTIBILITY IN PARKINSON'S, D. 2000. Association between early-onset Parkinson's disease and mutations in the parkin gene. *N Engl J Med*, 342, 1560-7.
- LUM, J. J., BAUER, D. E., KONG, M., HARRIS, M. H., LI, C., LINDSTEN, T. & THOMPSON, C. B. 2005. Growth factor regulation of autophagy and cell survival in the absence of apoptosis. *Cell*, 120, 237-48.
- LYLES, K. V. & EICHENBAUM, Z. 2018. From Host Heme To Iron: The Expanding Spectrum of Heme Degrading Enzymes Used by Pathogenic Bacteria. *Front Cell Infect Microbiol*, 8, 198.

- MA, Y., DENG, Q., LI, S., CHEN, M., JIN, B. & WANG, M. 2021. TRPV1, Targeted by miR-338-3p, Induces Neuropathic Pain by Interacting with NECAB2. *J Mol Neurosci*, 71, 55-65.
- MACVICAR, T. D., MANNACK, L. V., LEES, R. M. & LANE, J. D. 2015. Targeted siRNA Screens Identify ER-to-Mitochondrial Calcium Exchange in Autophagy and Mitophagy Responses in RPE1 Cells. *Int J Mol Sci*, 16, 13356-80.
- MAGALHAES, J., GEGG, M. E., MIGDALSKA-RICHARDS, A., DOHERTY, M. K., WHITFIELD, P. D. & SCHAPIRA, A. H. 2016. Autophagic lysosome reformation dysfunction in glucocerebrosidase deficient cells: relevance to Parkinson disease. *Hum Mol Genet*, 25, 3432-3445.
- MANDRIANI, B., CASTELLANA, S., RINALDI, C., MANZONI, M., VENUTO, S., RODRIGUEZ-AZNAR, E., GALCERAN, J., NIETO, M. A., BORSANI, G., MONTI, E., MAZZA, T., MERLA, G. & MICALE, L. 2016. Identification of p53-target genes in *Danio rerio*. *Sci Rep*, 6, 32474.
- MARCHI, S., PATERGNANI, S., MISSIROLI, S., MORCIANO, G., RIMESSI, A., WIECKOWSKI, M. R., GIORGI, C. & PINTON, P. 2018. Mitochondrial and endoplasmic reticulum calcium homeostasis and cell death. *Cell Calcium*, 69, 62-72.
- MATSUDA, N., SATO, S., SHIBA, K., OKATSU, K., SAISHO, K., GAUTIER, C. A., SOU, Y. S., SAIKI, S., KAWAJIRI, S., SATO, F., KIMURA, M., KOMATSU, M., HATTORI, N. & TANAKA, K. 2010. PINK1 stabilized by mitochondrial depolarization recruits Parkin to damaged mitochondria and activates latent Parkin for mitophagy. *J Cell Biol*, 189, 211-21.
- MCBRIDE, H. M., NEUSPIEL, M. & WASIAK, S. 2006. Mitochondria: more than just a powerhouse. *Curr Biol*, 16, R551-60.
- MCWILLIAMS, T. G. & MUQIT, M. M. 2017. PINK1 and Parkin: emerging themes in mitochondrial homeostasis. *Curr Opin Cell Biol*, 45, 83-91.
- MCWILLIAMS, T. G., PRESCOTT, A. R., MONTAVA-GARRIGA, L., BALL, G., SINGH, F., BARINI, E., MUQIT, M. M. K., BROOKS, S. P. & GANLEY, I. G. 2018. Basal Mitophagy Occurs Independently of PINK1 in Mouse Tissues of High Metabolic Demand. *Cell Metab*, 27, 439-449 e5.
- MECO, G., PRATESI, L. & BONIFATI, V. 1991. Cardiovascular reflexes and autonomic dysfunction in Parkinson's disease. *J Neurol*, 238, 195-9.
- MICHIORRI, S., GELMETTI, V., GIARDA, E., LOMBARDI, F., ROMANO, F., MARONGIU, R., NERINI-MOLTENI, S., SALE, P., VAGO, R., ARENA, G., TOROSANTUCCI, L., CASSINA, L., RUSSO, M. A., DALLAPICCOLA, B., VALENTE, E. M. & CASARI, G. 2010. The Parkinson-associated protein PINK1 interacts with Beclin1 and promotes autophagy. *Cell Death Differ*, 17, 962-74.
- MIJALJICA, D., PRESCOTT, M. & DEVENISH, R. J. 2007. Different fates of mitochondria: alternative ways for degradation? *Autophagy*, 3, 4-9.
- MORIMOTO, B. H. & KOSHLAND, D. E., JR. 1990. Induction and expression of long- and short-term neurosecretory potentiation in a neural cell line. *Neuron*, 5, 875-80.
- MULLIN, S. & SCHAPIRA, A. 2013. alpha-Synuclein and mitochondrial dysfunction in Parkinson's disease. *Mol Neurobiol*, 47, 587-97.

- NAKAGAWA, T. & YUAN, J. 2000. Cross-talk between two cysteine protease families. Activation of caspase-12 by calpain in apoptosis. *J Cell Biol*, 150, 887-94.
- NARENDRA, D., TANAKA, A., SUEN, D. F. & YOULE, R. J. 2008. Parkin is recruited selectively to impaired mitochondria and promotes their autophagy. *J Cell Biol*, 183, 795-803.
- NAVARRO-ROMERO, A., MONTPEYO, M. & MARTINEZ-VICENTE, M. 2020. The Emerging Role of the Lysosome in Parkinson's Disease. *Cells*, 9.
- NISHIDA, Y., ARAKAWA, S., FUJITANI, K., YAMAGUCHI, H., MIZUTA, T., KANASEKI, T., KOMATSU, M., OTSU, K., TSUJIMOTO, Y. & SHIMIZU, S. 2009. Discovery of Atg5/Atg7-independent alternative macroautophagy. *Nature*, 461, 654-8.
- PADDOCK, M. L., WILEY, S. E., AXELROD, H. L., COHEN, A. E., ROY, M., ABRESCH, E. C., CAPRARO, D., MURPHY, A. N., NECHUSHTAI, R., DIXON, J. E. & JENNINGS, P. A. 2007. MitoNEET is a uniquely folded 2Fe 2S outer mitochondrial membrane protein stabilized by pioglitazone. *Proc Natl Acad Sci U S A*, 104, 14342-7.
- PANG, Z. P., MELICOFF, E., PADGETT, D., LIU, Y., TEICH, A. F., DICKEY, B. F., LIN, W., ADACHI, R. & SUDHOF, T. C. 2006. Synaptotagmin-2 is essential for survival and contributes to Ca²⁺ triggering of neurotransmitter release in central and neuromuscular synapses. *J Neurosci*, 26, 13493-504.
- PENG, C., FURLAN, A., ZHANG, M. D., SU, J., LUBKE, M., LONNERBERG, P., ABDO, H., SONTHEIMER, J., SUNDSTROM, E. & ERNFORS, P. 2018. Termination of cell-type specification gene programs by the miR-183 cluster determines the population sizes of low-threshold mechanosensitive neurons. *Development*, 145.
- REINHARDT, P., GLATZA, M., HEMMER, K., TSYTSYURA, Y., THIEL, C. S., HOING, S., MORITZ, S., PARGA, J. A., WAGNER, L., BRUDER, J. M., WU, G., SCHMID, B., ROPKE, A., KLINGAUF, J., SCHWAMBORN, J. C., GASSER, T., SCHOLER, H. R. & STERNECKERT, J. 2013a. Derivation and expansion using only small molecules of human neural progenitors for neurodegenerative disease modeling. *PLoS One*, 8, e59252.
- REINHARDT, P., SCHMID, B., BURBULLA, L. F., SCHONDORF, D. C., WAGNER, L., GLATZA, M., HOING, S., HARGUS, G., HECK, S. A., DHINGRA, A., WU, G., MULLER, S., BROCKMANN, K., KLUBA, T., MAISEL, M., KRUGER, R., BERG, D., TSYTSYURA, Y., THIEL, C. S., PSATHAKI, O. E., KLINGAUF, J., KUHLMANN, T., KLEWIN, M., MULLER, H., GASSER, T., SCHOLER, H. R. & STERNECKERT, J. 2013b. Genetic correction of a LRRK2 mutation in human iPSCs links parkinsonian neurodegeneration to ERK-dependent changes in gene expression. *Cell Stem Cell*, 12, 354-67.
- REMEC PAVLIN, M. & HURLEY, J. H. 2020. The ESCRTs - converging on mechanism. *J Cell Sci*, 133.
- ROBERTS, M. E., CRAIL, J. P., LAFFOON, M. M., FERNANDEZ, W. G., MENZE, M. A. & KONKLE, M. E. 2013. Identification of disulfide bond formation between MitoNEET and glutamate dehydrogenase 1. *Biochemistry*, 52, 8969-71.
- ROUZIER, C., BANNWARTH, S., CHAUSSENOT, A., CHEVROLIER, A., VERSCHUEREN, A., BONELLO-PALOT, N., FRAGAKI, K., CANO, A., POUGET, J., PELLISSIER, J. F., PROCACCIO, V., CHABROL, B. & PAQUIS-FLUCKLINGER, V. 2012. The MFN2 gene is responsible for mitochondrial DNA instability and optic atrophy 'plus' phenotype. *Brain*, 135, 23-34.

- SAKOWSKI, Ł. 2016. *Moje drogie mitochondrium - My dear mitochondrium* [Online]. Available: <https://www.totylikoteoria.pl/2016/05/mitochondrium.html> [Accessed February 9th, 2021].
- SALEM, A. F., WHITAKER-MENEZES, D., HOWELL, A., SOTGIA, F. & LISANTI, M. P. 2012. Mitochondrial biogenesis in epithelial cancer cells promotes breast cancer tumor growth and confers autophagy resistance. *Cell Cycle*, 11, 4174-80.
- SANDERS, M., PETRASCH-PARWEZ, E., HABBES, H.-W., DÜRING, M. V. & FÖRSTER, E. 2021. Postnatal Developmental Expression Profile Classifies the Indusium Griseum as a Distinct Subfield of the Hippocampal Formation. *Frontiers in Cell and Developmental Biology*, 8.
- SCHAPIRA, A. H. 2006. Mitochondrial disease. *Lancet*, 368, 70-82.
- SCHONDORF, D. C., AURELI, M., MCALLISTER, F. E., HINDLEY, C. J., MAYER, F., SCHMID, B., SARDI, S. P., VALSECCHI, M., HOFFMANN, S., SCHWARZ, L. K., HEDRICH, U., BERG, D., SHIHABUDDIN, L. S., HU, J., PRUSZAK, J., GYGI, S. P., SONNINO, S., GASSER, T. & DELEIDI, M. 2014. iPSC-derived neurons from GBA1-associated Parkinson's disease patients show autophagic defects and impaired calcium homeostasis. *Nat Commun*, 5, 4028.
- SCHÜNKE, M., SCHULTE, E., SCHUMACHER, U. 2012. *Kopf, Hals und Neuroanatomie*, Stuttgart : Georg Thieme Verlag.
- SCHWEERS, R. L., ZHANG, J., RANDALL, M. S., LOYD, M. R., LI, W., DORSEY, F. C., KUNDU, M., OPFERMAN, J. T., CLEVELAND, J. L., MILLER, J. L. & NEY, P. A. 2007. NIX is required for programmed mitochondrial clearance during reticulocyte maturation. *Proc Natl Acad Sci U S A*, 104, 19500-5.
- SENER, A. & MALAISSE, W. J. 1980. L-leucine and a nonmetabolized analogue activate pancreatic islet glutamate dehydrogenase. *Nature*, 288, 187-9.
- SIDRANSKY, E., NALLS, M. A., AASLY, J. O., AHARON-PERETZ, J., ANNESI, G., BARBOSA, E. R., BARSHIRA, A., BERG, D., BRAS, J., BRICE, A., CHEN, C. M., CLARK, L. N., CONDROYER, C., DE MARCO, E. V., DURR, A., EBLAN, M. J., FAHN, S., FARRER, M. J., FUNG, H. C., GAN-OR, Z., GASSER, T., GERSHONI-BARUCH, R., GILADI, N., GRIFFITH, A., GUREVICH, T., JANUARIO, C., KROPP, P., LANG, A. E., LEE-CHEN, G. J., LESAGE, S., MARDER, K., MATA, I. F., MIRELMAN, A., MITSUI, J., MIZUTA, I., NICOLETTI, G., OLIVEIRA, C., OTTMAN, R., ORR-URTREGER, A., PEREIRA, L. V., QUATTRONE, A., ROGAEVA, E., ROLFS, A., ROSENBAUM, H., ROZENBERG, R., SAMII, A., SAMADDAR, T., SCHULTE, C., SHARMA, M., SINGLETON, A., SPITZ, M., TAN, E. K., TAYEBI, N., TODA, T., TROIANO, A. R., TSUJI, S., WITTSTOCK, M., WOLFSBERG, T. G., WU, Y. R., ZABETIAN, C. P., ZHAO, Y. & ZIEGLER, S. G. 2009. Multicenter analysis of glucocerebrosidase mutations in Parkinson's disease. *N Engl J Med*, 361, 1651-61.
- SIEKEVITZ, P. 1957. Powerhouse of the Cell. *Scientific American*, 197, 131-144.
- SIMONS, S. B., ESCOBEDO, Y., YASUDA, R. & DUDEK, S. M. 2009. Regional differences in hippocampal calcium handling provide a cellular mechanism for limiting plasticity. *Proc Natl Acad Sci U S A*, 106, 14080-4.
- SINGH, I. N., SULLIVAN, P. G., DENG, Y., Mbye, L. H. & HALL, E. D. 2006. Time course of post-traumatic mitochondrial oxidative damage and dysfunction in a mouse model of focal traumatic brain injury: implications for neuroprotective therapy. *J Cereb Blood Flow Metab*, 26, 1407-18.

- SMIRNOVA, E., GRIPARIC, L., SHURLAND, D. L. & VAN DER BLIEK, A. M. 2001. Dynamin-related protein Drp1 is required for mitochondrial division in mammalian cells. *Mol Biol Cell*, 12, 2245-56.
- SMITH, P. K., KROHN, R. I., HERMANSON, G. T., MALLIA, A. K., GARTNER, F. H., PROVENZANO, M. D., FUJIMOTO, E. K., GOEKE, N. M., OLSON, B. J. & KLENK, D. C. 1985. Measurement of protein using bicinchoninic acid. *Anal Biochem*, 150, 76-85.
- SOHN, Y. S., TAMIR, S., SONG, L., MICHAELI, D., MATOUK, I., CONLAN, A. R., HARIR, Y., HOLT, S. H., SHULAEV, V., PADDOCK, M. L., HOCHBERG, A., CABANCHICK, I. Z., ONUCHIC, J. N., JENNINGS, P. A., NECHUSHTAI, R. & MITTLER, R. 2013. NAF-1 and mitoNEET are central to human breast cancer proliferation by maintaining mitochondrial homeostasis and promoting tumor growth. *Proc Natl Acad Sci U S A*, 110, 14676-81.
- SONG, Z., GHOSHANI, M., MCCAFFERY, J. M., FREY, T. G. & CHAN, D. C. 2009. Mitofusins and OPA1 mediate sequential steps in mitochondrial membrane fusion. *Mol Biol Cell*, 20, 3525-32.
- SUGITA, S., HO, A. & SUDHOF, T. C. 2002. NECABs: a family of neuronal Ca²⁺-binding proteins with an unusual domain structure and a restricted expression pattern. *Neuroscience*, 112, 51-63.
- SUMIOKA, A., IMOTO, S., MARTINS, R. N., KIRINO, Y. & SUZUKI, T. 2003. XB51 isoforms mediate Alzheimer's beta-amyloid peptide production by X11L (X11-like protein)-dependent and - independent mechanisms. *Biochem J*, 374, 261-8.
- SUN, N., MALIDE, D., LIU, J., ROVIRA, II, COMBS, C. A. & FINKEL, T. 2017. A fluorescence-based imaging method to measure in vitro and in vivo mitophagy using mt-Keima. *Nat Protoc*, 12, 1576-1587.
- SWEET, S. & SINGH, G. 1999. Changes in mitochondrial mass, membrane potential, and cellular adenosine triphosphate content during the cell cycle of human leukemic (HL-60) cells. *J Cell Physiol*, 180, 91-6.
- TAMINELLI, G. L., SOTOMAYOR, V., VALDIVIESO, A. G., TEIBER, M. L., MARIN, M. C. & SANTA-COLOMA, T. A. 2008. CISD1 codifies a mitochondrial protein upregulated by the CFTR channel. *Biochem Biophys Res Commun*, 365, 856-62.
- TAMIR, S., PADDOCK, M. L., DARASH-YAHANA-BARAM, M., HOLT, S. H., SOHN, Y. S., AGRANAT, L., MICHAELI, D., STOFLETH, J. T., LIPPER, C. H., MORCOS, F., CABANTCHIK, I. Z., ONUCHIC, J. N., JENNINGS, P. A., MITTLER, R. & NECHUSHTAI, R. 2015. Structure-function analysis of NEET proteins uncovers their role as key regulators of iron and ROS homeostasis in health and disease. *Biochim Biophys Acta*, 1853, 1294-315.
- TOMITA, S., OZAKI, T., TARU, H., OGUCHI, S., TAKEDA, S., YAGI, Y., SAKIYAMA, S., KIRINO, Y. & SUZUKI, T. 1999. Interaction of a neuron-specific protein containing PDZ domains with Alzheimer's amyloid precursor protein. *J Biol Chem*, 274, 2243-54.
- TWIG, G., ELORZA, A., MOLINA, A. J., MOHAMED, H., WIKSTROM, J. D., WALZER, G., STILES, L., HAIGH, S. E., KATZ, S., LAS, G., ALROY, J., WU, M., PY, B. F., YUAN, J., DEENEY, J. T., CORKEY, B. E. & SHIRIHAI, O. S. 2008. Fission and selective fusion govern mitochondrial segregation and elimination by autophagy. *EMBO J*, 27, 433-46.

VALENTE, E. M., ABOU-SLEIMAN, P. M., CAPUTO, V., MUQIT, M. M., HARVEY, K., GISPERT, S., ALI, Z., DEL TURCO, D., BENTIVOGLIO, A. R., HEALY, D. G., ALBANESE, A., NUSSBAUM, R., GONZALEZ-MALDONADO, R., DELLER, T., SALVI, S., CORTELLI, P., GILKS, W. P., LATCHMAN, D. S., HARVEY, R. J., DALLAPICCOLA, B., AUBURGER, G. & WOOD, N. W. 2004. Hereditary early-onset Parkinson's disease caused by mutations in PINK1. *Science*, 304, 1158-60.

VANCE, J. E. 1990. Phospholipid synthesis in a membrane fraction associated with mitochondria. *J Biol Chem*, 265, 7248-56.

WALKER, F. O. 2007. Huntington's disease. *Lancet*, 369, 218-28.

WIEMERSLAGE, L. & LEE, D. 2016. Quantification of mitochondrial morphology in neurites of dopaminergic neurons using multiple parameters. *J Neurosci Methods*, 262, 56-65.

WILEY, S. E., ANDREYEV, A. Y., DIVAKARUNI, A. S., KARISCH, R., PERKINS, G., WALL, E. A., VAN DER GEER, P., CHEN, Y. F., TSAI, T. F., SIMON, M. I., NEEL, B. G., DIXON, J. E. & MURPHY, A. N. 2013. Wolfram Syndrome protein, Miner1, regulates sulphhydryl redox status, the unfolded protein response, and Ca²⁺ homeostasis. *EMBO Mol Med*, 5, 904-18.

WILEY, S. E., MURPHY, A. N., ROSS, S. A., VAN DER GEER, P. & DIXON, J. E. 2007. MitoNEET is an iron-containing outer mitochondrial membrane protein that regulates oxidative capacity. *Proc Natl Acad Sci U S A*, 104, 5318-23.

WU, C. Y., CHEN, Y. F., WANG, C. H., KAO, C. H., ZHUANG, H. W., CHEN, C. C., CHEN, L. K., KIRBY, R., WEI, Y. H., TSAI, S. F. & TSAI, T. F. 2012. A persistent level of Cisd2 extends healthy lifespan and delays aging in mice. *Hum Mol Genet*, 21, 3956-68.

WU, H., LI, D., SHAN, Y., WAN, B., HEXIGE, S., GUO, J., WU, C. & YU, L. 2007. EFCBP1/NECAB1, a brain-specifically expressed gene with highest abundance in temporal lobe, encodes a protein containing EF-hand and antibiotic biosynthesis monooxygenase domains. *DNA Seq*, 18, 73-9.

YEATS, C., BENTLEY, S. & BATEMAN, A. 2003. New knowledge from old: in silico discovery of novel protein domains in *Streptomyces coelicolor*. *BMC Microbiol*, 3, 3.

YONUTAS, H. M., HUBBARD, W. B., PANDYA, J. D., VEKARIA, H. J., GELDENHUYS, W. J. & SULLIVAN, P. G. 2020. Bioenergetic restoration and neuroprotection after therapeutic targeting of mitoNEET: New mechanism of pioglitazone following traumatic brain injury. *Exp Neurol*, 327, 113243.

YOO, J. C., CHANG, J. R., KIM, S. H., JANG, S. K., WOLGEMUTH, D. J., KIM, K. & RHEE, K. 2004. NIP1/XB51/NECAB3 is a potential substrate of Nek2, suggesting specific roles of Nek2 in Golgi. *Exp Cell Res*, 292, 393-402.

YUAN, H., LI, X., ZHANG, X., KANG, R. & TANG, D. 2016. CISD1 inhibits ferroptosis by protection against mitochondrial lipid peroxidation. *Biochem Biophys Res Commun*, 478, 838-44.

ZHANG, H., BOSCH-MARCE, M., SHIMODA, L. A., TAN, Y. S., BAEK, J. H., WESLEY, J. B., GONZALEZ, F. J. & SEMENZA, G. L. 2008. Mitochondrial autophagy is an HIF-1-dependent adaptive metabolic response to hypoxia. *J Biol Chem*, 283, 10892-903.

ZHANG, M. D., SU, J., ADORI, C., CINQUINA, V., MALENCZYK, K., GIRACH, F., PENG, C., ERNFORS, P., LOW, P., BORGIUS, L., KIEHN, O., WATANABE, M., UHLEN, M., MITSIOS, N., MULDER, J., HARKANY, T. & HOKFELT, T. 2018. Ca²⁺-binding protein NECAB2 facilitates inflammatory pain hypersensitivity. *J Clin Invest*, 128, 3757-3768.

ZHANG, M. D., TORTORIELLO, G., HSUEH, B., TOMER, R., YE, L., MITSIOS, N., BORGIUS, L., GRANT, G., KIEHN, O., WATANABE, M., UHLÉN, M., MULDER, J., DEISSEROTH, K., HARKANY, T. & HÖKFELT, T. G. 2014. Neuronal calcium-binding proteins 1/2 localize to dorsal root ganglia and excitatory spinal neurons and are regulated by nerve injury. *Proc Natl Acad Sci U S A*, 111, E1149-58.

ZIMMERMANN, B., GIRARD, F., MÉSZÁR, Z. & CELIO, M. R. 2013. Expression of the calcium binding proteins Necab-1,-2 and -3 in the adult mouse hippocampus and dentate gyrus. *Brain Res*, 1528, 1-7.

ZURIS, J. A., HARIR, Y., CONLAN, A. R., SHVARTSMAN, M., MICHAELI, D., TAMIR, S., PADDOCK, M. L., ONUCHIC, J. N., MITTLER, R., CABANTCHIK, Z. I., JENNINGS, P. A. & NECHUSHTAI, R. 2011. Facile transfer of [2Fe-2S] clusters from the diabetes drug target mitoNEET to an apo-acceptor protein. *Proc Natl Acad Sci U S A*, 108, 13047-52.

Acknowledgement

Curriculum Vitae

